University of New Mexico

UNM Digital Repository

5-4-1978

A Comprehensive Study Of Excimer Laser Systems

Robert Ray Butcher

Robert Ray Butcher
Candidate

Electrical Engineering and Computer Science
Department

This thesis is approved, and it is acceptable in quality
and form for publication on microfilm:

Approved by the Thesis Committee:

S.A. Gumbayani , Chairperson

Martin S. Piltch

Ruben D. Kelly

WW Grammann

Accepted:

Bernard Spolsky
Dean, Graduate School

May 4, 1978
Date

A COMPREHENSIVE STUDY OF EXCIMER LASER SYSTEMS

BY

ROBERT RAY BUTCHER

B. S., The University of New Mexico, 1975

THESIS

Submitted in Partial Fulfillment of the
Requirements for the Degree of
Master of Science in
Electrical Engineering
in the Graduate School of
The University of New Mexico
Albuquerque, New Mexico
May 1978

LA-UR

TITLE: A COMPREHENSIVE STUDY OF EXCIMER LASER SYSTEMS

AUTHOR(S): Robert R. Butcher, AP-2

SUBMITTED TO: GRADUATE SCHOOL
University of New Mexico

los alamos
scientific laboratory
of the University of California
LOS ALAMOS, NEW MEXICO 87545

An Affirmative Action/Equal Opportunity Employer

Acknowledgments

A COMPREHENSIVE STUDY OF EXCIMER LASER SYSTEMS

BY

Robert Ray Butcher

ABSTRACT OF THESIS

Submitted in Partial Fulfillment of the

Requirements for the Degree of
Master of Science in
Electrical Engineering
in the Graduate School of

The University of New Mexico

Albuquerque, New Mexico
May 1978

A COMPREHENSIVE STUDY OF EXCIMER LASER SYSTEMS

ABSTRACT

Rare gas halogen lasers are finding increasing usage as an intense source of ultraviolet energy. Many applications require a high energy laser capable of operation at reasonably high repetition rates. Electrical discharge pumping satisfies these requirements quite nicely, however to date little has been reported on the discharge characteristics of this class of laser. This paper describes a parametric study done on electrical discharge excimer laser systems.

We have designed and tested a flashboard pre-ionized excimer laser utilizing a cable pulse forming network (PFN) for the main discharge. Extensive voltage and current data were taken with various gas mixtures at various pressures. The voltage and current data were digitized and used to find such parameters as dynamic impedance of the load, energy deposited in the gas, and peak power during the pulse. The effects of varying the length and impedance of the cable PFN were studied. Several interesting relationships were discovered between the various parameters.

A computer simulation was used to verify the consistency of the data. A comparison of the computer simulated voltage and current pulse

to the measured data indicates the data is internally consistent.

Two experiments are described using the lasers studied. The threshold for laser induced air breakdown was measured at 193 nm and at 248 nm. A series of Raman scattering experiments was conducted to obtain levels of energy and wavelengths which were beyond the reach of other experimenters. The high power and beam quality achieved with these lasers was adequate for the purposes of the experiments.

In this paper conclusions are presented relating to the scaling factors for excimer laser systems. These conclusions are expected to have an impact on future rare gas laser system design.

TABLE OF CONTENTS

List of Figures

List of Tables

CHAPTER I. INTRODUCTION

Rare gas halogen lasers are finding increasing usage as a intense source of ultraviolet energy. Many applications require a high energy laser capable of operation at reasonably high repetition rates. Electrical discharge pumping satisfies these requirements quite nicely, however to date little has been reported on the discharge characteristics of this class of laser. This paper describes a parametric study done on electrical discharge excimer laser systems.

Four separate laser systems were designed and built. The details of the four different systems are described in Chapter 2-1, while the instrumentation and measurement procedures are explained in chapter 2-2. The electrical considerations of the various systems are discussed in chapter 2-3, and the parameter studies and most of the data are presented in chapter 3. Chapter 4 describes the details of the air breakdown and Raman shifting experiments. Finally chapter 5 wraps up the effort, and discusses the implications of the parameter studies.

This work represents what is the most extensive engineering study done to date on excimer laser systems. In spite of this many areas are covered only briefly, and many questions are left unanswered. The experiments conducted in air breakdown and Raman scattering are not exhaustive by any means; these areas are broad enough to be a research problem by themselves. The only intent in doing the experiments was to fill a gap in existing data. The conclusions presented provide an insight into the electrical characteristics of an important class of lasers.

CHAPTER II.   DESIGN OF THE LASER SYSTEMS

2-1.   Mechanical Design

During the course of this work, three different lasers were built
and operated.   These will be referred to as 1) Early model, 2) 1.2 m
laser, 3) 0.6 m laser. The general features of all three are shown in
Figure 1. A rectangular box of insulating material provided the body
for the laser. Aluminum plates were attached to the open sides of the
box and sealed with viton O-rings. Electrodes were bolted to these
plates and O-ring seals were used around the bolts. Windows were
attached to the ends of the box to permit extraction of the laser
output. Some type of pre-ionization source was included in the box to
stabilize the discharge. All three lasers utilized a line type pulse
forming network (PFN) consisting of a number of coaxial cables. The
center conductors of the cables were connected to the anode plate, while
the outer shields were connected to the cathode plate. The other ends
of the cables were attached to the electrical driver, which consisted of
a high voltage discharge capacitor (or capacitors) and a switch. Dif-
ferences between the three lasers were primarily in the physical size
and material of the box, the electrode length and shape, the window
material and method of attachment, the method of pre-ionization, the
number and type of cables, and the details of the high voltage driver.
These differences are discussed and explained throughout this thesis.
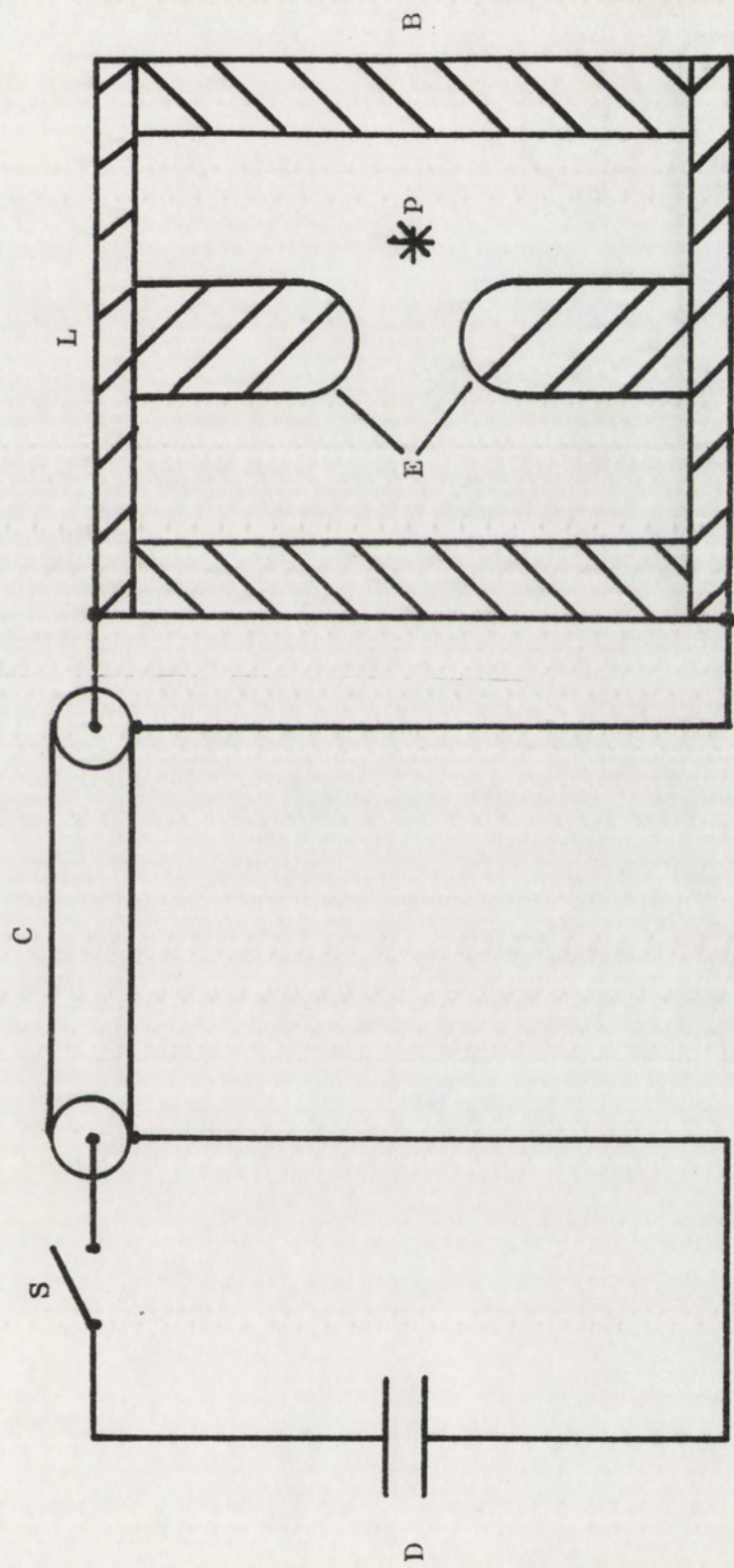
Figure 1. Typical Excimer Laser. D— driver capacitor; S— switch; C— cable PFN; L— aluminum plate; E— electrodes; P— preionization source; B— rigid dielectric body

Early Model

The early model used an acrylic body machined from a solid plate. The available material determined to some extent the 600 x 150 x 50 mm dimensions of the box. The electrodes used were simple half cylinders of 19 mm radius separated by 13 mm and tapered on the ends to reduce field enhancement. Quartz windows were installed at Brewster's angle and sealed to the window holders with epoxy. The window holders were bolted to the body and sealed with viton O-rings. Pre-ionization of the gas was achieved by a double-discharge corona technique. Three lengthwise slots were machined into the cathode and fitted with quartz tubing. Small diameter wires inside the tubing were capacitor coupled to the anode as shown in Figure 2. Thirty-two low impedance cables (YK-198) of 1 m length were used to provide a 0.5 ohm, 6 nsec (one way transit time) PFN. The cables were pulse charged by a 0.15 μf capacitor (Maxwell 31159) switched by a grounded grid thyratron (E. G. & G. HY-3202). The thyratron and capacitor were mounted in a low inductance configuration to permit a fast voltage risetime on the PFN. The optical cavity consisted of a 5 m radius of curvature aluminum mirror and a quartz etalon separated by 0.9 m. The acrylic body of this laser cracked after two weeks of testing, which led to the 1.2 m laser design.

1.2 m Laser

The 1.2 m laser utilized two acrylic boxes (Tachisto, Inc.) attached end to end. The resulting body dimensions were 1420 x 140 x 90 mm. Aluminum Rogowski electrodes (Tachisto, Inc.) of 600 mm length were spaced 20 mm apart in each box. This resulted in an electrode
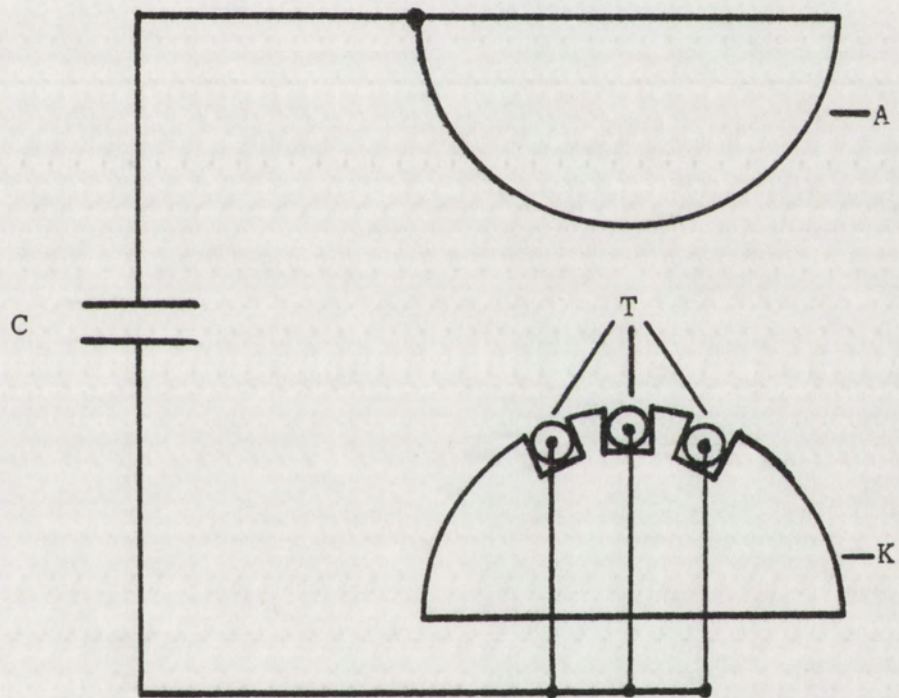
Figure 2. Corona Preionization. A- anode; K- cathode;
C- coupling capacitor; T- quartz tubing

length of 1.2 m; hence the name. Quartz Brewster angle windows were fitted similar to the early model. These were later changed to a tilted (5°) window in a teflon mount sealed by O-rings. This permitted the windows to be changed more easily.

Figure 3 shows one flashboard pre-ionizer of the type used in this laser. Two such flashboards were mounted along one side of the laser through holes in the body. Each flashboard consisted of a series of 49 flathead brass screws (1/4-20) threaded into a 660 x 50 x 6 mm strip of plastic (acrylic and polycarbonate were both tried) on 12.7 mm centers. This resulted in a gap between screw heads of about 0.1 mm. The center screw on each board was grounded to the cathode and the end screws were connected through four 3 m lengths of coaxial cable (RG-214) to the flashboard driver. The flashboard driver consisted of a 0.15 µf capacitor (Maxwell 31159) and a spark gap switch (Tachisto ED 301).

Sixty-four 2.44 m lengths of graded dielectric cable (Essex 40/100) were attached to form a 0.5 ohm impedance 15 nsec (one way) electrical length PFN for the main discharge. The cable driver used on this laser was a two stage Marx bank using 0.15 µf capacitors (Maxwell 31159) and spark gap switches (Tachisto SG 301). The first Marx Bank incorporated air and mylar insulation, but a second version was soon built with oil insulation to permit operation above 30 kV DC per stage.

The first 1.2 m laser was committed to a series of experiments so a second identical laser was built. This laser used field distortion spark gaps (Maxwell 40044) in the Marx bank to permit low jitter triggering. Two thyratron pulsers were built to provide accurate timing
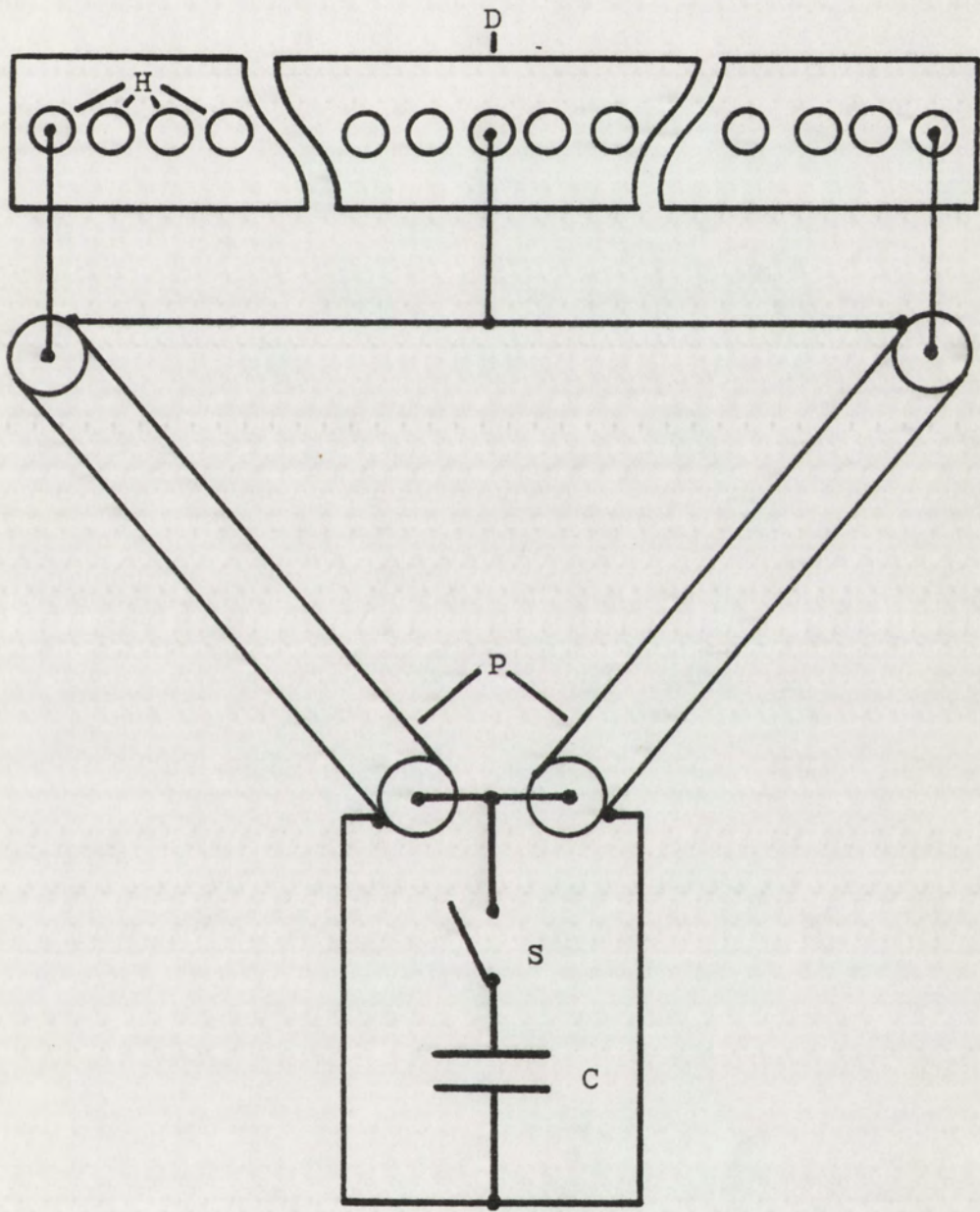
Figure 3. Flashboard Preionizer. C- capacitor; S- switch;
P- cable PFN; D- plastic strip; H- screw head

of the pre-ionizer and main discharge pulses. These units are described in chapter 2-3. Several different optical cavities were used with this laser and will be discussed in detail in Chapter 4. This laser had a problem similar to the early model and after repairing and/or replacing six acrylic bodies which developed cracks, work was begun on the 0.6 m laser.

0.6 m Laser

The 0.6 m laser was designed to be more compatible with the fluorine gas mixes used. Other work done at LASL indicated that a cast epoxy body (EPON 828) might have a much higher strength and better fluorine resistance (Willis, 1977). Helicoil inserts were used on all threaded holes. Since only one such body was available, a single box of 710 x 140 x 90 mm was used. Two electrodes from the 1.2 m laser were used first, however, these were replaced later on with a pair of nickel plated brass electrodes having a Chang profile. The Chang profile utilizes a larger volume in the same length and spacing. The 1.2 m laser windows were replaced with CaF_2 windows in an epoxy holder to reduce window damage and permit operation at higher pressures. The same type of flashboards as on the 1.2 m laser were fabricated from Teflon TFE since both acrylic and polycarbonate developed many cracks after long exposures to fluorine gas mixes. One flashboard was mounted on each side of the laser to permit symmetrical pre-ionization and increase the discharge volume as shown in Figure 4. The 1.2 m laser pre-ionizer driver was used. All gas and pre-ionizer feed through connections were
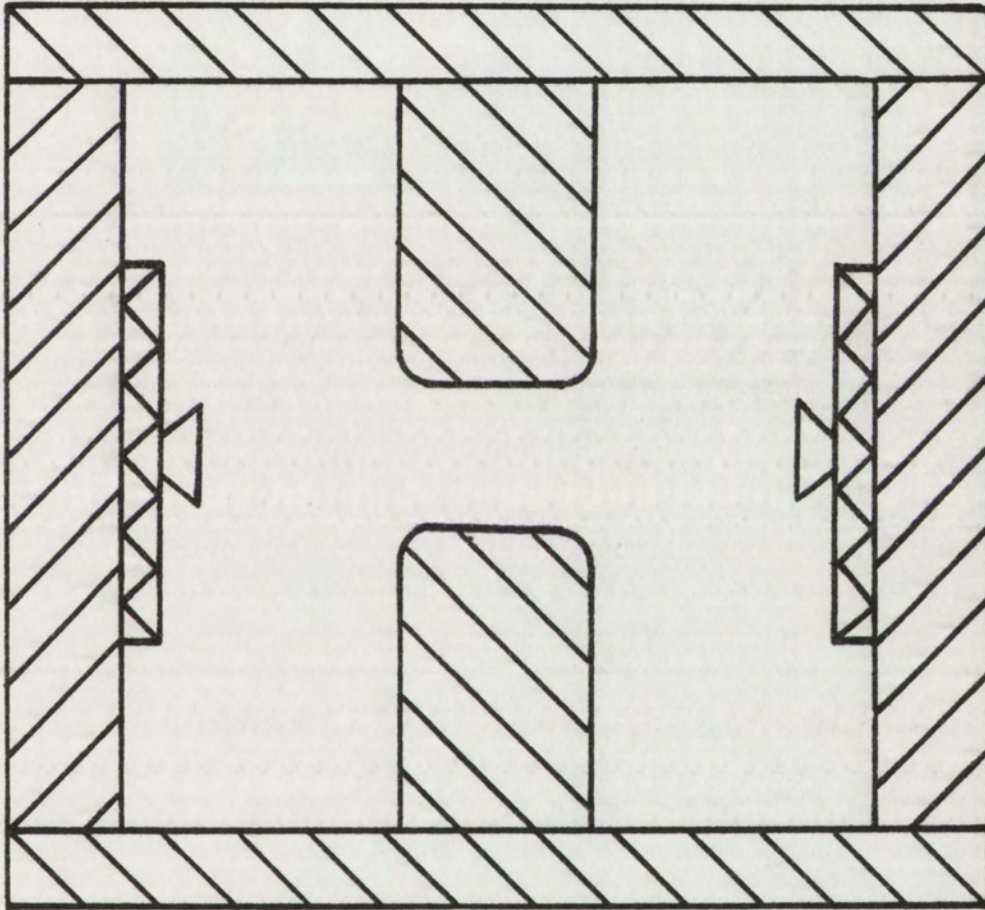
Figure 4. Cross-section of 0.6 m Laser Head

made in the cathode (grounded) aluminum plate to reduce the stress
points in the epoxy body to a minimum. The shorter length of the single
box limited the number of PFN cables to 48 without hardware modifi-
cations. The same cable PFN used on the 1.2 m laser was used on this
device. The driver was the same Marx bank used on the 1.2 m laser.

2-2.   MEASUREMENT TECHNIQUES

Data were obtained from a variety of sensors. Voltage measurements were made at the laser cavity electrodes using a resistive divider voltage probe which incorporates a grading shield to minimize the time constants associated with stray capacitance. The probe has an impedance of 50 k Ω and an attenuation ratio of 1000:1 when terminated in 50 Ω. The rise-time is less than 10 nsec. Current measurements were made by installing a current viewing resistor (CVR) having a nominal resistance of 1 x 10^{-3} Ω and a frequency response of 300 MHz (risetime of 1.2 nsec) in series with the ground return braid of one of the PFN cables. Total discharge current was then calculated as N (the number of cables) times the measured current. A length of solid copper tubing was installed around the shield on the coaxial cable between the CVR and the screen room to reduce high frequency noise pickup.

The inductance of the driver was calculated from the relation

$$f = \frac{1}{2\pi \ (LC)^{\frac{1}{2}}} \tag{1}$$

rearranged to

$$L = \frac{1}{4\pi^2 \ f^2 \ C} \ = \ \frac{T^2}{4\pi^2 C} \tag{2}$$

where T is one period of the ringing waveform of the shorted driver and

C is the driver capacitance. The resistance of the driver was cal-
culated from the relation

$$\left| I_2 \right| = \left| I_1 \right| \exp \left| \frac{(-RC)}{L} \right| \tag{3}$$

rearranged to

$$R = \frac{L}{C} \ln \left| \frac{I_1}{I_2} \right| \tag{4}$$

where I_1 and I_2 are the magnitudes of consecutive current peaks of
opposite amplitude.

The laser output was monitored using a fast photodiode (ITT F128)
having a 0.5 nsec response time located as near as practical to the
laser output and suitably attenuated. All cable lengths between the
sensors and the oscilloscope were matched to provide accurate timing of
data. A fast (3.5 nsec risetime) storage oscilloscope (Tektronix 7633)
was used inside the screen room to record the data. Since this oscillo-
scope was not a dual beam device, measurements were made in the alter-
nate mode, using the pulse from the voltage probe as a trigger source.
Multiple sweeps were taken periodically to assure overlap of several
pulses and avoid errors in timing or magnitude of the data. Energy
measurements were made using either a calorimeter (Scientech 362), or a
pyroelectric energy meter (Gen-Tec ED-500). The energy meter was
periodically compared to the calorimeter. The active volume in the
laser was calculated from the product of electrode length and area of
burn spots taken near the output of the laser. Wavelength measurements

were made using either a rapid scan spectrometer (RSS, Tektronix 7J 20)
or an optical multichannel analyzer (OMA, Princeton Applied Research
1205A with intensified scintillator head).

A desk top calculator (Hewlett Packard 9830) with digitizer and
plotter was used to reduce the data. A program was written to digitize
and store the voltage, current, and laser signal from photographs of
oscilloscope traces and calculate various parameters. Power was cal-
culated from the product of instantaneous voltage and current. Impedance
was calculated from the ratio of voltage to current. Charge and energy
were calculated from the time integrals of current and power. By
rearranging the formula for energy stored in an inductor

$$E = \frac{1}{2} LI^2 \tag{5}$$

to

$$L = \frac{2E}{I^2} \tag{6}$$

the inductance of the load was calculated from the energy stored in the
magnetic field and the current at the time of power reversal. This
inductance was used along with the time derivative of the current to
calculate the reactive portion of the measured voltage using the re-
lation

$$V_L(t) = L \frac{dI(t)}{dt} \tag{7}$$

This voltage drop was then used to calculate the voltage, power, and

energy due to the resistive component of the load by the relations

$$V_R(t) = V \text{ measured } - V_L(t) \tag{8}$$

$$P_R(t) = V_R(t).I(t) \tag{9}$$

$$E_r(t) = \frac{1}{T} \int_o^T P_R(t) \, dt \tag{10}$$

The resistance of the load was calculated from the relation

$$R(t) = V_R(t)/I(t) \tag{11}$$

A smoothing function was written into the program to reduce the effects of high frequency noise which was apparent on some of the data. This was extremely beneficial when derivatives of the waveforms were required, as differentiation tends to accentuate high frequency noise. The technique which produced the best results was a simple averaging function

$$V(T_n) = \frac{V(T_n - \Delta) + V(T_n + \Delta)}{2} \tag{12}$$

which could be repeated as many times as needed to reduce noise.

Output from the program was available in either tabular or graphical form.

In order to check the data obtained, a network analysis program (NET-2, Release 9) was used. A circuit resembling the actual laser circuit was devised to verify the magnitude and temporal shape of

the voltage and current waveforms. Component values used in the program
were identical to the measured or calculated values obtained from the
actual circuit, including a time dependent resistance for the load. A
switch was closed at the appropriate time to simulate the avalanche
breakdown in the laser. Equations previously applied to spark gaps were
used to calculate the time constants associated with the time varying
resistance of the laser gas.

2-3. Electrical Design

Several different electrical drivers and trigger systems were used on the three laser systems, as mentioned in the design section of this paper. The various systems had some good and some bad features, which are discussed in this section.

A cable discharge PFN was used on all the lasers studied. This type of energy storage has the best defined inductance, capacitance, and electrical length of any common technique. Very low impedances are possible, and defective cables are easily replaced. For pulse lengths of a few tens of nanoseconds the physcial lengths are reasonable. The most serious limitation of this type of PFN is the large volume required for storage of reasonable energies.

The voltage on the cables at the time of onset of laser current is determined primarily by electrode spacing and the gas pressure. Gas composition and voltage risetime have an effect on breakdown voltage as well. Allowing the laser to operate as its own switch has the advantage of a minimum inductance in the discharge path and a greatly simplified design. The greatest disadvantage of this technique is the limited control over the voltage (and hence stored energy) on the cables at the time of switch closure.

The early model used 32 parallel coaxial cables of 1 m length for the PFN. These cables (Belden YK-198) had an inductance of 92 nH per meter and a capacitance of 362.5 pF per meter. The cable impedance calculated from

$$Z_o = (L/C)^{1/2} \tag{13}$$

is 15.92 ohms. The total impedance of the PFN is

$$Z = Z_o/32 \tag{14}$$

calculated to be 0.4975 ohms. The total cable capacitance available for energy storage calculated from the relation

$$C_c = nC\ell \tag{15}$$

is 11.6 nF, where C is capacitance per unit length, ℓ is the cable length, and n is the number of cables.

The one way transit time of a transmission line can be calculated from

$$\tau = \frac{\ell}{v} \tag{16}$$

where ℓ is the length of the cable and v is the velocity of propagation in the cable, derived from

$$v = \frac{c}{(\varepsilon_r)^{\frac{1}{2}}} = \frac{1}{(\varepsilon_r \varepsilon_o U_o)^{\frac{1}{2}}} \tag{17}$$

where c is the velocity of light in free space, ε_r is the relative dielectric constant, and ε_o and U_o are the permittivity and permeability of free space. An alternate equation for calculating the transit of a transmission line is

$$\tau = (LC)^{1/2} \tag{18}$$

where L and C are the inductance and capacitance of the length of transmission line.

For the 1 m length cables used on this laser, the one way electrical length is 5.77 nsec. For a matched impedance load, the pulsewidth of the current pulse will be twice the one way transit time of the cables. For the early model this time is 11.54 nsec which is considerably shorter than the laser pulsewidth of 30 nsec expected from a KrF laser. A longer electrical length line should couple more energy into the gas during this 30 nsec period. The electrical insulation on these cables is only 1.2 mm, which limits the voltage to about 24 kV.

Cables of 2.44 m length were used on the 1.2 m laser and the 0.6 m laser to more nearly match the laser pulsewidth. These cables (Essex 40/100) are special cables having a nominal d-c voltage rating of 60 kV an impedance of 30.4 ohms (from a capacitance of 204 pF per meter and an inductance of 188 nH per meter), and a propagation time of 6.2 nsec per meter. Essex 40/100 cable utilizes carbon-loaded PVC jackets to reduce local field stress points resulting from imperfections in the braid conductors. This produces a highly reliable cable capable of much higher voltages than any encountered in either of the lasers. The number of cables was varied between 8 and 64 to obtain data on these two lasers. In addition longer cables (6.1 m) were tried in one experiment to increase the width of the electrical pulse to 75.6 nsec.

Several different electrical drivers were used to pulse charge the cables to the breakdown voltage of the gas load. For charging times which are long compared to the cable transit time, and neglecting any resistive losses, the voltage on the cables can be approximated by the equation

$$V_c(t) = Vm \ (1 - \cos wt) \tag{19}$$

where the ringing frequency is calculated from

$$w = \frac{1}{(L_d C_{eq})^{1/2}} \tag{20}$$

where L_d is the inductance of the driver and the equivalent series capacitance is expressed by

$$C_{eq} = \frac{C_s \ C_c}{C_s + C_c} \tag{21}$$

where C_s is the capacitance of the storage capacitor (or equivalent series capacitance in the case of a Marx generator) and C_c is the cable capacitance. Since the charge divides between series capacitors, the peak voltage is expressed by the formula

$$Vm = V_o \ (\frac{C_s}{C_s + C_c}) \tag{22}$$

where V_o is the initial voltage on the storage capacitor or nV_o in the case of an n-stage Marx generator. It is worth noting that if $C_s \gg C_c$ the ringing frequency is determined by primarily C_c and L_d. Also, if

the voltage is allowed to ring to its full peak value (wt = π radians) the voltage will nearly double. The time rate of change of voltage can be found by taking the derivative of equation (19) and is expressed as

$$\frac{dv}{dt} = V_m \, w \, \sin wt \tag{23}$$

which is useful for calculations involving this parameter.

Another point worth considering is the energy transfer efficiency

$$\eta_E = \frac{E_c}{E_s} \tag{24}$$

where the energies on the capacitors are found from

$$E_c = 1/2 \, C_c \, V_c^{\,2} \tag{25}$$

$$\dot{E}_s = 1/2 \, C_s V_o^{\,2} \tag{26}$$

and the voltage on the cable capacitor (assuming wt = π radians) is found from equations (21) and (22)

$$V_c = \frac{2 \, V_o \, C_s}{C_c + C_s} \tag{27}$$

The resulting energy transfer efficiency is calculated from equations (24), (25), (26), and (27).

$$\eta_E = \frac{4 \, C_c C_s}{(C_s + C_c)^2} \tag{28}$$

Solving for maximum transfer efficiency

$$0 = \frac{d\eta_E}{dC_c} = 4C_s \frac{d}{dC_c} \left[\frac{C_c}{(C_s + C_c)^2} \right] \qquad (29)$$

$$0 = \frac{4 C_s [C_s^2 - C_c^2]}{(C_s + C_c)^4} \qquad (30)$$

either $C_s = 0$ or $C_s = C_c$ will satisfy this equation. Obviously the latter condition will result in the maximum efficiency which from equation (28) becomes

$$\eta_E = \frac{4 C_c^2}{(2 C_c)^2} = 1 \qquad (31)$$

Therefore, the driver can be designed for maximum voltage gain or maximum efficiency, but not both.

The laser is usually operated at a voltage (V_o) high enough to reach the breakdown threshold of the gas well before the peak of the charging voltage, i.e. wt < π. In this case some energy is delivered to the laser gas from the driver directly, since the PFN is being charged by the driver while being discharged by the gas load. This usually raises the laser output somewhat, but results in extra heat into the laser gas after the useful work is done, and a reduced overall efficiency.

The early model used a single capacitor with a thyratron switch for the driver. This driver had an inductance of 65 nH and a capacitance of 0.1 μF.

The current was not measured in this laser, and calculations requiring current were not possible.

The use of a thyratron switch for this laser permitted operation at a repetition rate limited by the power supply current rating. The charge on the capacitor is calculated from

$$Q = CV \tag{32}$$

to be 2×10^{-3} coulomb. The average current drawn from the supply is calculated from

$$i = nQ \tag{33}$$

where i is the current in amperes and n is the number of pulses in one second. The 200 milliampere limit of the supply is reached at a repetition rate of 100 Hz.

Figure 5 shows a block diagram of the 1.2 m and the 0.6 m laser systems. A 2 stage Marx generator was used for a cable driver to pulse charge the main discharge PFN.

The Marx generator was charged to voltages of up to the power supply limit of 48 kV per stage. The inductance of the bank was calculated to be approximately 360 nH resulting in a typical voltage rise-time on 48 - 2.44 m cables of 85 nsec to the breakdown voltage of 40 kV. Data were taken with various numbers of cables at different initial voltages and pressures, and with different gas mixtures. These data are presented in Chapter 3.

A single 0.15 uF capacitor and field distortion spark gap were used in the pre-ionizer driver. A PFN composed of four parallel lengths of co-ax cable provided adequate ballast ot insure all four flashboard sections would fire everytime. No attempt was made to reduce the
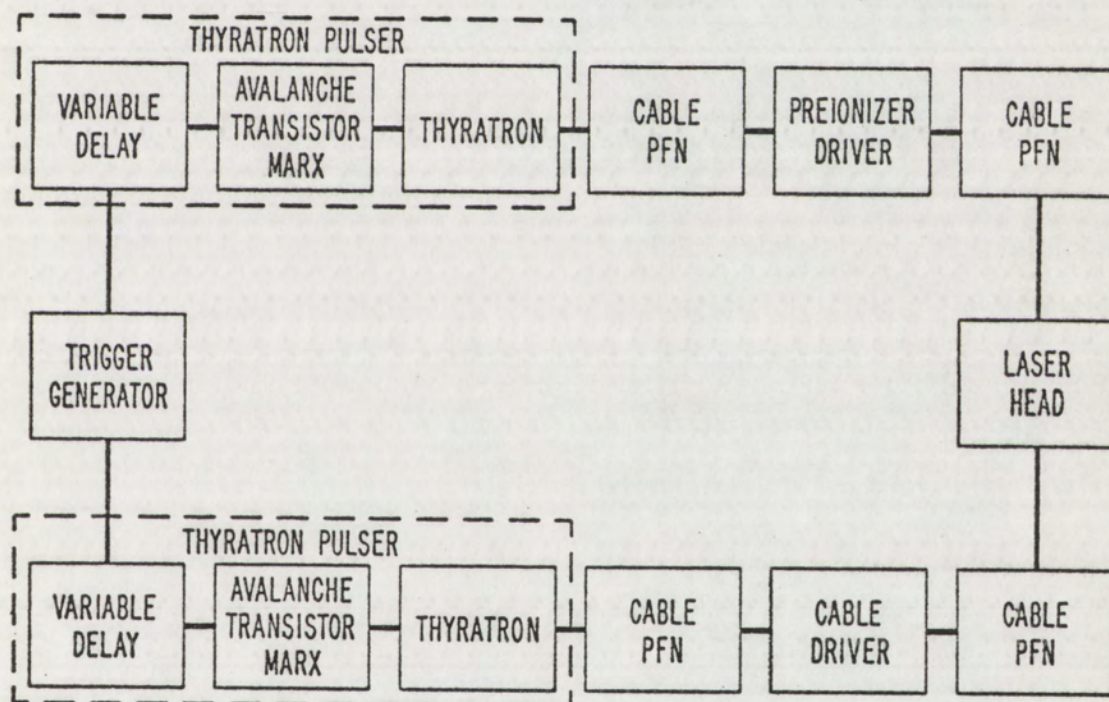
Figure 5. Block Diagram of Laser Systems

inductance of this circuit and the resulting current risetime was 345 nsec. The voltage on the driver was varied between 15-30 kV.

Reliable triggering was accomplished by the use of two thyratron pulsers. Each pulser had two capacitors charged to 20 kV and switched into two 5 m lengths of RG 214 cable by a thyratron (E G & G HY 1102) as shown in Figure 6. The cable PFN is initially terminated in a very high impedance and the voltage pulse nearly doubles on arrival at the spark gap. In practice, the voltage reaches 37 kV when the capacitors are charged to 20 kV. When the spark gap breaks down the 5 m cable PFN supplies sufficient energy to trigger the discharge. The mid-plane of the spark gap reaches very high voltages when the gap triggers, and a series resistor and capacitor (50 Ω and 170 pF 90 kV) limit the voltage transmitted back down the cable toward the thyratron pulser.

The thyratron cathode is biased at +100 volts and is pulsed negative by a 3 stage avalanche transistor Marx generator shown in Figure 7. A series resistor of 100 ohms limits the grid to cathode current. The pulse on the cathode reaches a negative 600 volt level in less than 10 nsec. The resulting jitter is less than one nsec between pulses of the thyratron.

A variable delay circuit is incorporated into each thyratron pulser to permit a several usec delay between the trigger pulse and thyratron breakdown. This allows precise adjustments of the delay between the flashboard firing and erection of the main discharge voltage. This delay is very important for some rare gas halides, as discussed in chapter 3.
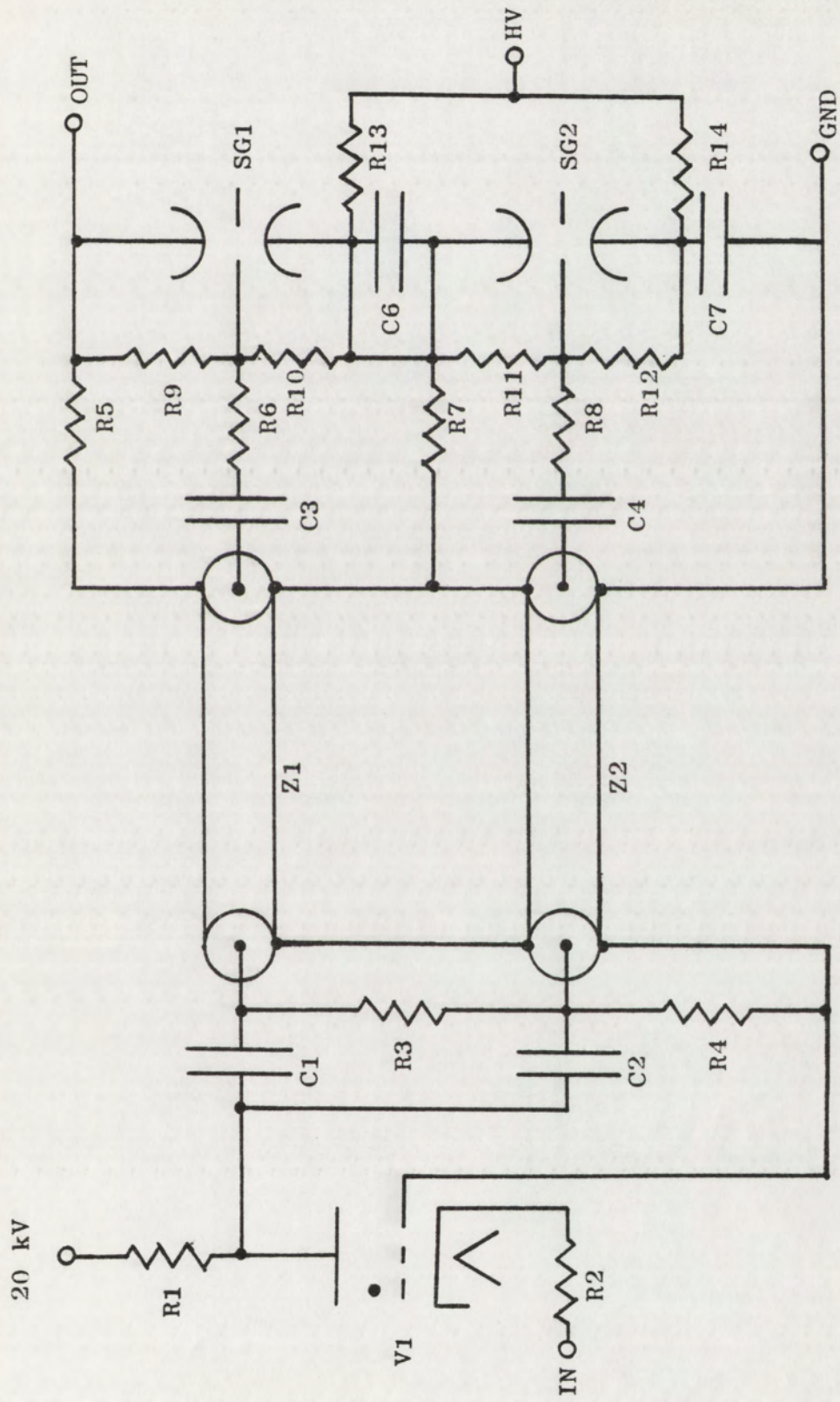
Figure 6. Thyratron Pulser and Marx Generator

R1, 3, 4, 5, 7	- 500 K	50kV
R2	- 100	
R6, 8	- 100	50kV
R9, 11	- 100 M	50kV
R10, 12	- 200 M	50kV
R13, 14	- 2 Meg	50kV
C1, 2	- 8.1 nF	40kV
C3, 4	- 170 pf	90kV
C6, 7	- .15 μF	50kV
V1	- HY 1102	
Z1, 2	- RG 214	
SG1, 2	- Maxwell 40044	

Table 1. Parts list for Thyratron Pulser and Marx Generator
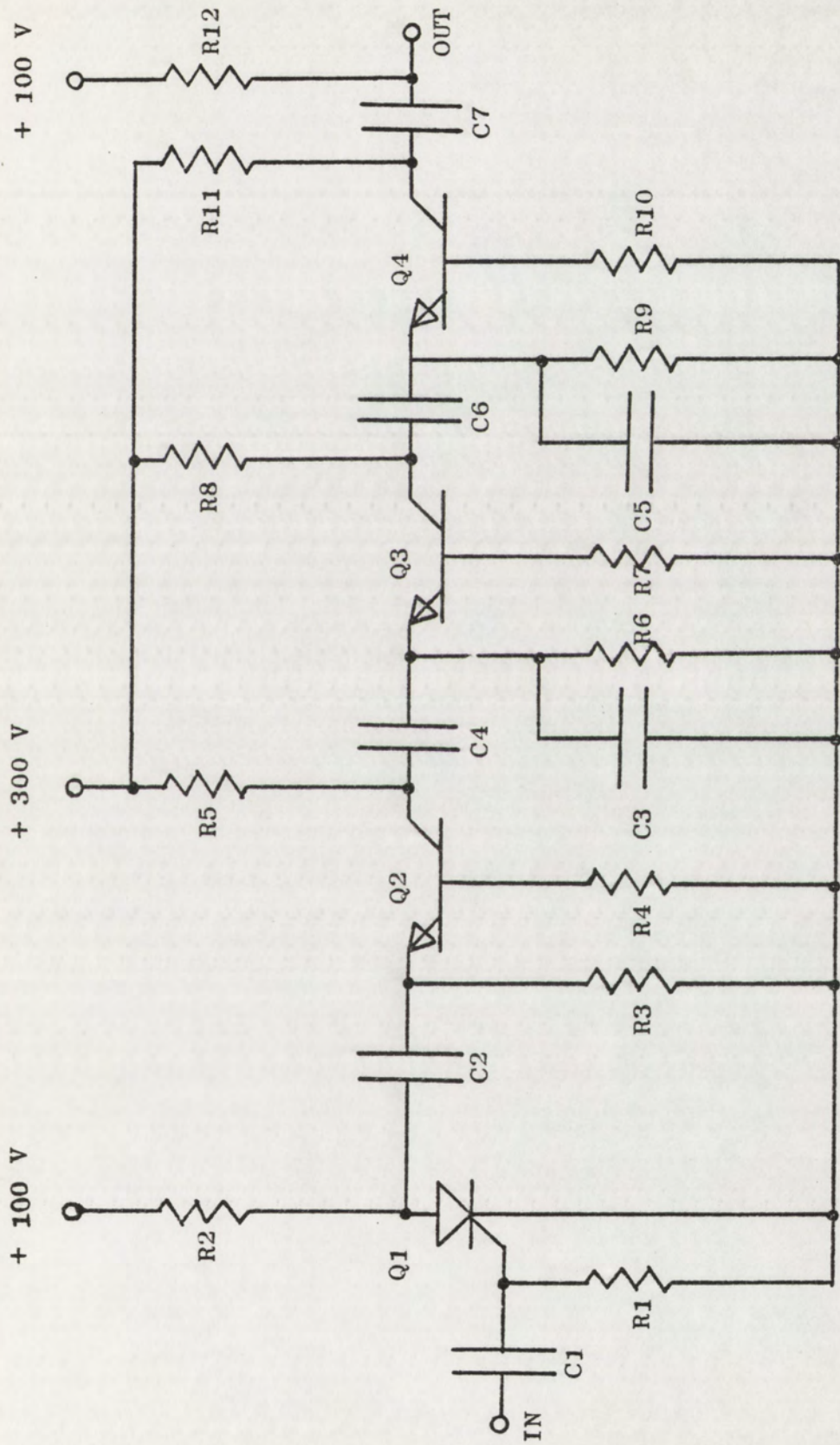
Figure 7. Avalanche Marx Generator

R1 - 100

R2, 5, 8, 11, 12 - 100 K

R3, 4, 6, 7, 9, 10 - 1000

C1   - 1nF

C2, 4, 6   - 3.3nF

C3, 5   - 33pF

Q1   - GA301

Q2, 3, 4 - MPS U04

Table 2. Parts list for Avalanche Marx Generator

CHAPTER III. DISCUSSION AND ANALYSIS

The goal of this research was to develop a better understanding
of the engineering requirements for rare-gas halogen lasers. This goal
was reached through a series of experiments and often by trial and error.
The basic approach was to build a laser and make modifications to
improve the energy output and reliability. This required the constru-
ction of three completely different lasers with numerous changes along
the way. These are referred to as 1) early Model, 2) 1.2 m Laser, 3)
0.6 m laser.

EARLY MODEL

The early model laser provided a means of getting started in rare-
gas excimer laser work and some encouragement. Under the best con-
ditions the laser output using KrF was 30 mJ per pulse at 1 Hz. The
electrode geometry and pre-ionization technique forced the discharge
into a volume of approximately 3 mm width. The corona pre-ionization
in the cathode seemed to be adequate to establish a multi-streamer
discharge. Unfortunately the pyrex and later quartz tubes housing the
trigger wires were quite fragile and broke on several occasions. No
provisions were made for gas exchange in the laser, and only a slow
longitudinal flow was possible. As a result the energy per pulse
decreased with increasing repetition rate until the lasing stopped near
70 Hz. Attempts at measuring voltage and current were not very success-
ful due to the lack of a screen room. It was not possible to increase
the pressure or the voltage in this laser beyond about 24 psia and 28

kVDC. The acrylic body developed fatal cracks after only a few days operation and brought to an end the early model. Meanwhile, Sze and Scott (1977) had been experimenting with a laser having a considerably longer active discharge volume, and were near 250 mJ per pulse with KrF.

1.2 m LASER

The 1.2 m laser was built similar to the one used by Sze and Scott, however several modifications were made. Sze and Scott were using 32 parallel cables for energy storage. These cables (YK-198) had a characteristic impedance of 16 ohms which resulted in a 0.5 ohm impedance PFN. The voltage rating on the cables was not adequate however, and they were replacing 3 or 4 cables per day. For my design I selected Essex 40/100 cable which has a nominal DC rating of 60 kV and has been used successfully at over 100 kV in pulsed applications. This cable has an impedance of 30.4 ohms (from an inductance of 188 nH per meter and a capacitance of 204 pF per meter) and 64 cables were required to produce a PFN impedance of less than 0.5 ohm.

The operation of this laser on a mixture of 0.2% F_2, 5% Kr, 10% Ar, 84.8% He resulted in energies of up to 215 mJ per pulse at a pressure of 32 psia and a voltage of 24 kVDC per stage on the two stage Marx generator. This energy was reached with external mirrors, as are all other energies reported (Sze and Scott used internal optics, which had a short life).

An aluminum coated pyrex flat having a magnesium fluoride overcoat was used for the rear total reflector, while the output coupler was an

uncoated quartz flat.[1] Other optical cavities were used in Raman scatt-
ering and air breakdown experiments as discussed elsewhere in this
paper.

As the system became passivated the energy from this laser grad-
ually increased to 254 mJ per pulse, using the original air insulated
Marx bank but the best gains were made after installation of the oil
insulated Marx generator.

The oil filled Marx generator permitted operation at voltages of up
to the power supply limit of approximately 45 kV resulting in an output
of 379 mJ/pulse at 32 psia which increased to 412 mJ/pulse at 38 psia.

In an attempt at more energy output, 20 ceramic capacitors of 2700
pF 40 kV rating were installed across the laser body in place of 20 of
the cables. This increased the energy output to 450 mJ/pulse at 40 psia
and 45 kVDC per stage on the Marx generator.

The laser was operated on ArF to see what output energy was avail-
able at the 193 nm wavelength. Using a mixture of 0.2% F_2, 10% Ar,
89.8% He the output was measured at 120 mJ per pulse. Three mixes were
tried to obtain lasing on KrCl at an expected wavelength of 222 nm.
These were 1) 1% Cl_2, 5% Kr, 10% Ar, 84% He; 2) 0.2% Cl_2, 5% Kr, 10% Ar,
84.8% He; 3) 0.2% Cl_2, 5% Kr, 1% Ne, 93.8% He. A dielectric mirror
cavity coated for 99% R and 87% R at 222 nm was used, but only strong
fluorescence was observed. The voltage was varied from 12-45 kV and the
pressures were varied between 12 and 44 psia.

---

[1]Aluminum mirrors purchased from Oriel have shown no tendency to
damage in this application, while similar mirrors purchased from NRC
were damaged in only a few pulses.

Pre-ionization inside the cathode was also tried with this laser. Since large screen electrodes are difficult to construct, electrodes having 32 screens of 12 mm diameter spaced along the center were used. An automotive spark plug was installed behind each screen. The spark plugs were inductively isolated and driven from the pre-ionization driver. The resulting main discharge consisted of 32 cylinders of 12 mm diameter along the length of the laser. The current was so well colli-mated that imprints of the screen were burned into the anode. Reversal of the polarity (pre-ionization in anode) produced in the same results. The laser output was very low using KrF. The same electrodes produced a normal discharge when the standard flashboard pre-ionization was used.

At this point the laser was committed to a series of experiments and became un-available for my research. Another identical laser was built, and installed in a lab with a screen room. Voltage and current measurements were taken for many different pressures, voltages and gas mixes. These data are best presented as graphs and tables.

Table 3 shows a list of various configurations used on this laser. In all cases the laser output produced a burn spot having dimensions of 4.75 mm x 19 mm. The assumed active volume based on these measurements and the 1.2 m electrode length is 0.108 liter. In the first five con-figurations the current was measured with a current probe (Rogowski loop) which was found to produce varying amplitudes depending on its position with respect to the surroundings. As a result no calculations involving current are presented for these 5 configurations. The re-maining data are calculated as explained in chapter 2-2.

CABLES	PRESSURE (psia)	VOLTAGE (kVDC)	POWER (GW)	POWER DENSITY (MW/cm^3)	ENERGY DEPOSITED (JOULES)	ENERGY DENSITY (J/cm^3)	EFFICIENCY (%)	ENERGY OUTPUT (mJ)
8-8.44m	42	30						50
20-2.44m	42	30						125
30-2.44m	42	30						175
38-2.44m	42	30						210
8-6.10m	42	30						50
16-6.10m	42	30	0.16	1.5	14.0	0.13	0.86	120
16-6.10m	42	40	0.22	2.1	17.0	0.16	0.88	150
16-2.44m	32	30	0.15	1.4	5.1	0.05	2.90	150
16-2.44m	42	40	0.18	1.7	6.3	0.06	3.4	215
32-2.44m	32	20	0.26	2.4	11.1	0.10	1.3	140
32-2.44m	32	30	0.41	3.8	15.4	0.14	1.1	175
32-2.44	42	20	0.34	3.1	14.8	0.14	1.2	175
32-2.44m	42	30	0.51	4.7	21.3	0.20	1.1	225
32-2.44m	42	40	0.65	6.1	26.7	0.25	0.86	230
32-2.44m	52	40						350

Table 3. Various Laser Configurations

Figure 8 shows a typical voltage, current and laser output wave-form. This data was taken with 16 - 6.1 m cables and a mixture of 0.15% F_2, 3.75% Kr, 20% Ne, 76.1% He at 42 psia. The charging voltage was 30 kVDC.

The same data are presented in Figure 9 after computer averaging to reduce the noise.

Figure 10 shows the calculated power, energy, and impedance as a function of time.

The current in Figure 9 can be approximated by

$$I(t) = Im [1-\exp(-(t-t_0)/\tau)] \tag{34}$$

as calculated from a least squares fit of the measured current over the period 83 nsec $\leq t \leq$ 150 nsec where $Im = 3.97 \times 10^4$ amperes, $t_0 = 82.4$ nsec, and $\tau = 45.6$ nsec. The measured current and the approximation are shown in Figure 11.

The power in the circuit can be found from

$$P = I^2R \tag{35}$$

Since the power over the interval 83 nsec $\leq t \leq$ 150 nsec is nearly a constant (2×10^8 watts) the resistance can be found from

$$R(t) = \frac{P}{I^2} = \frac{Pm}{Im^2[1-\exp(-(t-t_0)/\tau)]^2} \tag{36}$$

Figure 12 shows the calculated impedance and this approximation over the same time interval. Likewise the power can be expressed as

$$P = VI \tag{37}$$

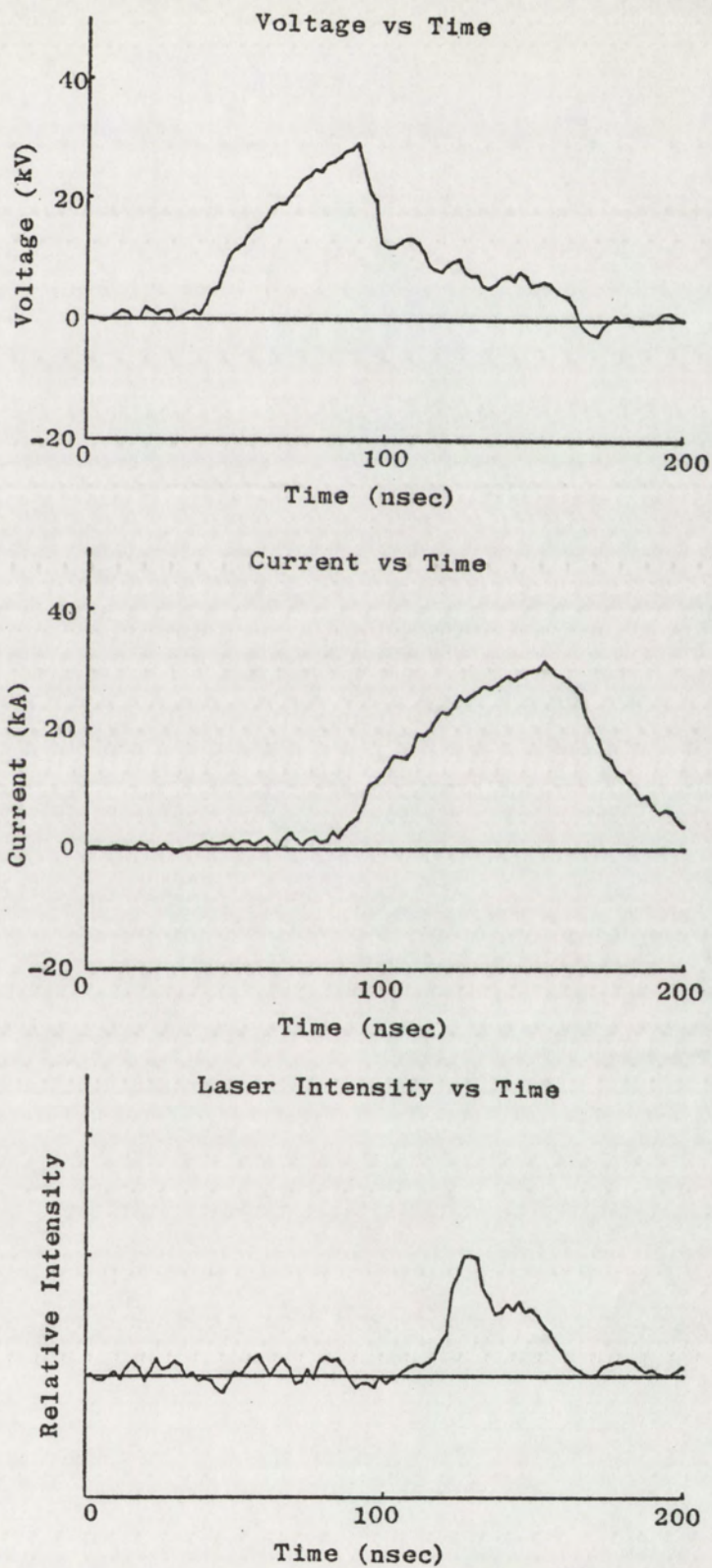which can be solved for the voltage
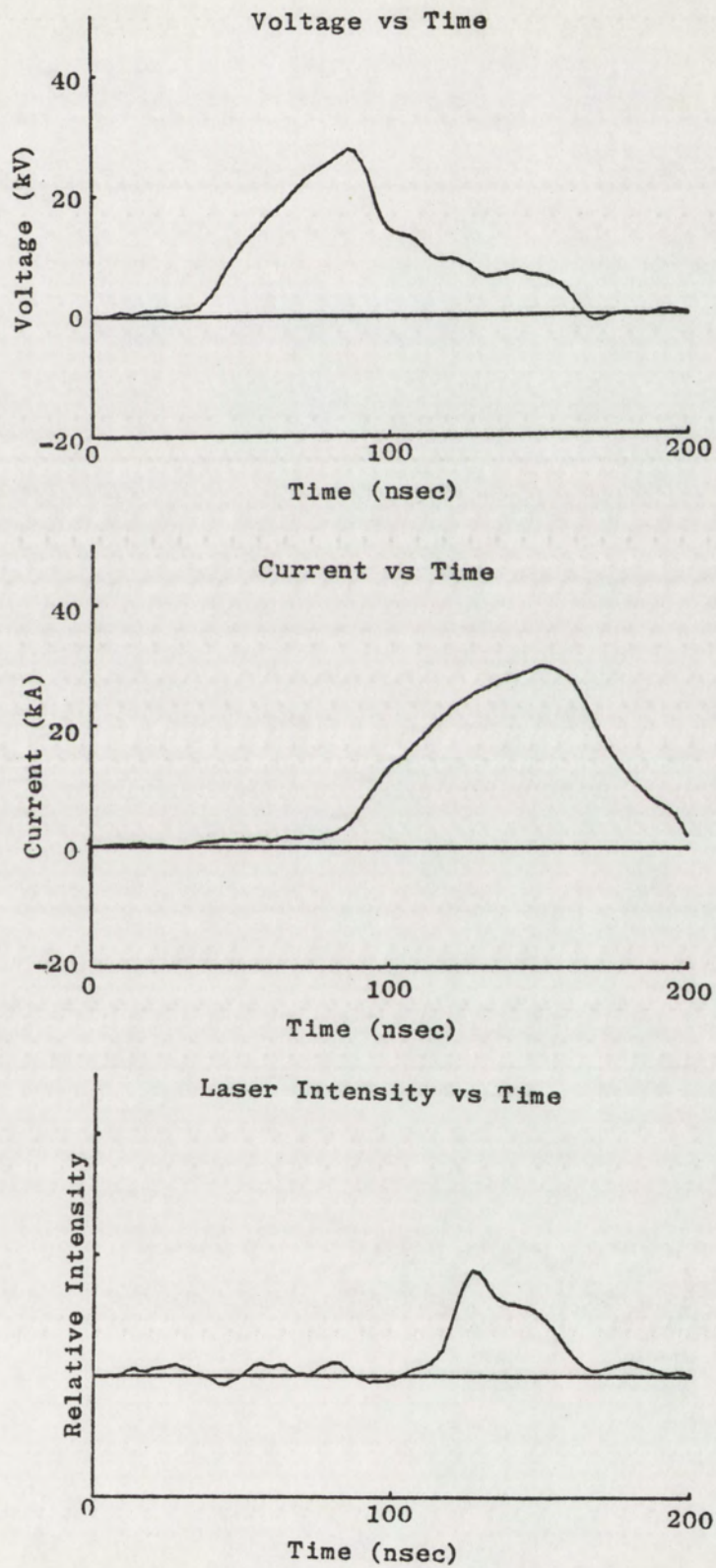
Figure 8. Raw Voltage, Current, and Laser Signal

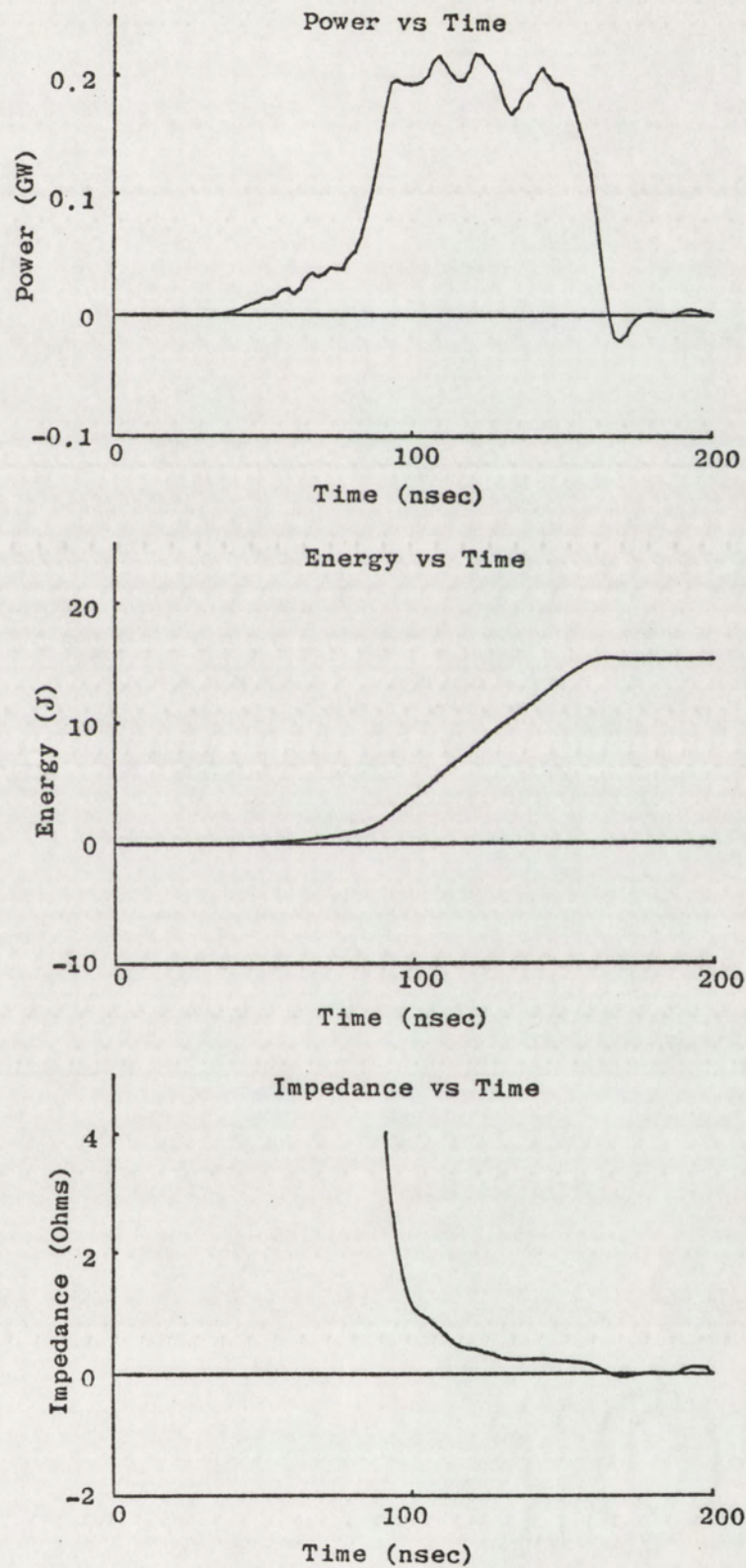Figure 9. Averaged Voltage, Current, and Laser Signal
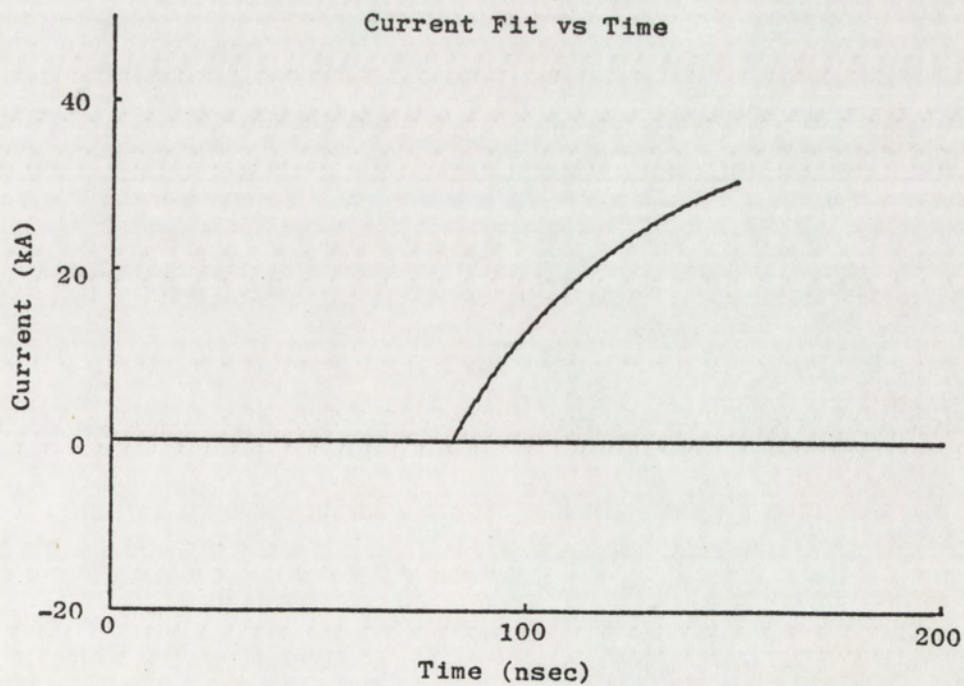
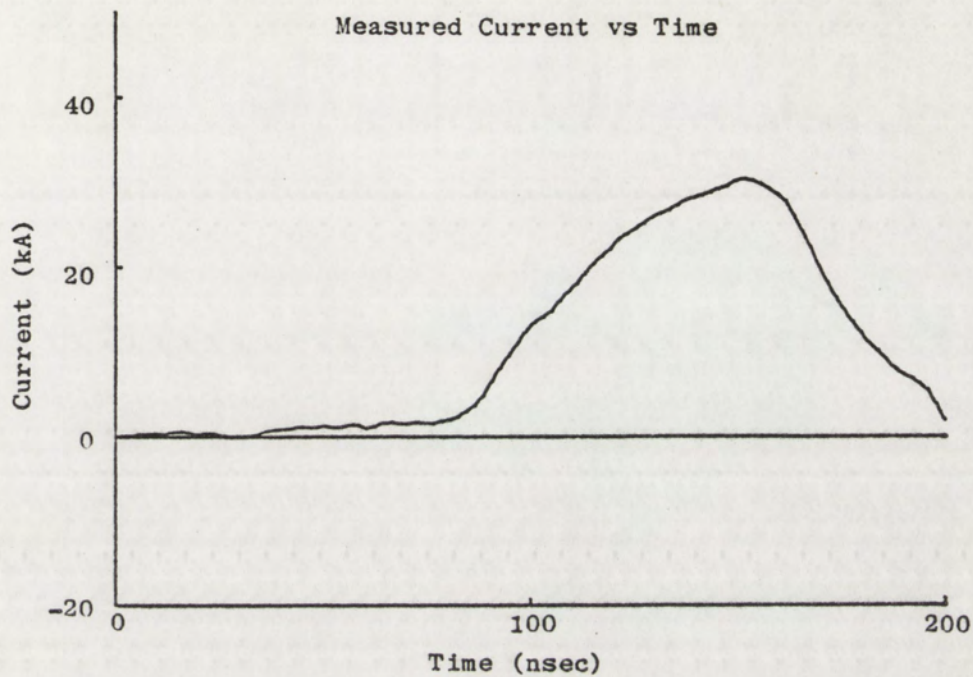Figure 10. Power, Energy, and Impedance

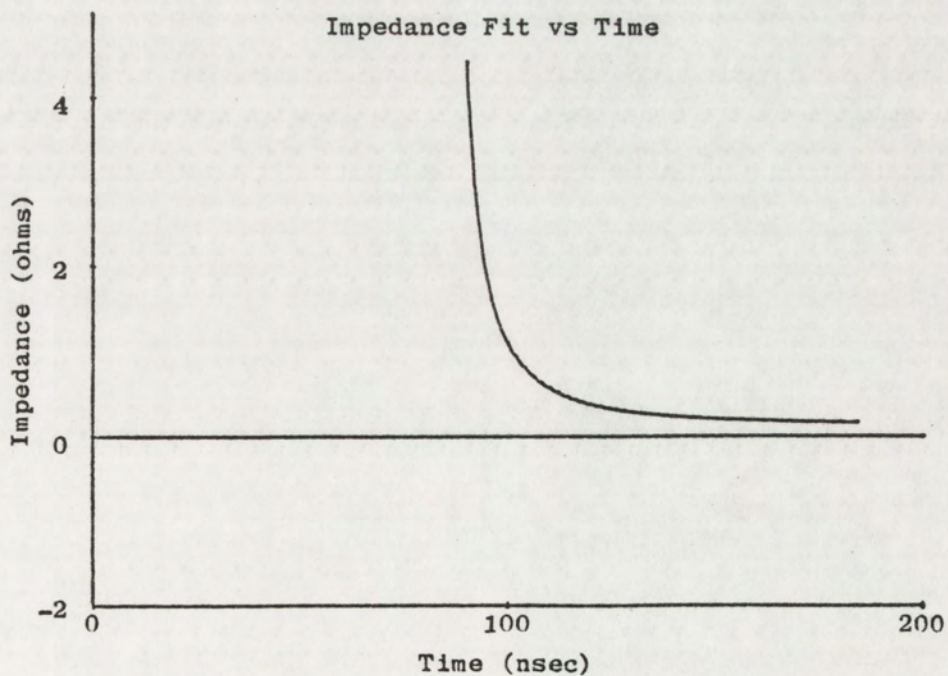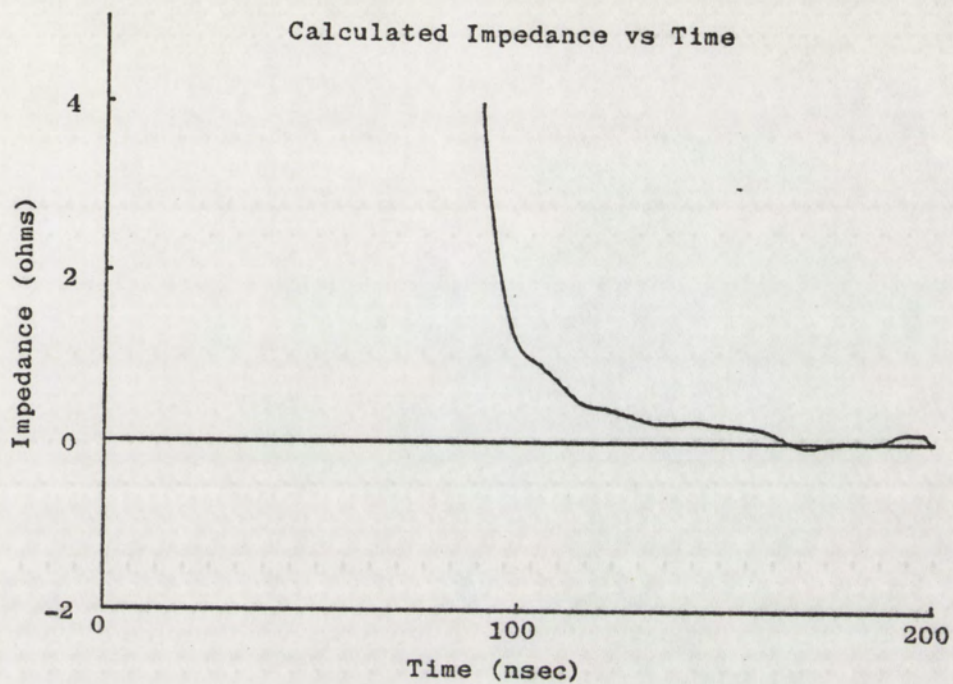Figure 11. Measured Current and Fit Expression

Figure 12. Calculated Impedance and Fit Expression

$$V = \frac{P}{I} \qquad (38)$$

Over the same interval the voltage can be approximated by the formula

$$V(t) = \frac{Pm}{Im[1-\exp(-t-t_o)/\tau)]} \qquad (39)$$

which is compared to the measured voltage in Figure 13.

It is worth noting that the laser pulse begins about 23 ns after the start of the current pulse and ends when the power pulse ends. Examination of the energy vs. time curve (Figure 10) shows very little if any energy returned to the system after the end of the positive power pulse. This implies that the inductance of the laser head was very low for this particular configuration. The energy returned was approximately 0.3 J which implies an inductance of 0.6 nH calculated from equation (6) since the current is 3×10^4 amps at the time of power reversal. This is abnormally low, and probably is the result of the relatively high impedance of the cable PFN damping out the inductive effect.

Voltage, current and laser pulse data are presented in Figure 14 for the case of 16 - 2.44 m cables with the same pressure and charging voltage. Figure 15 shows the calculated power, energy, and impedance for this case. The equations describing the current, voltage, and resistance over the interval 77 nsec $\leq$ t $\leq$ 108 nsec are the same as as the previous case (i.e. equations (34), (36), and (39)) with only the constants being different. The constants required for a fit are
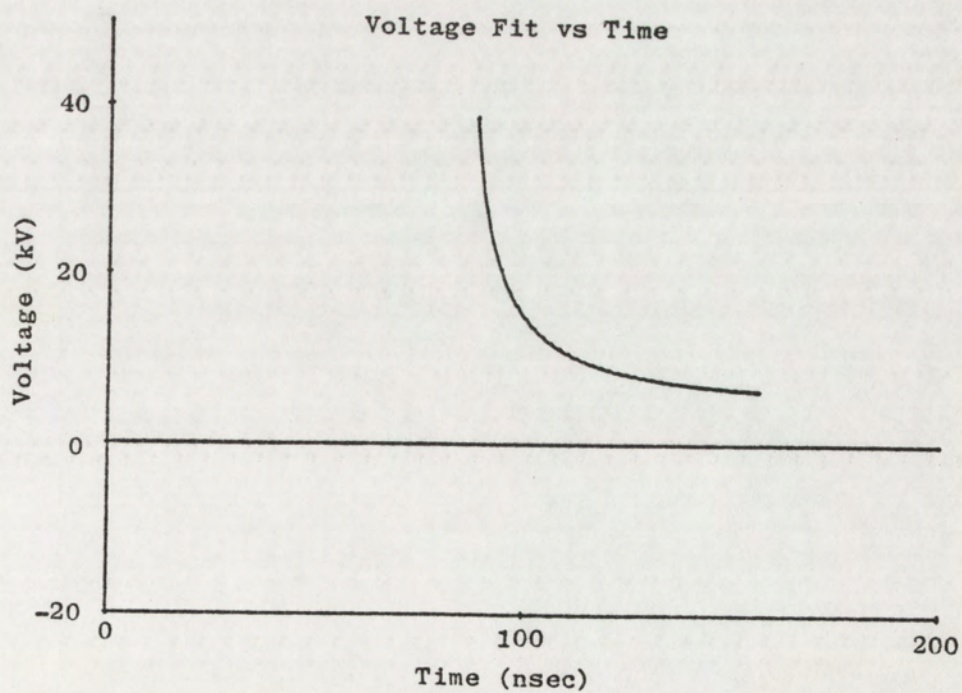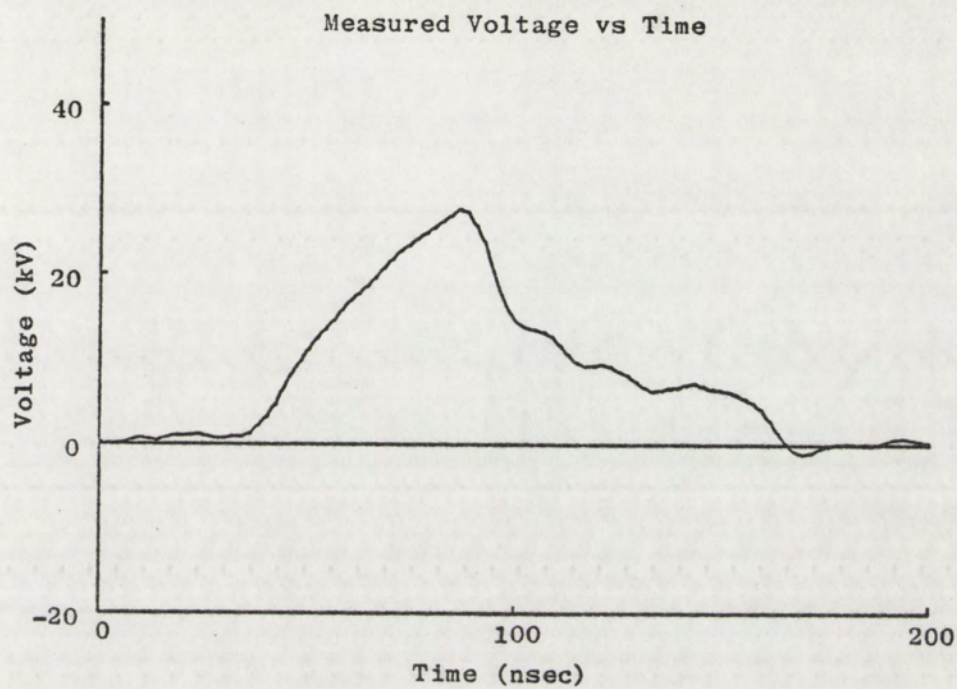
Measured Voltage vs Time

Voltage Fit vs Time
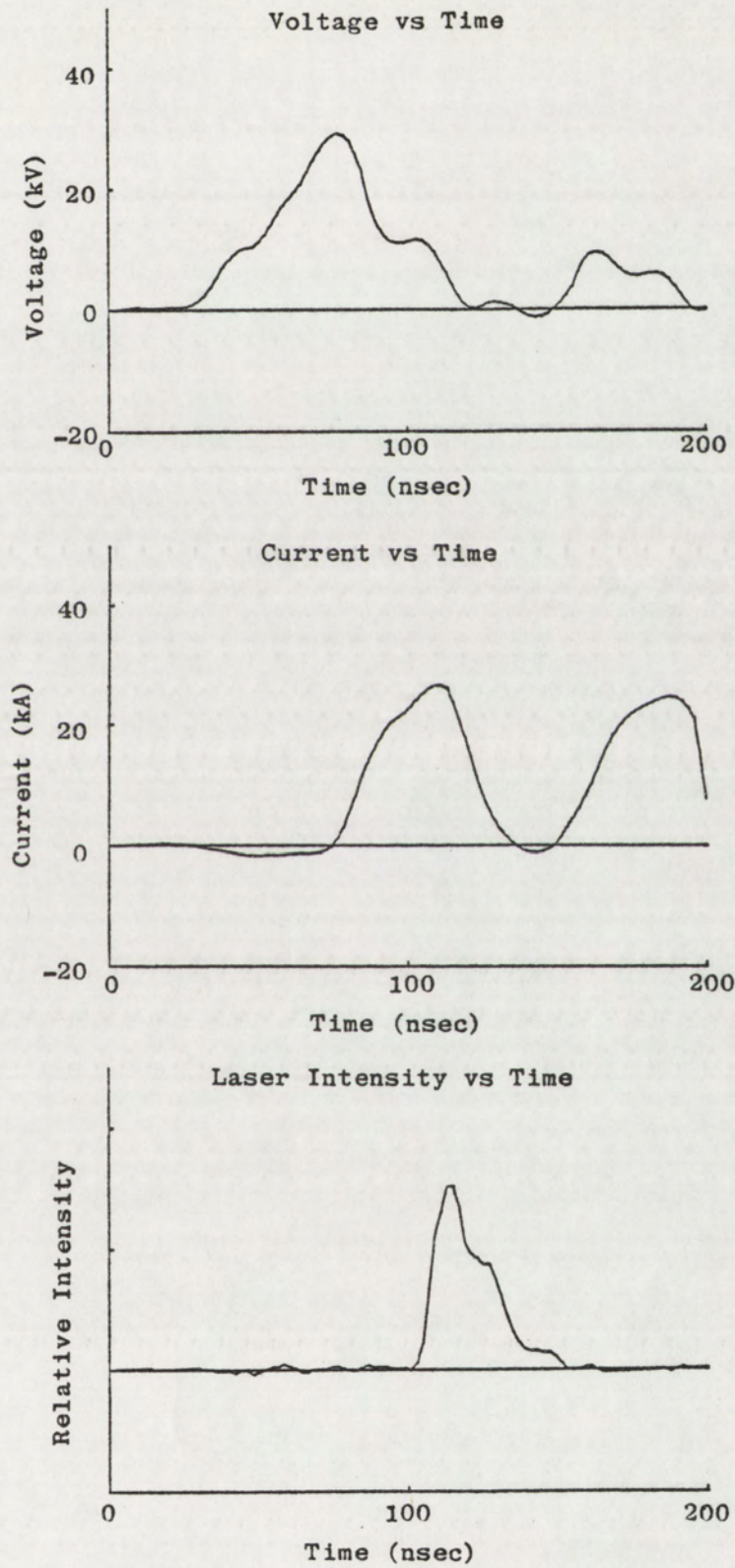

Figure 13. Measured Voltage and Fit Expression
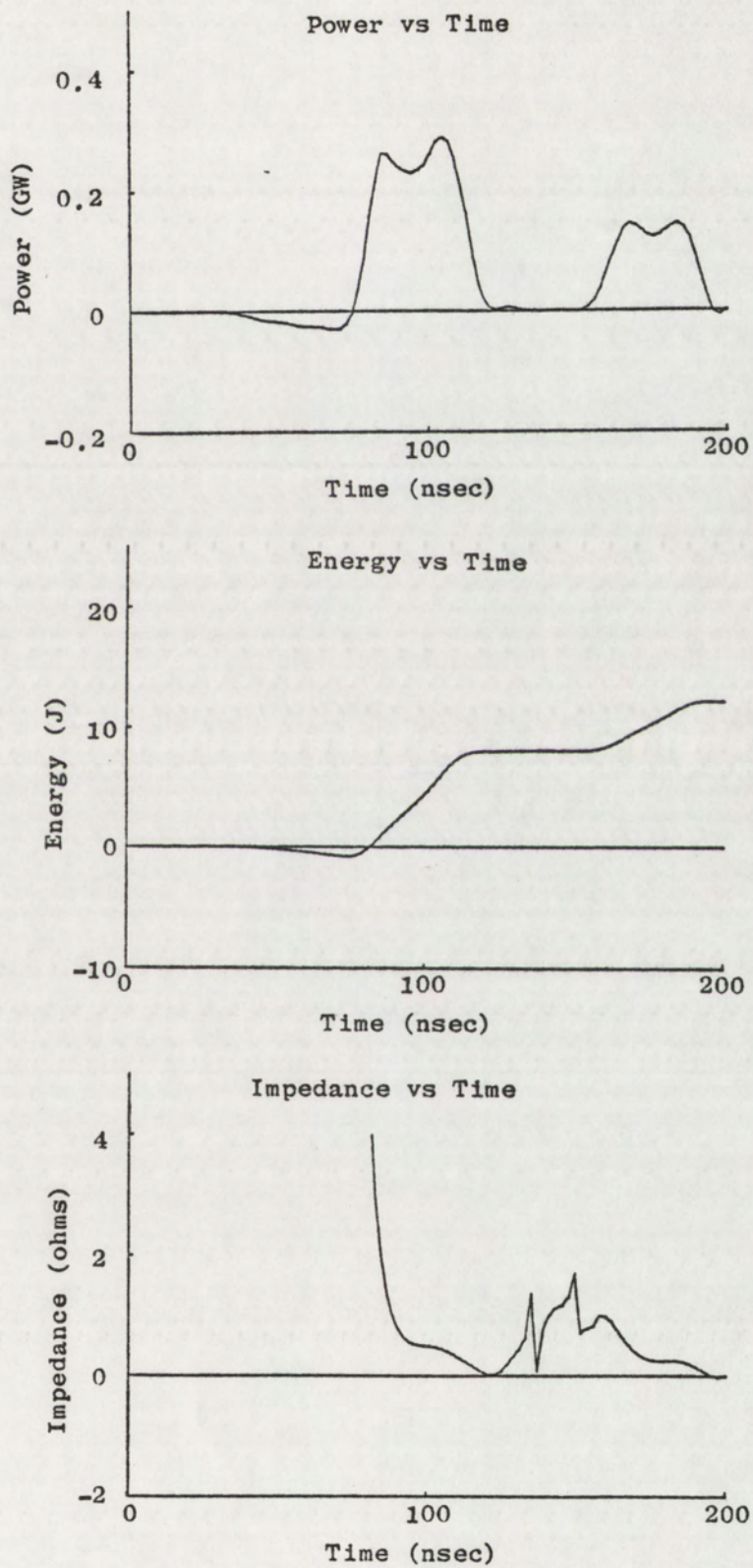
Figure 14. Voltage, Current, and Laser Signal

Figure 15. Power, Energy and Impedance

$Im = 3.77 \times 10^4$, $\tau = 26.1$ nsec, $t_o = 76.7$ nsec, and $Pm = 2.5 \times 10^8$ watts. The voltage on the PFN has a slightly faster risetime than the 6.1 m case, and rises to a higher voltage before the current starts (29.4 kV compared to 27.8 kV). The current pulse rises faster, but reaches a lower peak value (26.7 kA compared to 30.4 kA). The current pulse is considerably narrower in time for the shorter PFN (35.2 nsec FWHM compared to 69.6 nsec FWHM) which is to be expected. The faster risetime on the current pulse resulted in a peak power pulse of greater average magnitude (2.5 x 10^8 watts compared to 2 x 10^8 watts), but the shorter current duration resulted in a shorter power pulsewidth (34 nsec FWHM compared to 74 nsec FWHM). The energy deposited in the gas was less for the shorter PFN (8.6 J compared to 14 J). The laser pulse was of a shorter duration with the shorter PFN (20.8 nsec FWHM compared to 32.8 nsec FWHM) and continued after the end of the power pulse. In the case of the shorter PFN the laser pulse started about 27 nsec after the power pulse began and ended 31 nsec after the end of the power pulse. Perhaps the most surprising result is the energy contained in the laser pulses. The pulse from the shorter cable PFN contained more energy (180 mJ compared to 125 mJ). This results in some very interesting energy, power and efficiency data which are discussed later in this chapter.

An experiment was conducted to observe the effect of varying the number of cables in the PFN for this laser. The voltage and pressure were held constant at 30 kVDC and 42 psia (0.15% F_2, 3.75% Kr, 20% Ne, 76.1% He) and the laser output energy was measured for different numbers

of 2.44 m length cables. The results are presented in Figure 16. It appears that considerable gains could be realized by the addition of even more cables to the PFN. The curve is not linear, and the departure from linearity is probably due to the longer voltage risetime associated with the increased capacitance of additional cables.

0.6 m LASER

The 0.6 m laser was basically half of the 1.2 m laser, with a flashboard mounted on either side of the electrodes to provide more uniform pre-ionization. This combined with the Chang profile electrodes permitted an increased volume utilization and resulted in burn spots of 19 mm x 12 mm (compared to 19 mm x 4.75 mm in the 1.2 m laser) and an active volume of 0.138 liters for the 600 mm electrode length. Although the electrode length is only half that of the 1.2 m laser, the double flashboard and balanced cable PFN (equal number of cables on each side of laser head) allowed the discharge to fill the electrodes. This did not result in an energy increase over the single flashboard case however, as indicated in Table 4. The top two experiments were done at the same voltage and pressure with the same gas mix. In the first case one flashboard was simply disconnected, which resulted in 375 mJ output in an irregular shaped area of 193 mm^2. Connecting the second flashboard and repeating the measurement produced the same 375 mJ of energy, but over a nice rectangular area of 230 mm^2. A slight difference in the voltage and current waveforms produces a difference in the peak power pulse between these two configurations in the same ratio as the area. This leads to an interesting result discussed later.
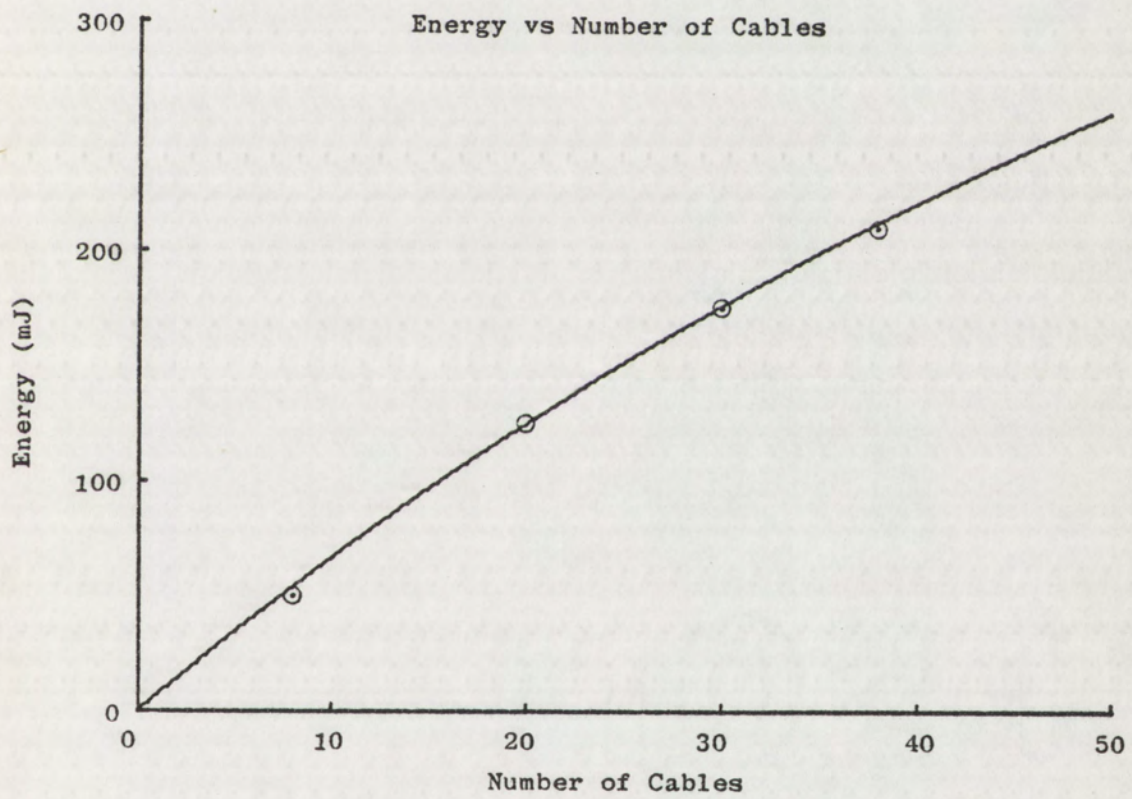
Figure 16.   Effect of Varying PFN

CABLES	PRESSURE (psia)	VOLTAGE (kVDC)	POWER (GW)	ENERGY DEPOSITED (JOULES)	EFFICIENCY (%)	BURN AREA (cm^2)	ACTIVE VOLUME (cm^3)	ENERGY OUTPUT (mJ)
48-2.44m	52	40	0.87	18.7	2.0	1.93	116	375
48-2.44m	52	40	1.0	28.3	1.3	2.3	138	375
48-2.44m	62	48	1.8	53.4	1.1	2.3	138	580
48-2.44m	62	48	1.6	50.0	0.88	2.3	138	440

Table 4. 0.6 m Laser Configurations

The time delay between the pre-ionization and the main discharge was varied using the 0.6 m laser for two different gas mixes. Figure 17 shows the pre-ionizer fluorescence signal vs time, the normalized laser amplitude from a mixture of ArF gas (0.2% F_2, 10% Ar, 89.8% He) at 52 psia and the normalized laser amplitude from a mixture of KrF gas (0.12% F_2, 3% Kr, 20% Ne, 86.88% He) at 52 psia. The abscissa in the laser signals is delay after pre-ionization begins, plotted on the same time scale as the pre-ionizer fluorescence. Note that the time delay is much more critical for the ArF mixture than for the KrF mixture. The error bars represent pulse to pulse variations, which were quite pronounced in the ArF mix for all but two values of delay, corresponding to the first two maxima of the fluorescent signal. The pre-ionizer voltage was also varied from 15 kV to 30 kV, with no measurable effect on either gas mix. The maximum laser output in either case occurs at the first maxima of the pre-ionizer.

In order to exceed the performance of the 1.2 m laser, the 0.6 m laser was operated on a KrF mixture (0.095% F_2, 1.71% Kr, 98.195% He) at 62 psia. The voltage on the Marx bank was increased to the power supply limit of 48 kV. The resulting voltage and current waveforms are shown in Figure 18. The current fits the form of equation (34) over the interval 125 nsec $\leq$ t $\leq$ 157 nsec. The parameters required for a fit are Im = 1.3 x 10^5, t_o = 120 nsec, and τ = 39.3 nsec. Using a constant power, P_m = 1.59 x 10^9 watts, which is the average of the resistive power over the interval results in a fit to the voltage and resistance of the form of equations (39) and (36). The laser was connected with
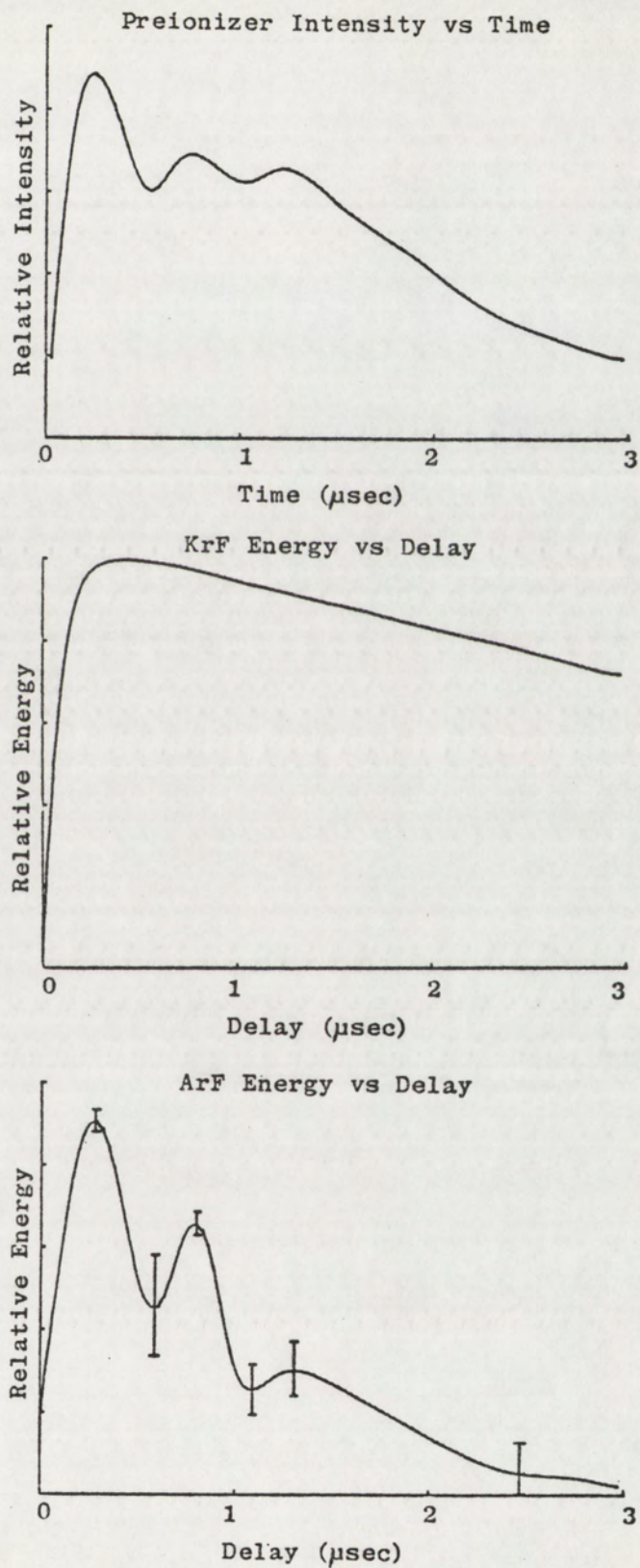
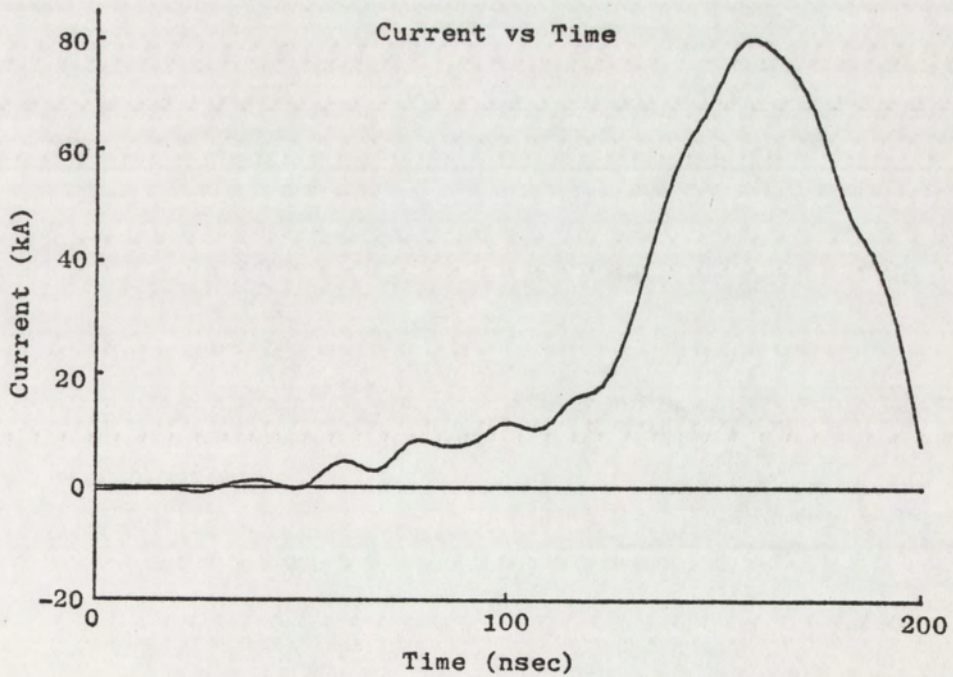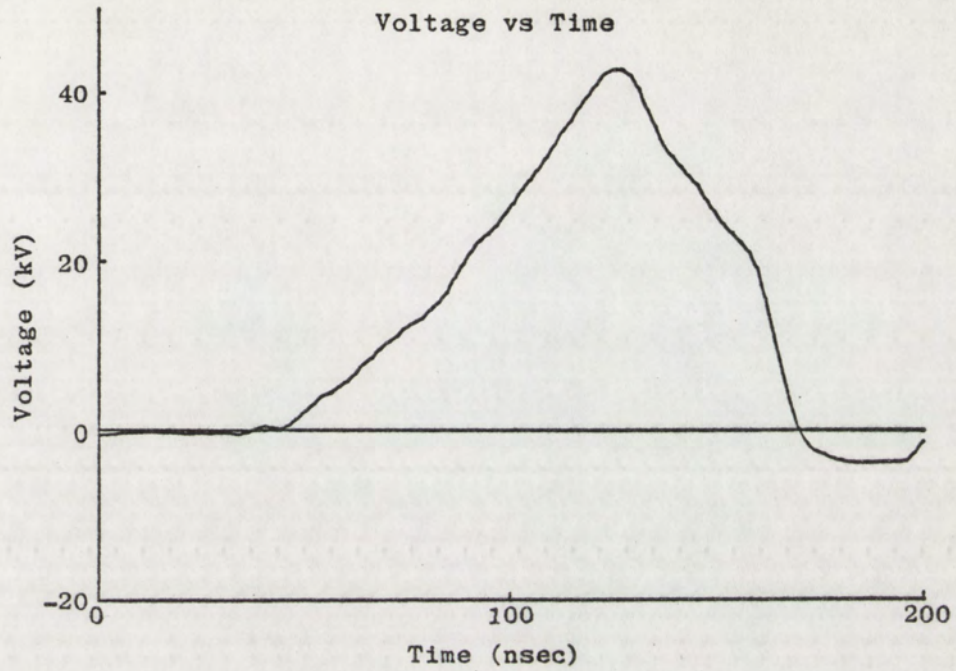Figure 17. Effect of Varying Time Delay

Figure 18. Voltage and Current

38 - 2.44 m cables between the Marx bank and the laser head, plus 5

more peaking cables of 4.88 m length connected at both ends to the

laser head. This provides an effective PFN of 48 cables, as far as

the discharge is concerned, however during the charging cycle current

is drawn through the CVR by the 5 peaking cables. This is the current

seen in the waveform of Figure 18 during the interval $0 \leq t \leq 125$ nsec,

which results in an apparent power and energy deposition before

actual gas breakdown, as seen in Figure 19. This effect is taken

into account in calculations of energy deposited and efficiency.

The impedance of the gas decreases with time and appears to

become negative during the power reversal. This negative impedance

is explained by the inductance of the discharge circuit which is

calculated from the energy returned to the system (about 4 J) using

equation (6) to be 2 nH. This inductance was used in conjunction

with the time rate of change of current shown in Figure 20 to calculate

the resistive component of the voltage, which is compared to the

measured voltage. The resistive voltage is slightly lower than the

measured voltage, and does not reverse to any extent. The resulting

resistive component of the power is compared to the calculated power

in Figure 21. The amplitude is somewhat lower, and very little

negative power is observed, as should be the case for real power.

Comparison of the energy deposited in Figure 22 shows no energy

returned to the circuit as expected. Figure 23 shows a comparison of

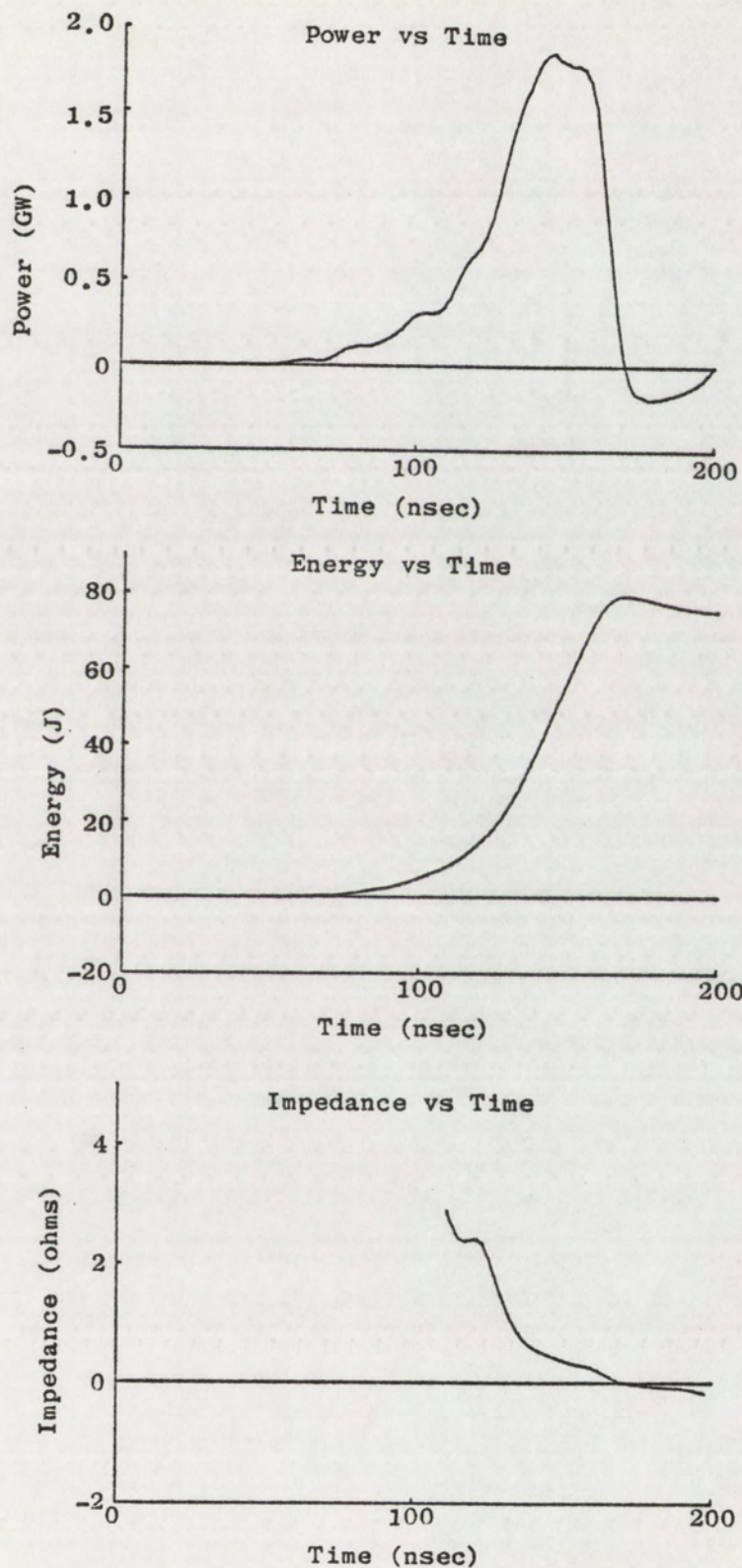the impedance and resistance of the gas during the discharge. The
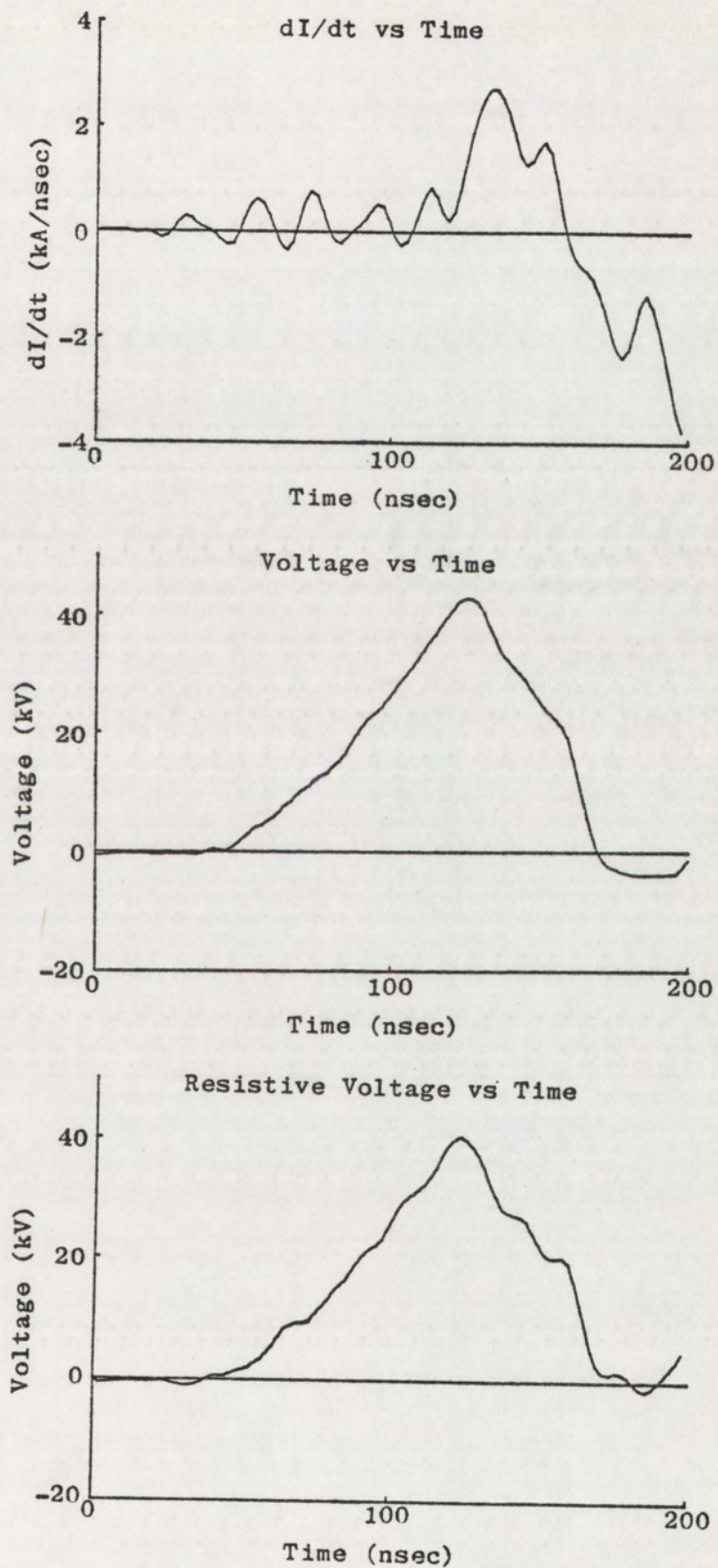
Figure 19. Power, Energy, and Impedance
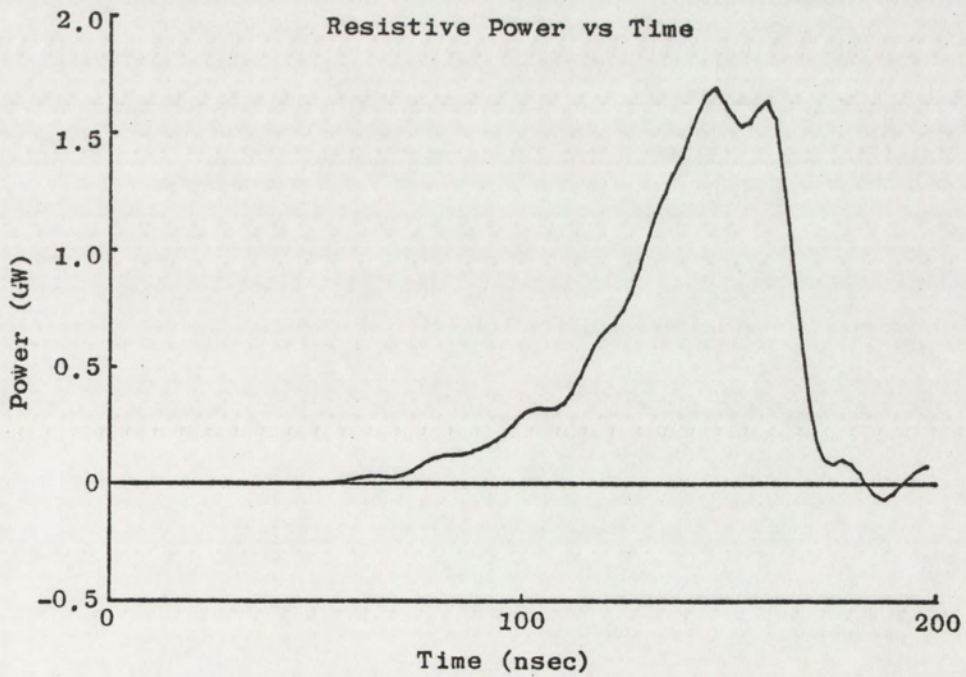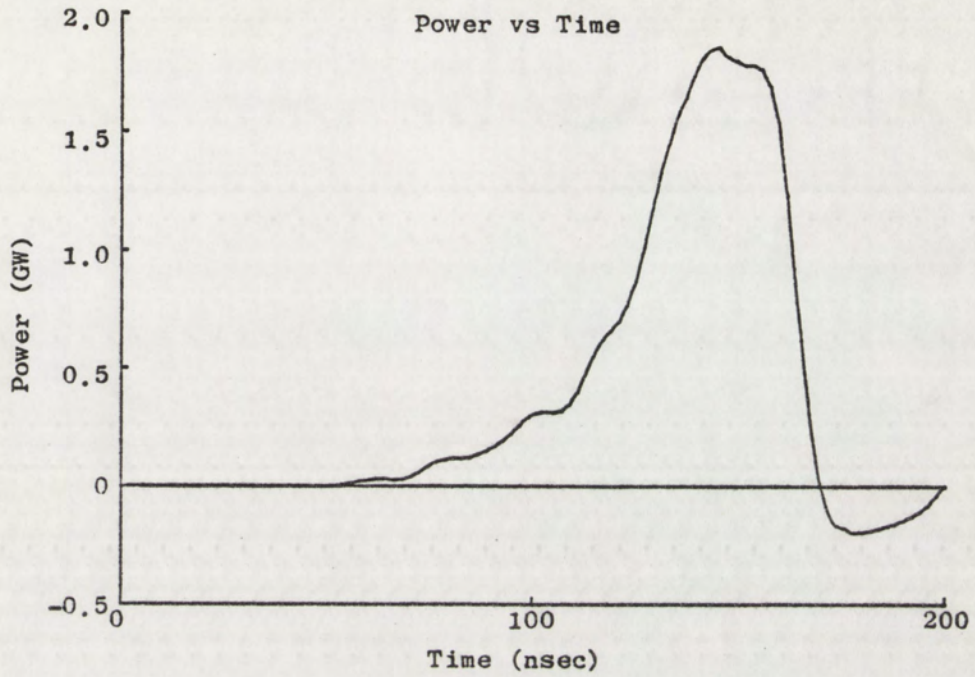
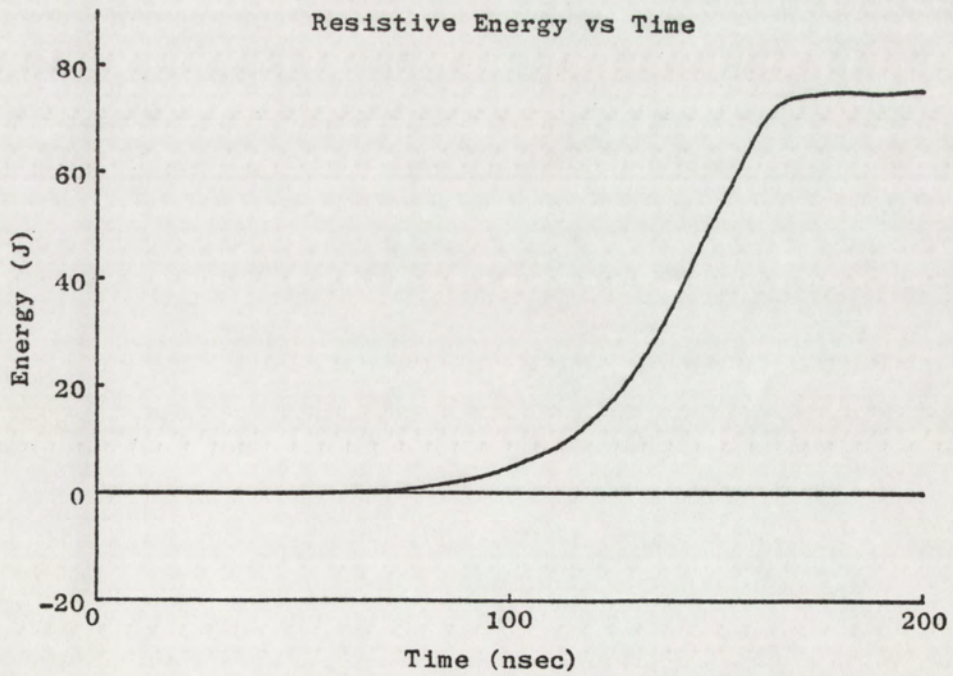Figure 20. Inductive Effects on Voltage

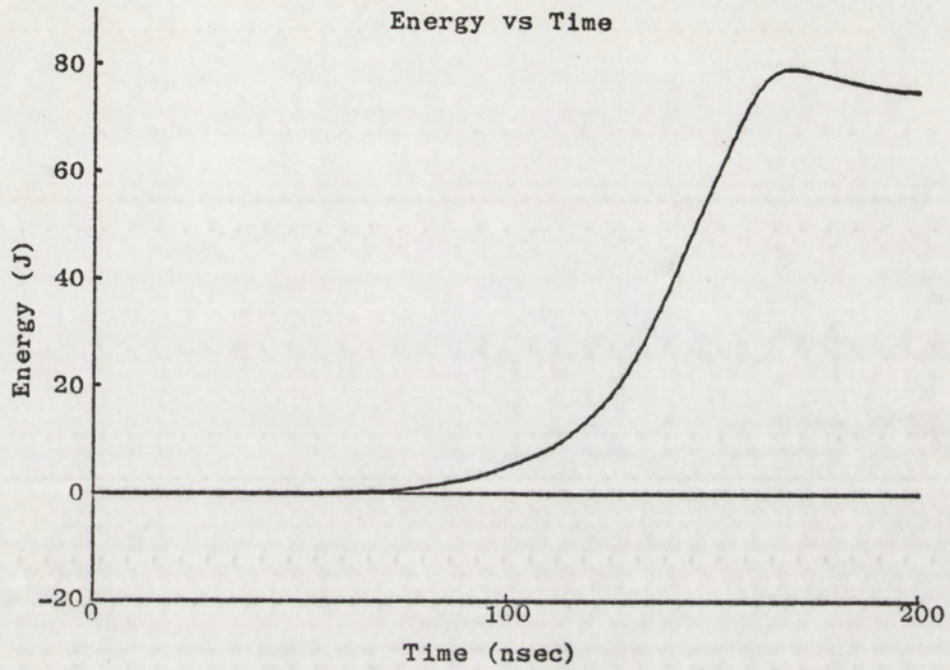Figure 21.   Inductive Effects on Power
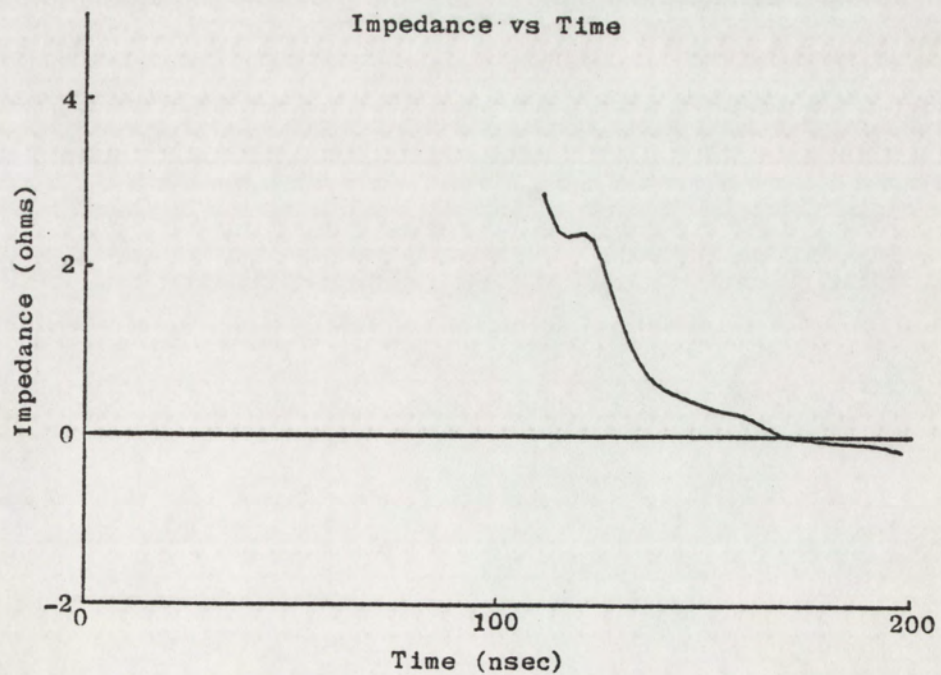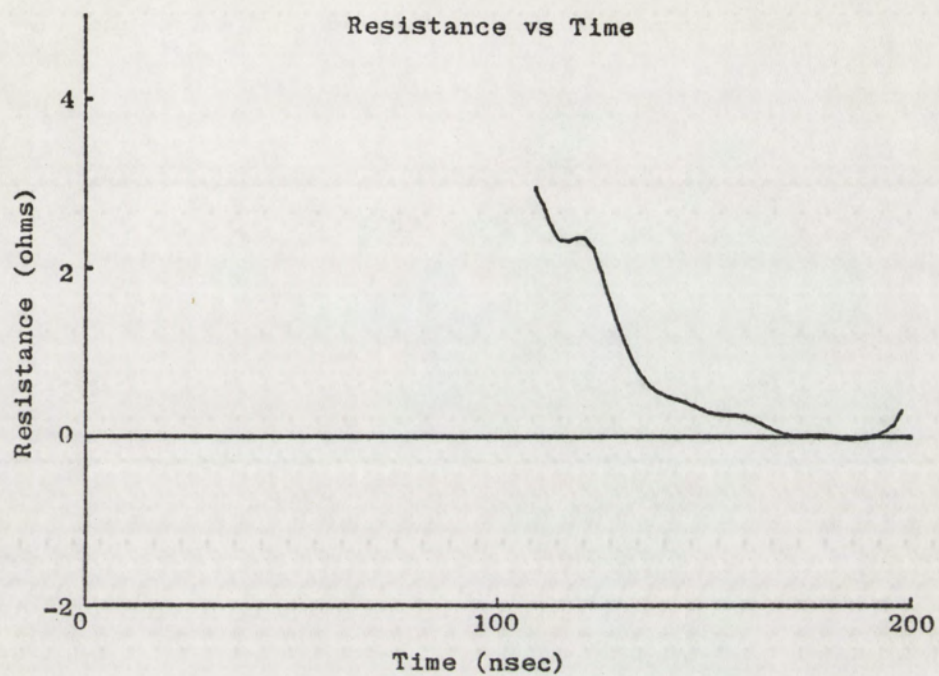
Figure 22. Inductive Effects on Energy

Figure 23. Comparison of Resistance and Impedance

only apparent difference is the resistance remaining positive while
the impedance goes slightly negative late in the discharge. The
resistance appears to drop to zero at about t = 172 nsec, indicative
of an arc. The value of resistance predicted by equation (36) with
the added drop to zero at t = 172 nsec was used in a computer simulation
of the circuit. The other parameters used were 96 kV charging voltage
(the dc voltage of the Marx generator into an infinite impedance
load), 2 nH load inductance, 360 nH driver inductance, 75 nF driver
capacitance (the equivalent series capacitance of the Marx generator),
38 series cables and 5 longer peaking cables in the PFN, and switch
closures between the driver and cables timed to start the voltage
waveform at t = 42 nsec (the point of measured voltage inflection).
The load resistance was assumed to be infinite for all time less than
t = 120 nsec.

The resulting simulated voltage is compared to the measured
value in Figure 24. The agreement is remarkable, with only very
slight deviations over the entire pulse width.

The predicted current pulse is compared to the measured current
in Figure 25. Again the agreement is very good, with deviations
during the cable charging interval, a slight difference in amplitude,
and a slight difference in overall width. The simulated current
amplitude was multiplied by 48/38 to account for the difference
between the current measured flowing in only 38 cables, while the
discharge current flows in all 48 cables. (A similar correction was
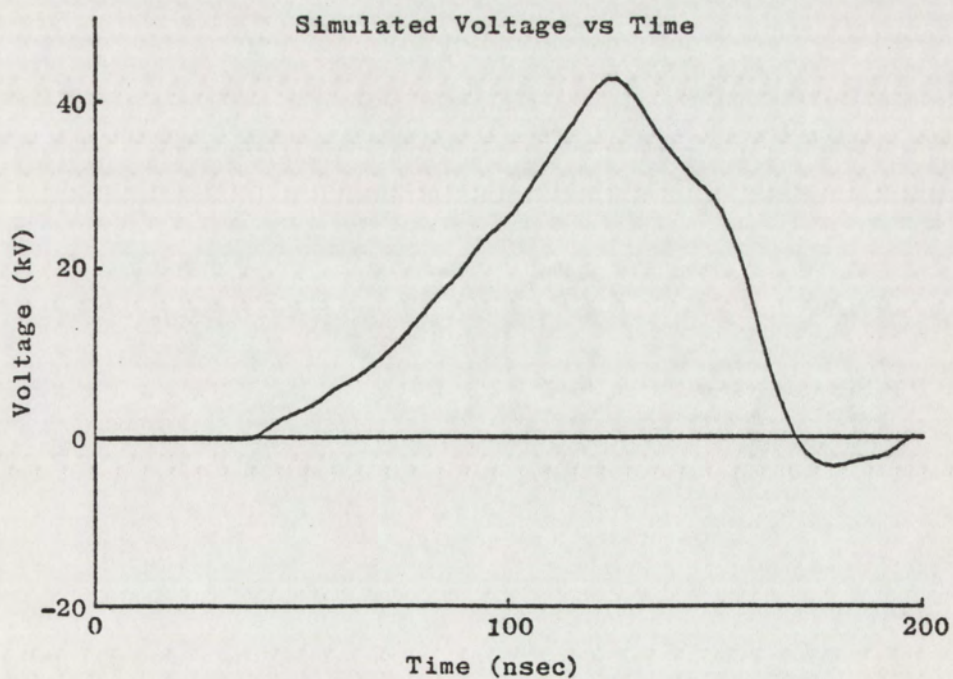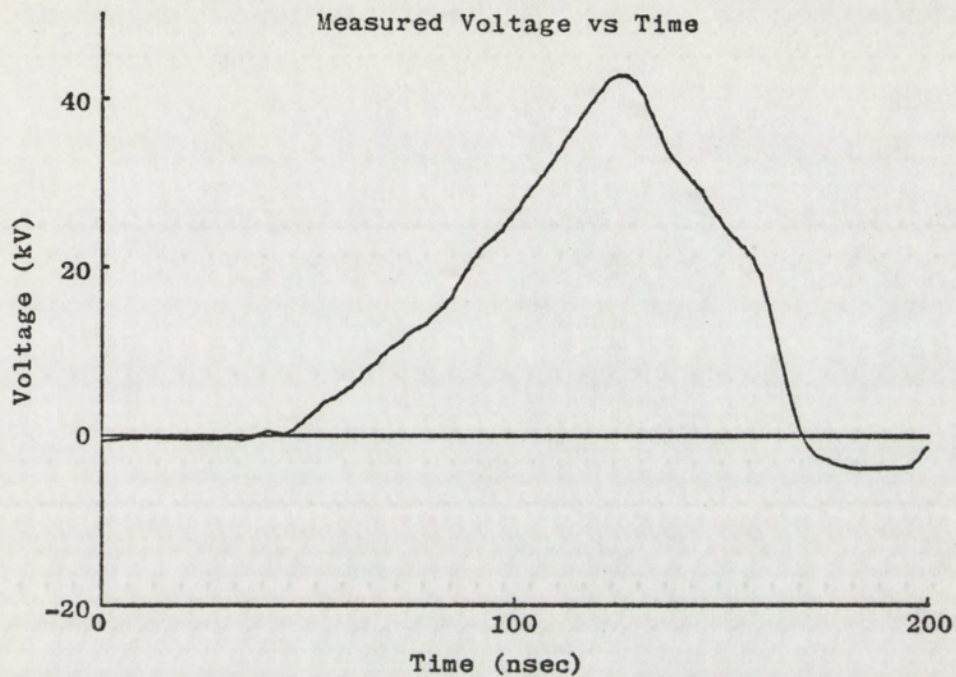done in the actual circuit, since the measured current only flows in

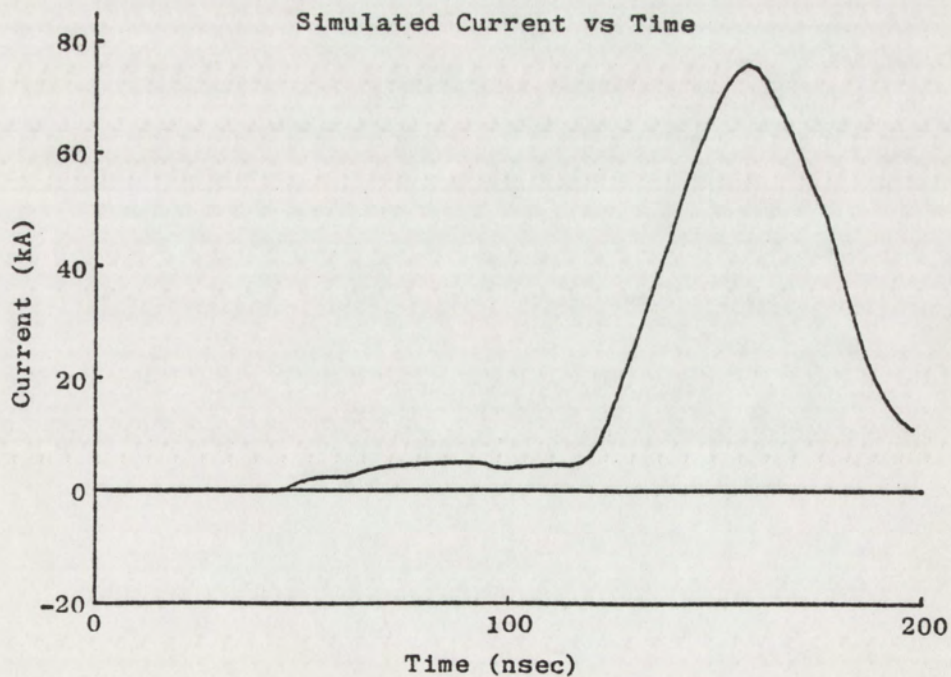Figure 24. Comparison of Measured and Simulated Voltage
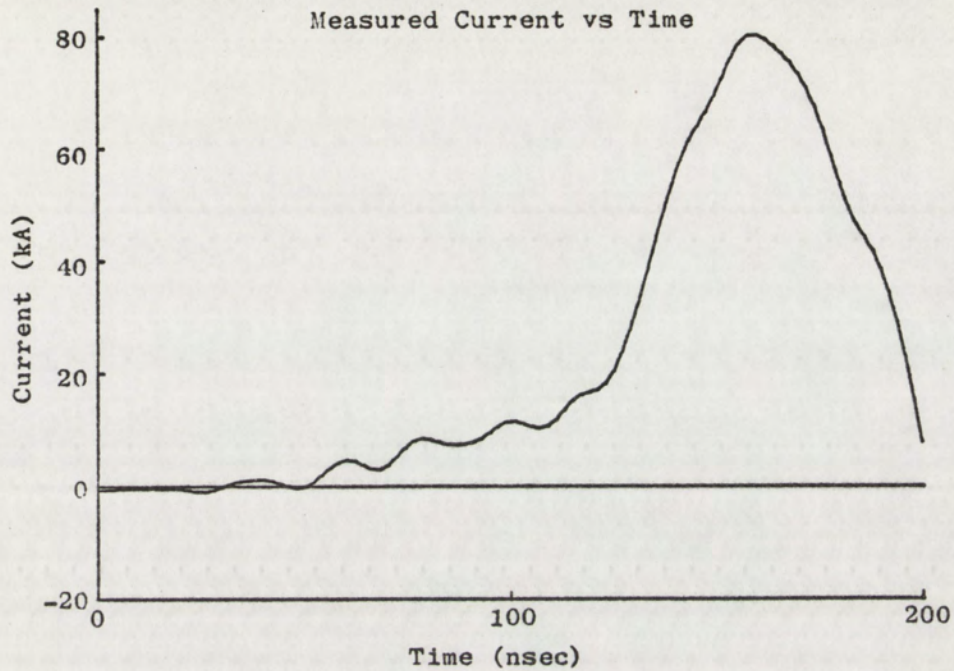
Figure 25. Comparison of Measured and Simulated Current

one of the 38 cables).

Since the current was not actually measured in the main dis-
charge, there was some question as to the validity of the current
measurement. Figure 26 shows a comparison of the computer simulated
current in the load resistor and the current at the point the measure-
ments were taken in the laser. There is a slight difference in
amplitude and of course the charging current for the additional 5
cables doesn't flow through the load. If anything, it appears the
measured values of current may be a bit larger than the actual discharge
current.

Probably the best test of the data is a comparison of the
simulated power and the calculated power as shown in Figure 27. The
amplitudes are in very close agreement, and the width of the pulses
is only slightly different. It appears the data is self consistent,
and the resistance approximation is reasonable.

The voltage and current fit expressions discussed in this section
have so far been presented with no justification for the equations.
Since the laser operates much like a spark gap it seems reasonable to
treat the voltage-current characteristics in a similar manner. J. C.
Martin (1970) presents a formula for the resistive phase time constant
of a spark gap

$$T_R = \frac{88}{Z^{1/3} E^{4/3}} \left(\frac{\rho}{\rho_o}\right)^{\frac{1}{2}} \tag{40}$$

where the time is in nanoseconds, Z is the impedance of the PFN in ohms,
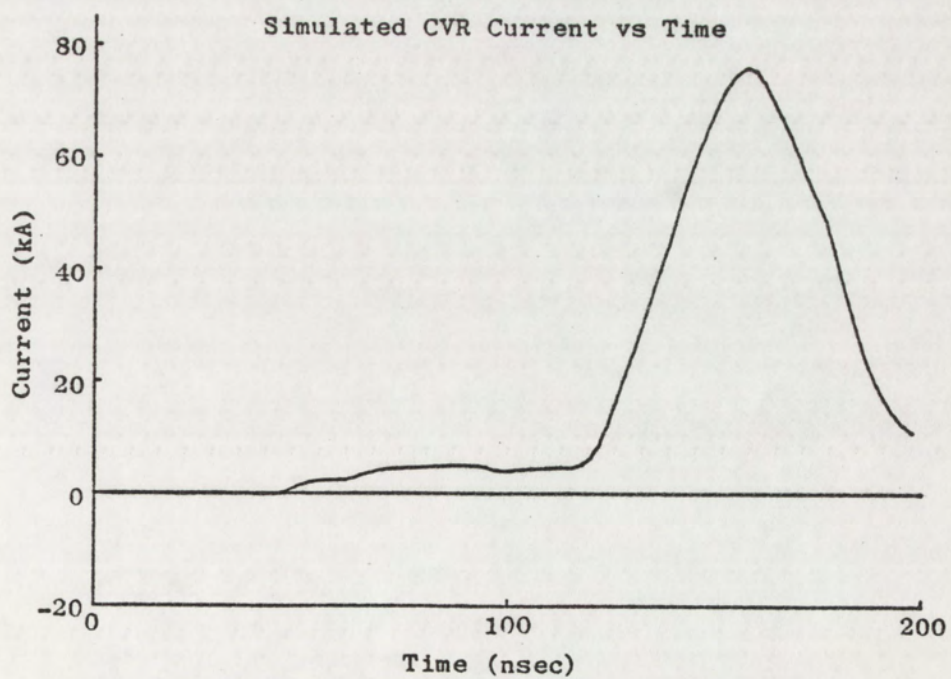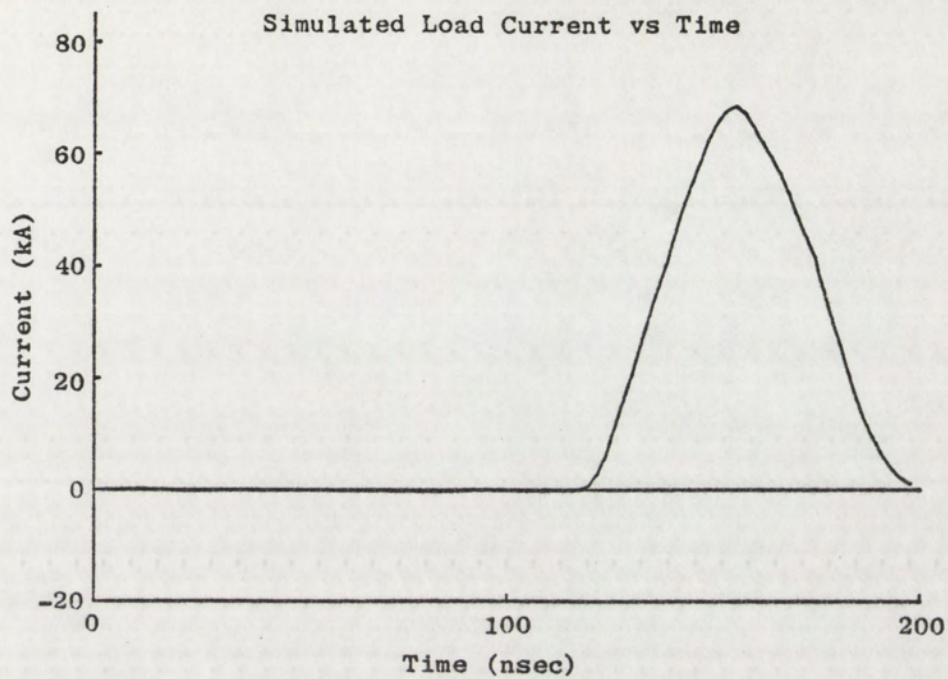
Figure 26. Comparison of Load Current and CVR Current
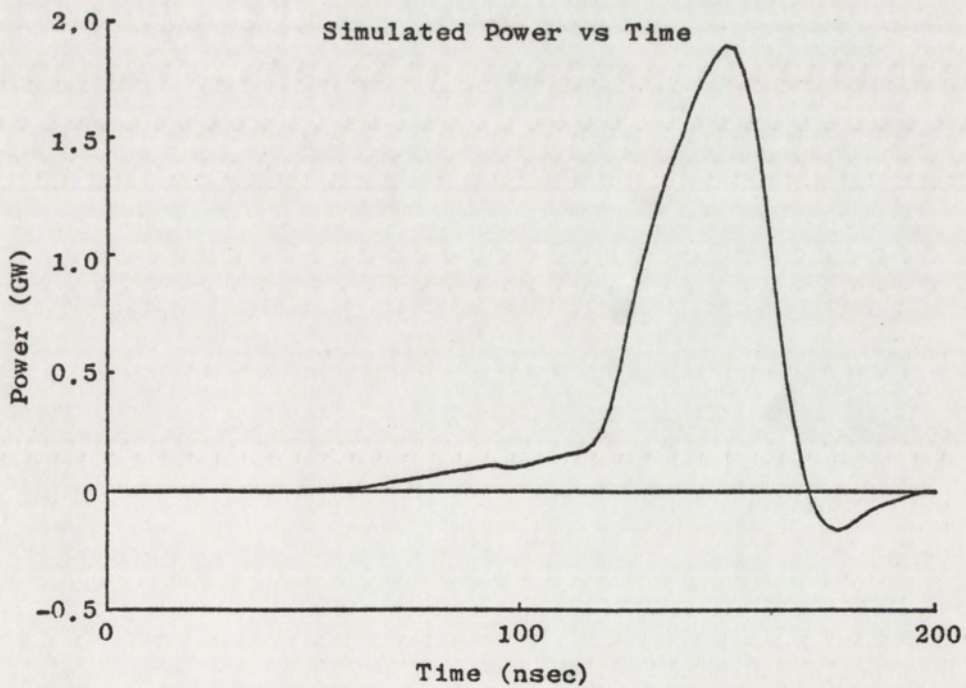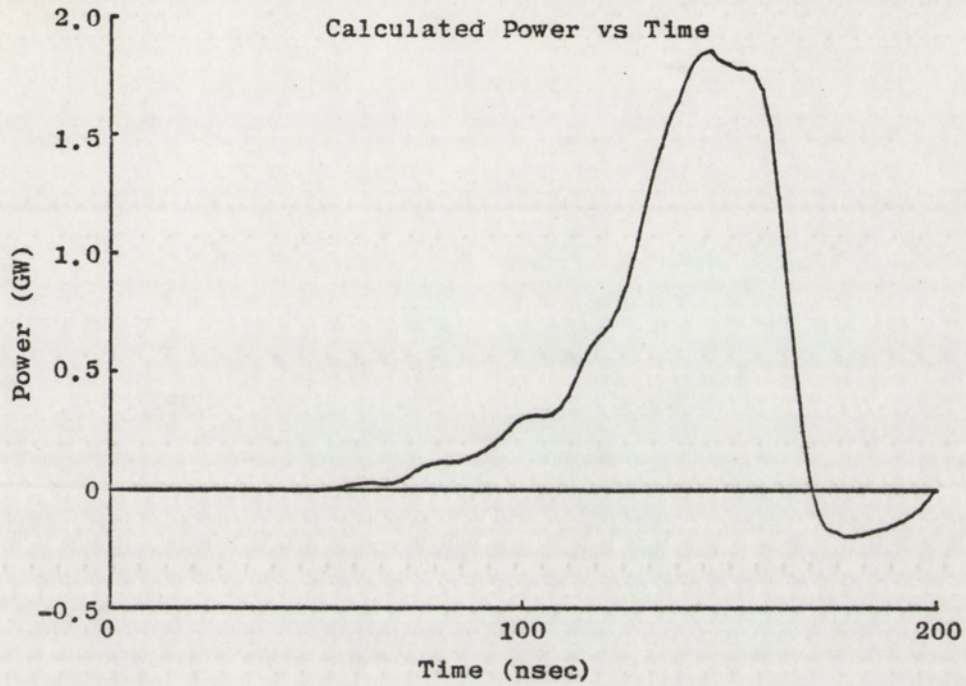
Figure 27. Comparison of Calculated and Simulated Power

E is the electric field in MV/m, ρ is the density of the gas used, and ρ_o is the density of air at NTP. This time constant can be treated like an inductive time constant and used to calculate a resistive phase inductance

$$L_R = \tau_R \, Z \tag{41}$$

To find the total effective circuit inductance the fixed inductance of the unit (L) is added in quadrature to the resistive phase contribution

$$L_{eff} = \left(L^2 + L_R{}^2\right)^{\frac{1}{2}} \tag{42}$$

Since the components of inductance add in quadrature, the fixed inductance (L) will have negligible effects on the current pulse whenever the resistive phase inductance (L_R) is appreciably larger. This is the case for most of the systems studied to date.

Assuming $L_R \gg L$ the equation for load current is

$$I(t) = Im \, [1 - \exp \, (-t/\tau_R)] \tag{43}$$

which has the same form as equation (34). The value of maximum current available from a transmission line is

$$Im = \frac{V_{BD}}{Z_o} + I_s \tag{44}$$

where V_{BD} is the breakdown voltage of the gas, Z_o is the characteristic impedance of the line, and I_s is the charging current flowing from the cable driver

$$I_s = C_c \, \frac{dv}{dt} \tag{45}$$

found from equations (15) and (23).

The voltage across the load is expressed by

$$(V(t) = V_{BD} \exp (-t/\tau_R) \tag{46}$$

from which the impedance of the load can be found by

$$R(t) = \frac{V(t)}{I(t)} = \frac{V_{BD}}{Im} \frac{\exp (-t/\tau)}{[1 - \exp(-t/\tau)]} \tag{47}$$

These equations for voltage and current are only a slightly different form from equations (36) and (39) presented earlier.

From equations (43) and (46) the power can be expressed by

$$P (t) = V_{BD}Im \exp(-t/\tau_R)[1-\exp(-t/\tau_R)] \tag{48}$$

which reaches a maximum when t/τ_R is $\ln 2$. For maximum power transfer the resistive phase of the gas should be large compared to the fixed inductive time constant and short enough to reach maximum power. This can be expressed

$$\frac{L}{Z_o} < \tau_R < \frac{T}{\ln_2} \tag{49}$$

where T is twice the electrical length of the PFN.

These equations were tested by a comparison to the results previously obtained with the 48 - 2.44 m cable laser operating at 62 psia with a gas mixture of 0.095% F_2, 1.71% Kr, 98.195% He. The density ratio of this gas to air (ρ/ρ_o) is 0.834, the impedance of the PFN is 0.633 ohms, the electric field is 2.1277 M v/M (from a breakdown voltage of 42.55 kV and a separation of 2 cm). The resistive phase of this system is 34.2 nsec using these parameters. The ratio of Vm to Im used

for the gas resistance equation is 0.4726.

This time varying resistance was used to generate voltage and current data with the NET-2 computer program. Since the voltage on the PFN does not begin to drop until the load current equals the charging current, a value of load resistance was calculated at the time of voltage reversal. The value of this resistance can be found from

$$R_L = \frac{V_{BD}}{I_s} \tag{50}$$

which is 1.86 ohms for the conditions stated. The output switch was arranged to close at the time when the resistance had dropped to this value and the voltage on the PFN was at the correct breakdown voltage.

The resulting voltage and current, curves are shown overlayed with the measured data taken on the laser in Figure 28. Figure 29 shows the power and impedance calculated from the predicted curves compared to the measured data. The results are reasonably close to the measured data, and it appears the spark gap analysis provides a close approximation.

A series of experiments was done to determine the optimum gas ratios for KrF mixes. First the ratio of F_2 to Kr was held at a constant 1:25. The relative energy obtained from the laser vs. pressure is shown in Figure 30 for three different F_2 concentrations. Curve 1 is for a mixture of 0.2% F_2, 5% Kr, and 94.8% He. The maximum energy is available at approximately 37 psia and decreases at higher pressures. Curve 2 was obtained with a mixture of 0.15% F_2, 3.75% Kr, and 96.1% He. The maximum energy occurs at about 42 psia and decreases slowly at higher pressures. A mixture of 0.095% F_2, 2.375% Kr, and 97.53% He

Voltage vs Time

Measured
Predicted

Voltage (kV)

40

20

0

−20

0   100   200

Time (nsec)

Current vs Time

Measured
Predicted

Current (kA)
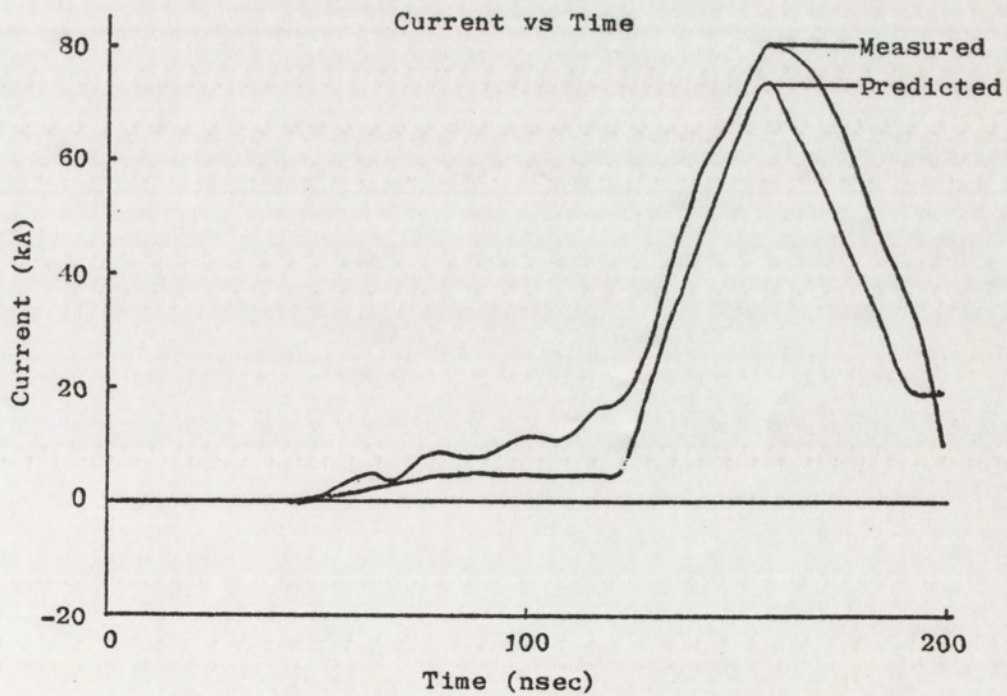
80

60

40

20

0

−20

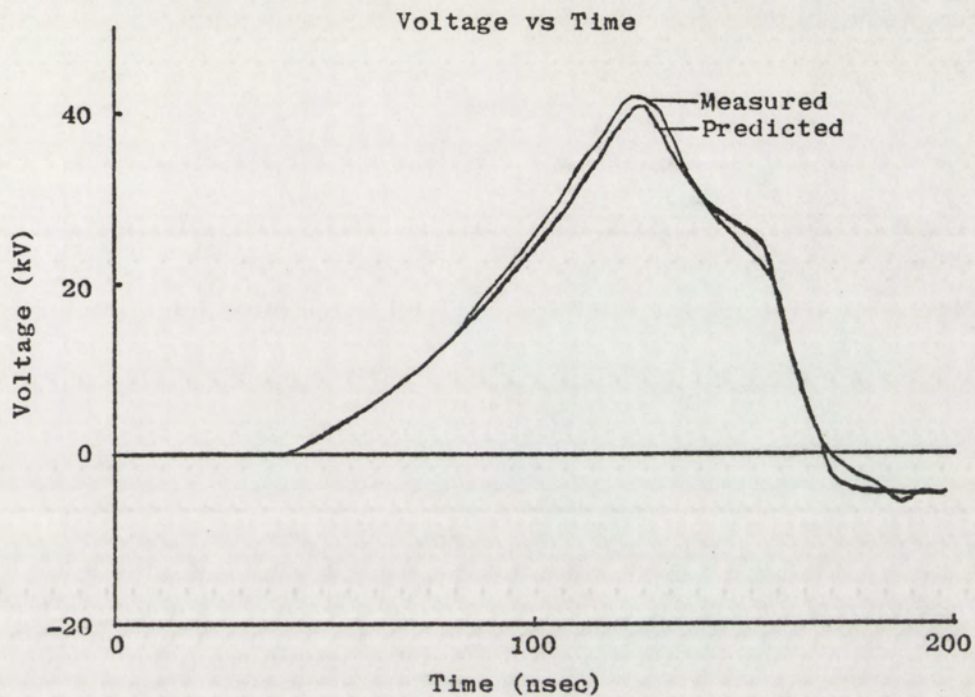0   100   200

Time (nsec)

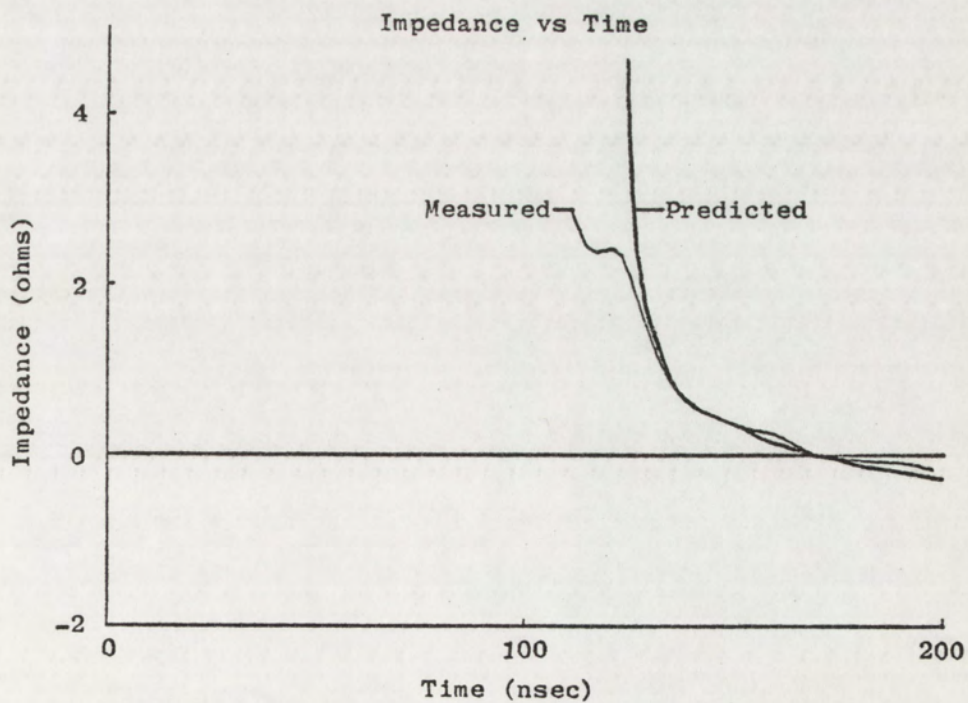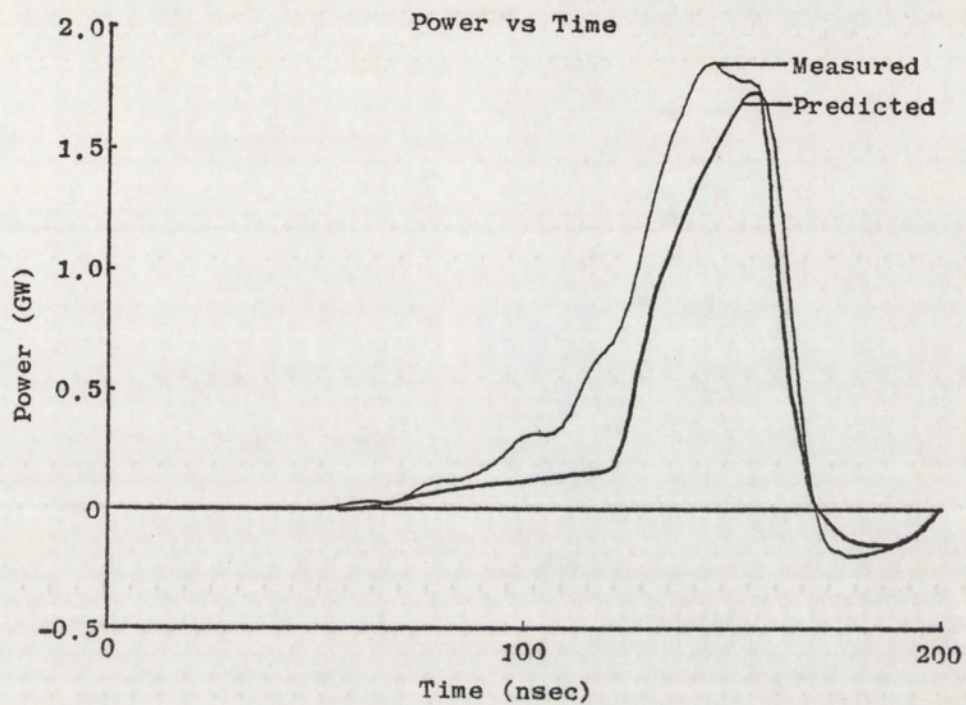Figure 28.   Comparison of Voltages and Currents

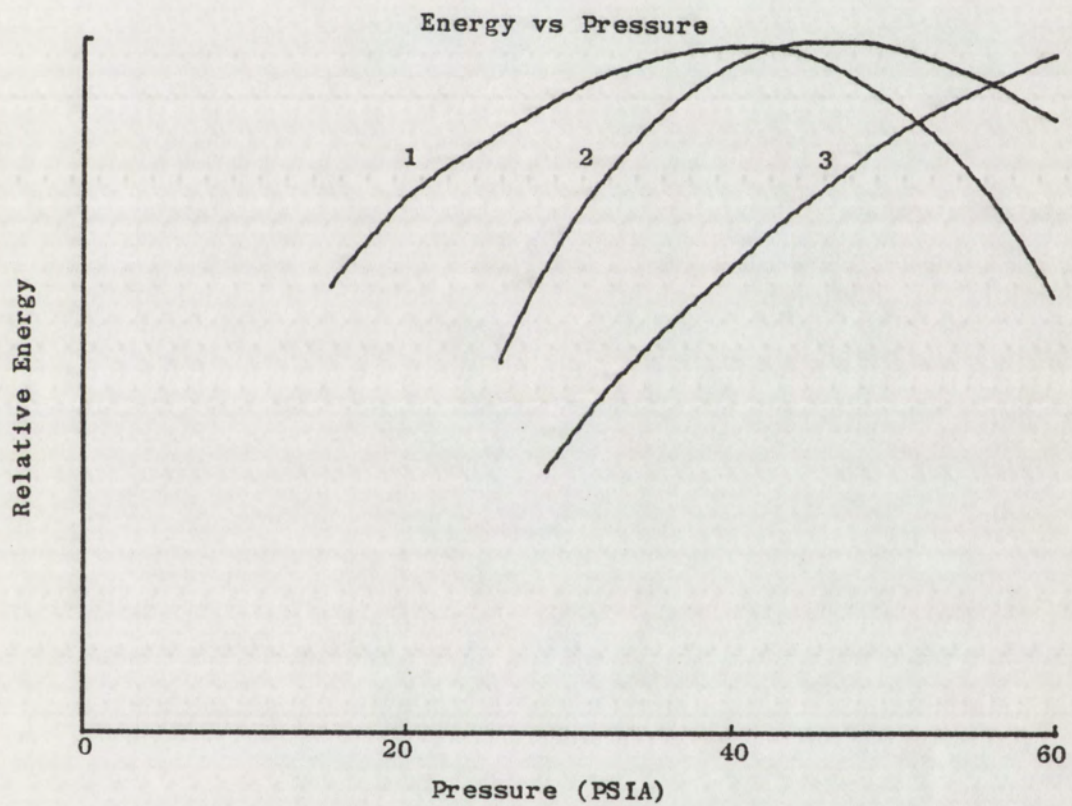Figure 29. Comparison of Powers and Impedances

Figure 30. Effects of Varying F_2 Concentration

was used to obtain curve 3. This curve has not reached the peak at 60 psia. All three curves were taken with different laser configurations, and the amplitudes are not normalized to each other. It is interesting to note that the partial pressure of F_2 at the peak of curve 1 is about 3.8 Torr while at the peak of curve 2 it is 3.3 Torr. At 60 psia the partial pressure of F_2 is only 2.9 Torr for curve 3 which implies the peak energy output is obtained at a partial pressure of F_2 of around 3.5 Torr, with He added to reach the final total pressure desired.

Next the F_2 concentration was held fixed at 0.095% and the Kr concentration was varied. Figure 31 shows the results of 3 different mixes. Curve A was obtained using a mixture of 0.095% F_2, 2.375% Kr, and 97.53% He. Curve B was taken with a mixture of 0.095% F_2, 3% Kr, and 96.905% He. A mixture of 0.095% F_2, 1.71% Kr, and 98.195% He was used for the data in curve C. These curves were taken in the same config- uration, and are normalized to each other. The mixture used in curve A is clearly superior to the other two mixtures over the pressure range tested. There is a slight tendency toward peaking at high pressure however, and a lower Kr concentration mix like mixture C may prove better at some higher pressure.

As mentioned in an earlier section of this paper the breakdown voltage of the gas is a function of pressure and risetime of the voltage pulse. Figure 32 shows the breakdown voltage versus pressure curves for 3 different initial charging voltages. Curve A is for a voltage of 40 kV which results in a dv/dt of 5.4×10^{11} volts/sec. Curve B was taken
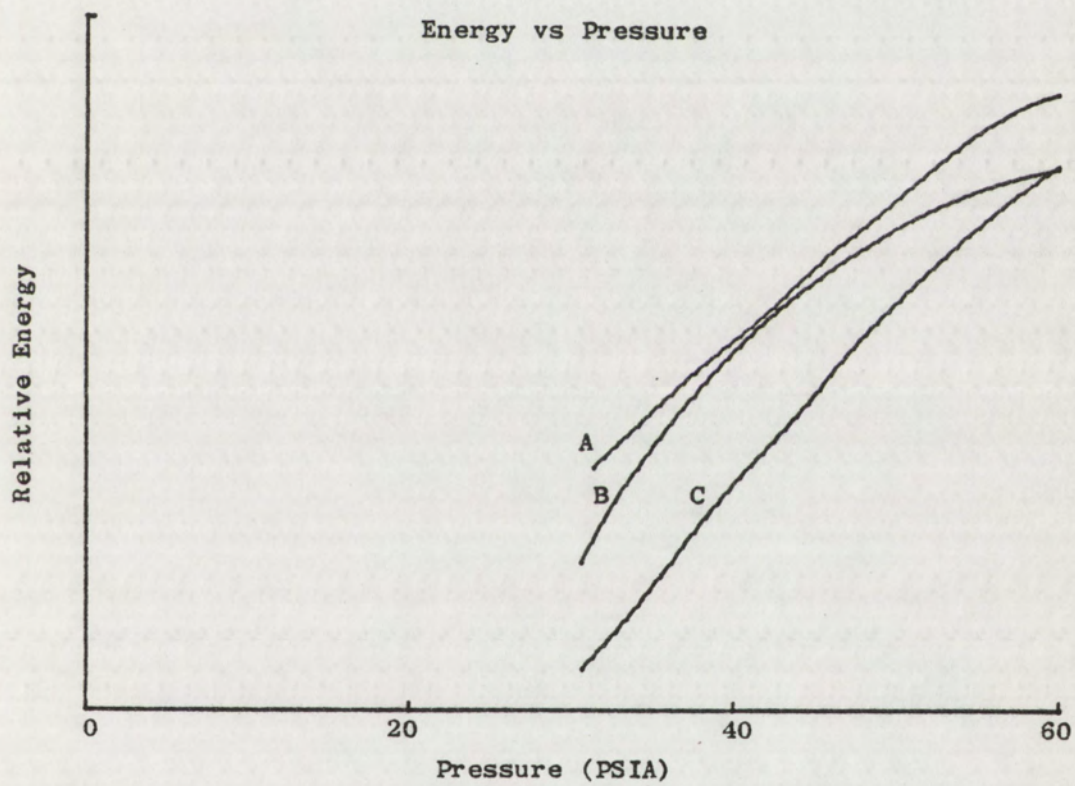
Figure 31. Effects of Varying Kr Concentration
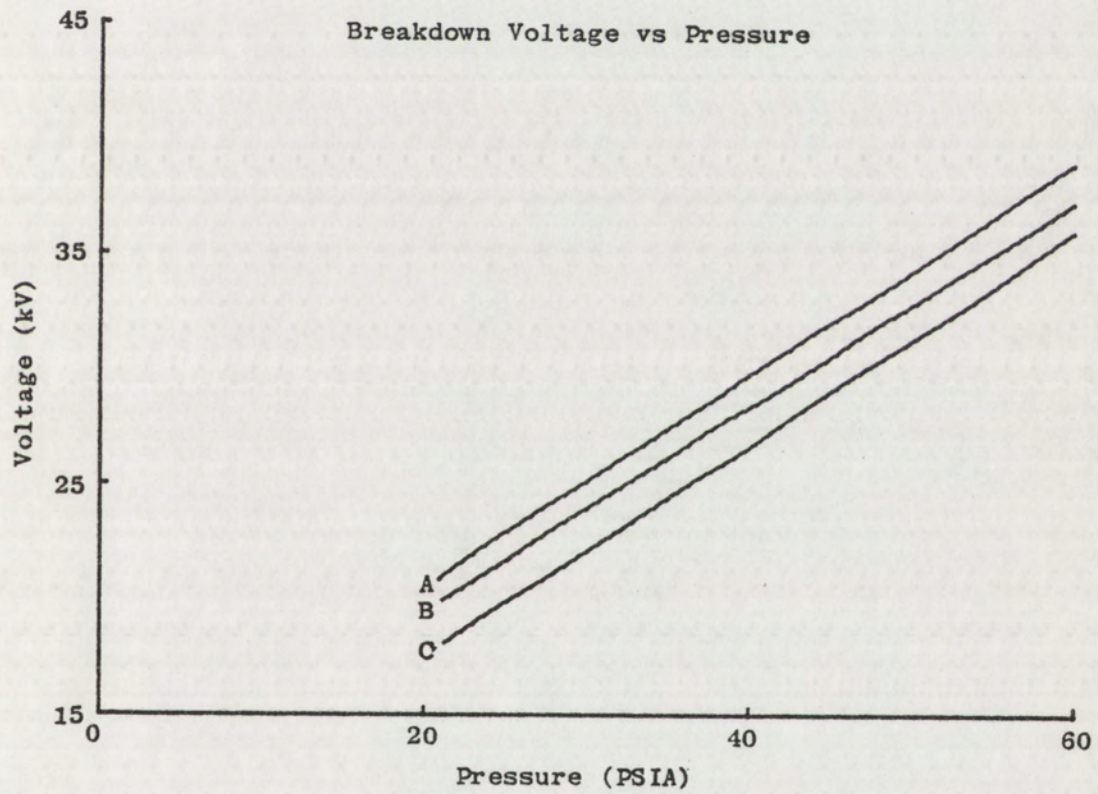
Figure 32. Measured Gas Breakdown Voltage

at an initial voltage of 30 kV resulting in a dv/dt of 4.7×10^{11} volts/ sec. Curve C was obtained at 20 kV initial voltage which produces a dv/dt of 3.9×10^{11} volts/sec. The slope of the three curves appears to be nearly the same, ie 456 v/psi while the y- intercept seems to be a function of the dv/dt. Curve A intercepts the y-axis at 11.76 kV, curve B at 10.14 kV, and Curve C at 8.38 kV. The ratio between the y-intercepts and the dv/dt appears to be nearly a constant 2.16×10^{-8}. This leads to an equation of the form

$$V_{BD} = K \frac{dv}{dt} + mP \tag{51}$$

where $K = 2.16 \times 10^{-8}$ sec, $\frac{dv}{dt}$ is the time rate of change of voltage in volts/sec, m = 456 V/psi, and P is the pressure in psia. This express- sion seems to be valid for the limited range of dv/dt and pressure en- countered in this laser.

An attempt was made to find a correlation between the laser output energy and some electrical parameter. Figure 33 shows the laser energy from many different configurations plotted against the calculated peak power, i.e. the rate of energy deposition.

The sample correlation coefficient for this data calculated from

$$r = \frac{S_{xy}}{(S_{xx} S_{yy})^{\frac{1}{2}}} \tag{52}$$

is 0.965 which indicates good correlation. A least squares fit to the data results in an equation of the form

Figure 33. Energy Dependence on Peak Power

$$E = E_o + m P \tag{53}$$

where $E_o = 1.01 \times 10^{-1}$ joules and $m = 2.55 \times 10^{-10}$ joules/watt, and P is the peak power in watts. Figure 34 shows the output energy plotted against peak power density, i.e. the rate of ener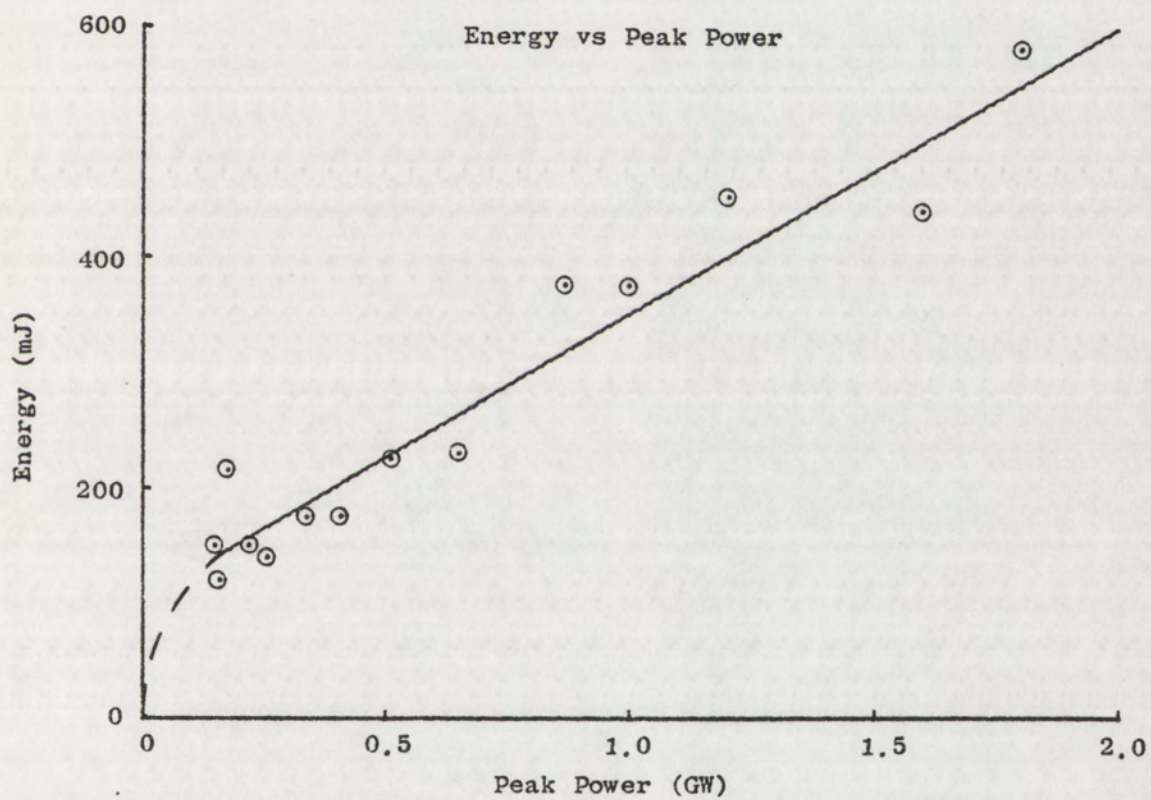gy deposition per unit volume. The correlation for this data is 0.962 which is not greatly different from the correlation obtained in Figure 31. There is not enough data at different volumes to determine whether the power or the power density is the important parameter. A least squares fit to the data results in an equation of the form

$$E = E_o + m \frac{P}{V} \tag{54}$$

where $E_o = 7.87 \times 10^{-2}$ J, $m = 3.517 \times 10^{-8}$ J . cm^3/W, P is the peak power in watts, and V is the active volume in cm^3. It is a bit disturbing however, to think of having an output energy with no power input whatever. Equations (53) and (54) must depart from a straight line approximation somewhere below the lowest power measured.

Attempts to find a correlation between the efficiency of the laser, i.e. energy out/energy deposited, and some electrical parameter were much less successful. Figure 35 shows two attempts, which indicate the efficiency is varying between 0.5% and 3.5%.

These figures were compiled from a number of different PFN geometries, gas mixes, pressures, voltages, and laser models. However when the efficiency of the 1.2 m laser was calculated using a fixed PFN (32-2.44 m cables) and a constant gas mix (0.15% F_2, 3.75% Kr, 20% Ne, 76.1% He) the data in Figure 36 were obtained. The trend is to lower effi-
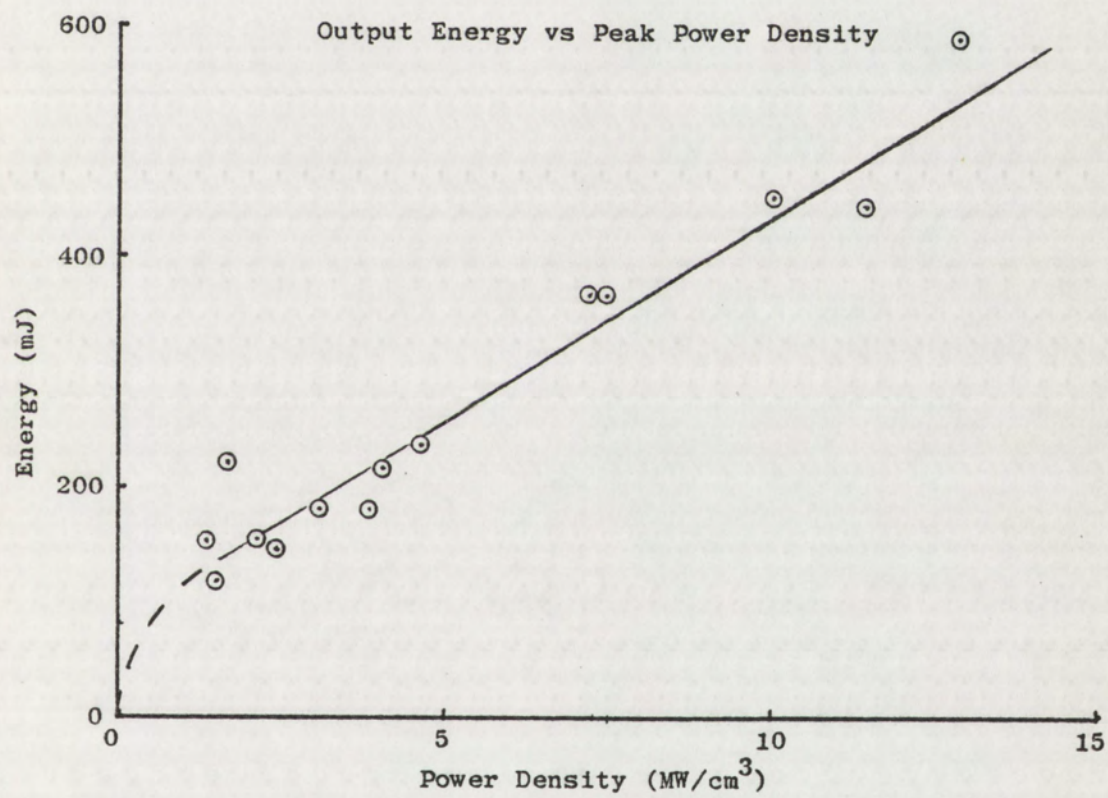
Figure 34. Energy Dependence on Power Density
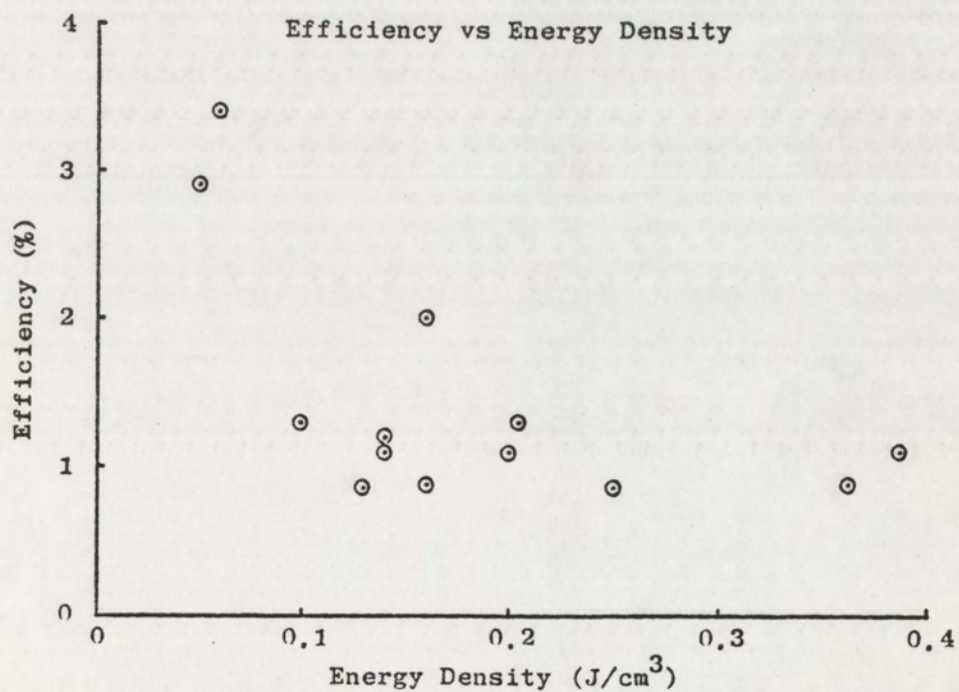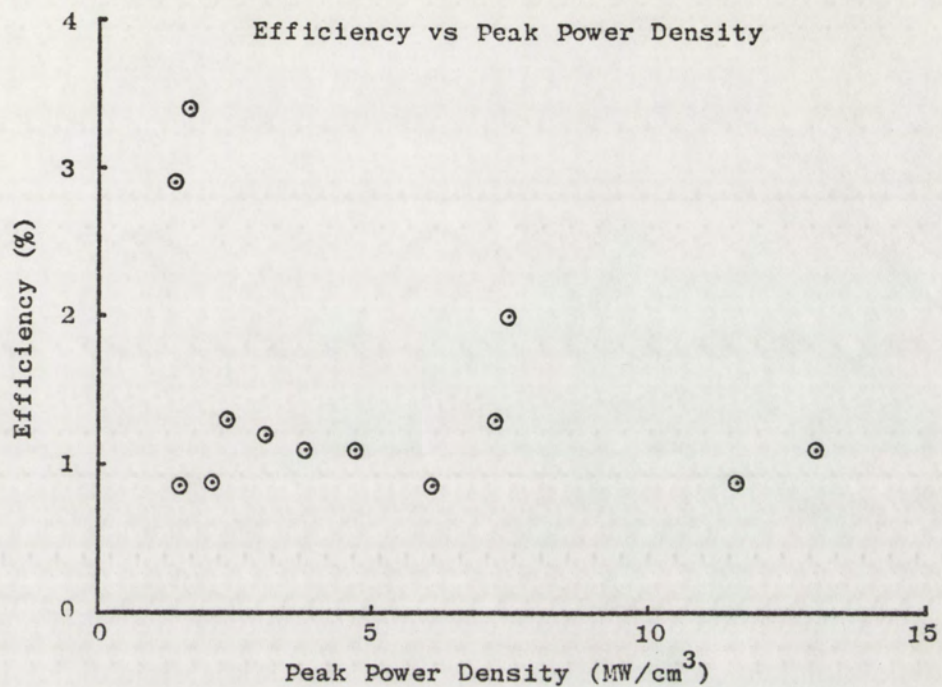
Figure 35. Efficiencies of Various Configurations

Efficiency vs Cavity Pressure
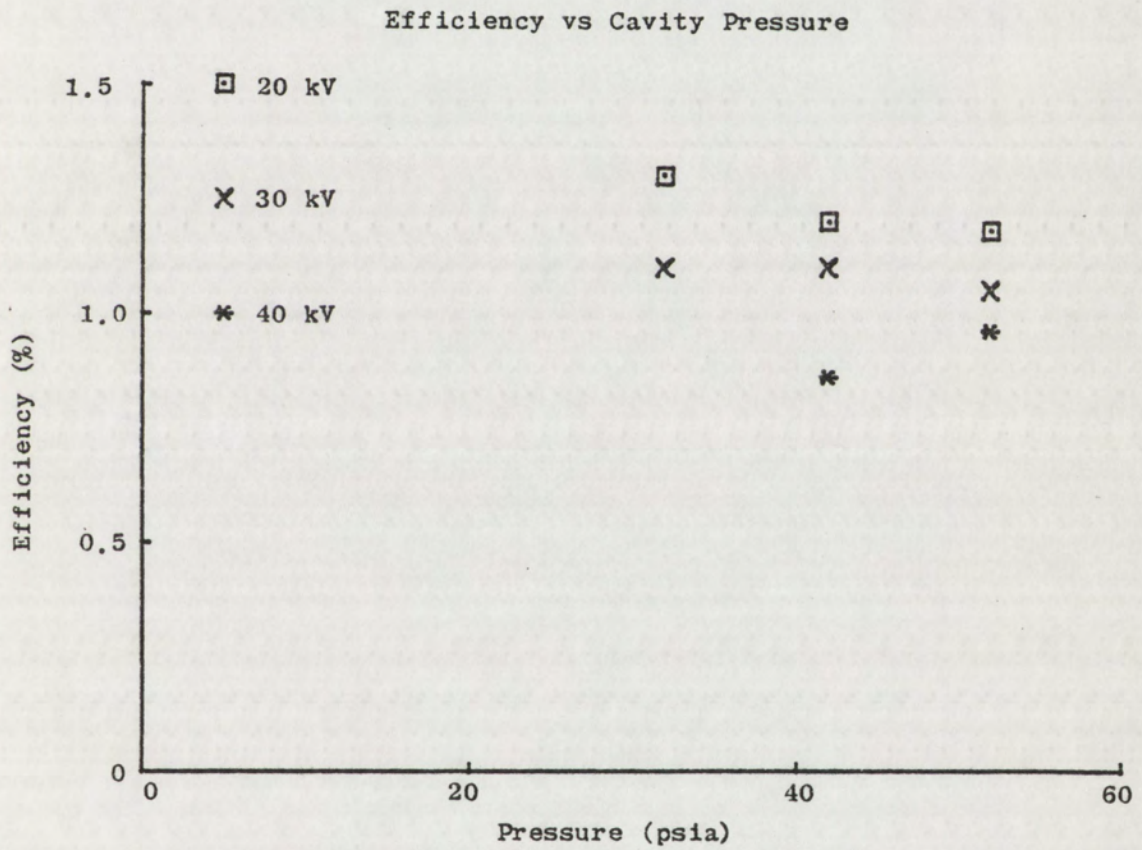
Figure 36. Efficiency of a Single Configuration

ciencies at higher initial voltages on the PFN driver, with the diff-
erences more pronounced at lower pressures. The efficiency appears to
be converging toward 1% at some pressure above 60 psia. This may be the
same effect observed in the data on varying gas concentrations, since
the peak energy is also expected to occur at a somewhat higher pressure
for this gas mixture.

The overall efficiency, i.e. the ratio of laser output energy to
energy stored in the capacitors behaves in a similar manner. As men-
tioned in the electrical section of this paper the overall efficiency
will vary with the breakdown voltage of the gas and the initial charging
voltage on the capacitors, as well as the value of the capacitance. In
an experiment to verify this effect the capacitors in the Marx generator
were changed to 0.06 µF to provide an effective driver capacitance of
0.03 µF. The laser was fitted with a 40 - 2.44 m cable PFN having a
total capacitance of 20 nF. The maximum energy transfer efficiency
calculated from equation (28) is 96% for this case. The laser was
operated on a KrF gas mixture of 0.1% F_2, 2.5% Kr, 20% Ne, and 77.4% He.
Figure 37 shows the overall efficiency plotted against pressure in the
laser cavity as a function of various initial charging voltages. The
best overall efficiency obtained occurred at about 55 psia and 20 kV
initial voltage.
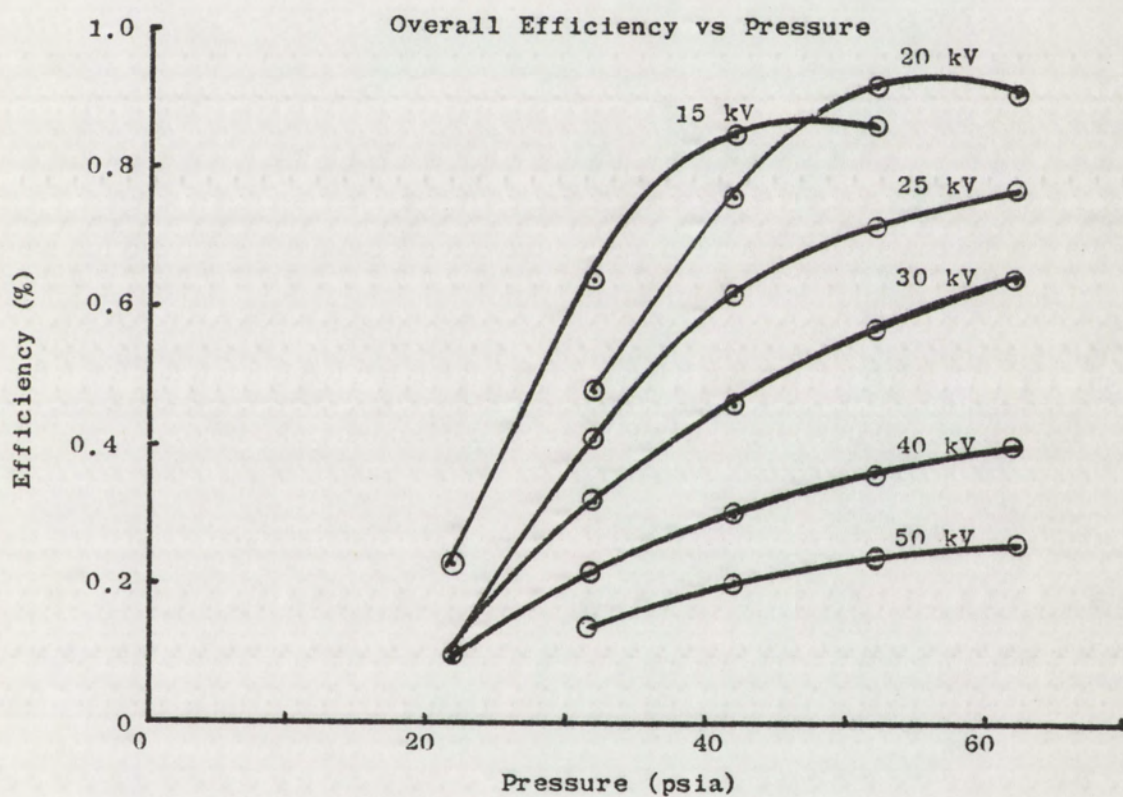
Figure 37. Overall Efficiency of Laser

CHAPTER IV. EXPERIMENTS

During this investigation two series of experiments were briefly pursued. These experiments were not intended to be comprehensive; they are included only as examples of the wide range of research made possible by the high power and beam quality obtained from these lasers.

The Raman scattering experiments were undertaken to expand the range of energies and frequencies obtained by other investigators (Loree 1977). The air breakdown study came about as an accident. When the laser was focused tightly for the Raman scattering experiments, a spark was observed in air at the focal plane of the lens. Since this phenomenon had not been observed previously, except at longer wavelengths (DeMichelis 1969), a brief attempt was made to measure the threshold power density. The measured threshold was found to be lower at shorter wavelengths, which is in agreement with the experimental data presented by DeMichelis.

4-1. Air Breakdown

Laser induced air breakdown has been of interest for a number of years. The early observations and measurements were at infra-red and visible wavelengths. Second harmonic generation of these lasers provided data at wavelengths in the near ultra-violet. Air breakdown has been observed with the 1.2 m laser operating on KrF, and with the 0.6 m laser operating on ArF. These new shorter wavelengths should provide a better understanding of this phenomenon.

In order to achieve the high power densities required for air breakdown, the quality of the beam must be improved over that possible with a plane-parallel cavity. In high gain large volume lasers one way to improve beam quality is by the use of an unstable resonator. Over the years several different unstable resonators have been used successfully. These resonators use high reflectivity curved optics with the output taken as "spillover" around the edge of one mirror. A new concept was tried recently, whereby one reflector is an uncoated convex lens (Barker, Loree, 1977). Output coupling is by transmission through this lens, with the output focused near the focal point of the lens.

The 1.2 m laser operating on KrF with this type of optical cavity reached air breakdown threshold at 50 mJ per pulse. A best form BaF_2 lens of 100 mm focal length was used as the output coupling element, with a 5 m radius of curvature aluminum rear reflector, and a separation of 1.9 m. Alignment of the lens was not critical and several degrees of rotation were required to eliminate the breakdown. Measurements of the

spot size were made by taking burn spots on several types of paper.
The diameter of the burn spots was measured with an optical loupe.
The bulk of the laser energy was focused to a diameter of 0.15 mm.
The divergence of the laser can be calculated from geometric optics as

$$\theta = \frac{D}{f} \qquad (55)$$

where f is the focal length of the lens and D is the diameter of the
spot. The full angle divergence thus is 1.5 mrad. This is far from the
diffraction limit calculated from

$$\theta = 1.22 \frac{\lambda}{D} \qquad (56)$$

where λ is the wavelength and D is the diameter, or width in this case,
of the laser beam in the cavity. Using the 5 mm dimension of the beam
in the laser results in a diffraction limit of 0.06 mrad full angle.

Power density was calculated from the relation

$$W/A = (E/\tau)/A \qquad (57)$$

where E is the laser energy, τ is the pulse-width measured at FWHM
and A is the area of the focal spot. Using the measured energy of 50
mJ, a pulsewidth of 25 nsec, and 0.15 mm diameter results in a threshold
of 1.1×10^{10} watts/ cm^2 for air breakdown at the 248 nm wavelength.

The 0.6 m laser operating on ArF reached optical air breakdown at
an energy of 30 mJ. A longer focal length (350 mm) plano convex quartz
lens was used as the output coupler (convex side towards laser). The
same aluminum rear reflector was used at a separation of 1 m. Measure-
ment of the burn spot resulted in a diameter of 0.2 mm. The divergence
of the beam is 0.57 mrad full angle which is well above the diffraction

limit of 0.047 mrad full angle.

Using the measured values of 30 mJ, 11 nsec pulsewidth, and 0.2 mm diameter results in a threshold for air breakdown of 8.7×10^9 watts/cm^2 at the 193 nm wavelength.

More accurate measurements of the threshold for air breakdown will require a better means of measuring the characteristics of the laser beam. Since the beam is quite far from the diffraction limit it appears the laser is operating in many transverse modes. This can cause local hot spots in the beam where the power density is very high and result in errors in the measurement. Burn spots are generally not the best means of determining spot size since they are subject to a number of errors, including non-linear intensity effects, and wavelength dependence. Interpretation of the burn spots is another area where errors can occur. Other methods could perhaps be devised, but the high power and small spot size lead to a number of problems. Further study is outside the scope of this thesis.

4-2. Raman Scattering

The Raman scattering process provides a convenient means of pro-
ducing high intensities at a variety of wavelengths. The Raman scat-
tering effect can be described by the interaction of a photon and a
molecule whereby the molecule gains one quantum of vibrational energy
and a photon is emitted having an energy reduced by the same amount.
This process can continue with further frequency shifts as the emitted
photons interact with molecules. The resulting Stokes lines (S_1, S_2,
S_3, etc) are shifted in frequency by an amount called the Stokes shift.
This value has been determined for a number of different molecules.

It is also possible for a photon to interact with a vibrating
molecule, the result being the emission of a higher energy photon as the
molecule relaxes to the ground state. These shorter wavelength emis-
sions are called Anti-Stokes lines (AS_1, AS_2). Experiments were con-
ducted with the 1.2 m laser operating on KrF to increase the output
energy obtained by Loree et al from a lower energy laser focused in high
pressure hydrogen. Later experiments were done with the 0.6 m laser
operating on ArF to attempt Raman scattering of the 193 nm wavelength in
high pressure deuterium, methane, and a mix of deuterium and hydrogen

gas. Loree et al were unable to reach the threshold power required for stimulated Raman scattering in these gases.

The 1.2 m laser operating·on KrF was used for the first series of experiments. The unstable optical resonator consisted of a flat aluminum reflector and a 250 mm focal length plano convex lens separated by 1.9 m. A H_2 cell pressurized to 900 psig was placed at the focus. The output was focused onto a ground glass diffuser and the RSS was positioned to observe the spot. With the laser operating at 200 mJ/pulse, outputs were observed at 206, 225, 248, 277, 313, 360, 423, and 513 nm. These correspond to the AS_2, AS_1, pump, S1, S2, S3, S4, and S5 lines of hydrogen.

Most of the energy appeared to be in the first Stokes line at 277 nm. A liquid filter solution was placed between the H_2 cell and an energy meter. A 10 mm cell of ethyl acetate effectively absorbs the pump and shorter wavelengths while transmitting all the Stokes lines with little loss. The energy converted to all Stokes lines was measured at different H_2 pressures to find an optimum (see Figure 38).

Operating the cell between 400 and 900 psig appears to produce the best results. A 10 mm cell containing a mixture of 90% ethyl acetate 10% toluene was inserted to absorb the S1 line and all shorter wavelengths. The output on S1 was then calculated from the difference as approximately 34 mJ, a significant improvement over the energy reported by Loree et al. This is a conversion of 17% of the pump energy into the first Stokes. Assuming a loss of 8% per window on the H_2 cell, and a measured
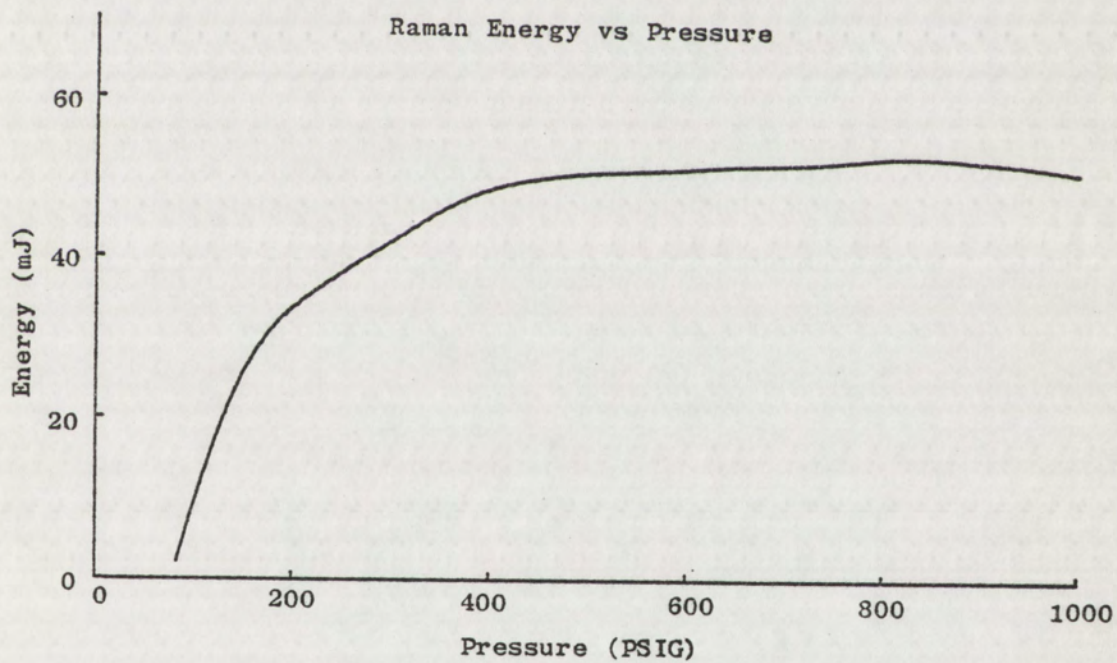
Figure 38. Raman Scattered KrF Energy in H_2

loss of 27% in the ethyl acetate filter (at 277 nm) results in 184 mJ
of pump energy reaching the H_2 gas, and 51 mJ of S1 leaving the H_2 gas.
This would imply an actual conversion efficiency 27.7% which is still
less than the maximum reported by Loree <u>et al</u>. Perhaps the longer laser
has reduced beam quality, which may well be the case judging from burn
spots taken at the focus. An additional problem encountered was the
deterioration of the ethyl acetate solution after exposure to the laser.
Absorption of wavelengths between 260 nm and 300 nm was increased con-
siderably after a few hundred pulses.

The 0.6 m laser operating on ArF gas produced sufficient power
density to achieve Raman Scattering in D_2 gas. A number of different
focal length lenses were used as output couplers, and the pressure was
varied in the D_2 cell. The output of the D_2 cell was refocused onto a
ground glass plate and the OMA was set up to measure the intensity of
the various lines. The OMA is a summing instrument, and each run con-
sisted of about 200 pulses from the ArF laser which was operating at
approximately 120 mJ/pulse. The relative amplitudes of the various
Stokes lines observed are plotted as a function of pressure for a 500
mm focal length output coupler and 500 mm length D_2 cell in Figure 39.

Figure 40 shows the same data obtained using a 350 mm focal length
output coupler and 300 mm length D_2 cell.

A 1 m focal length lens and 1 m length D_2 cell were used to obtain
the data in Figure 41.

A nitrogen purged housing was required to eliminate the oxygen
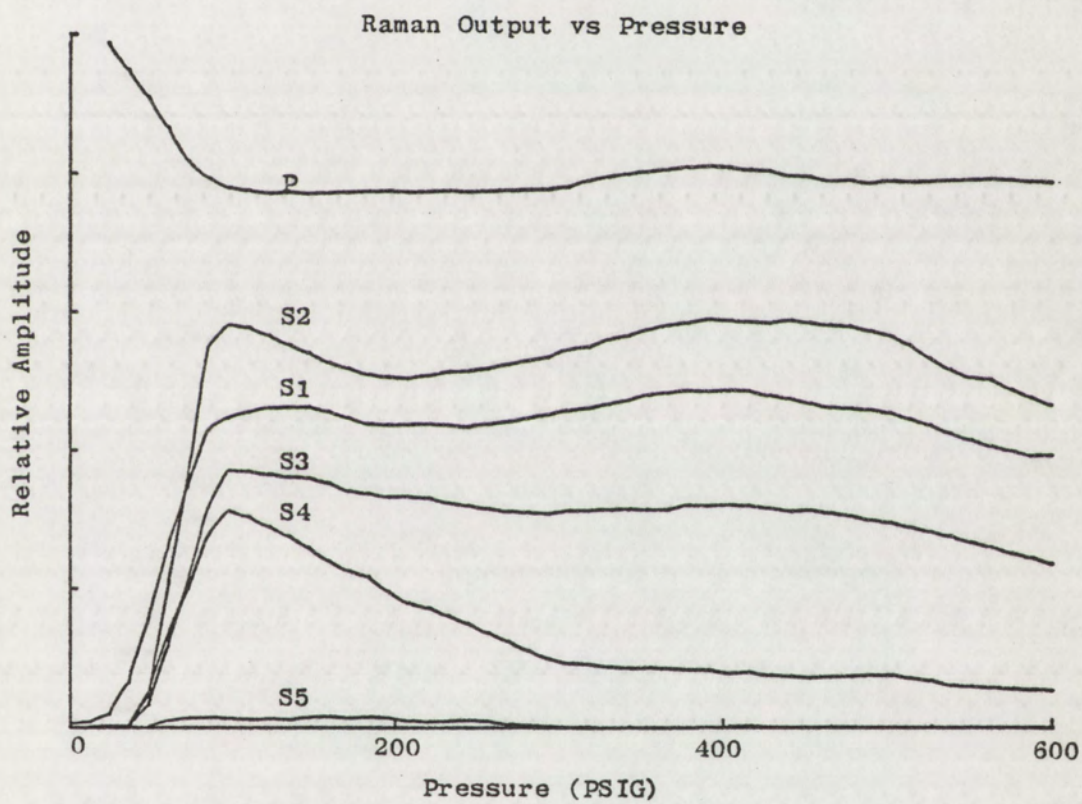
Raman Output vs Pressure

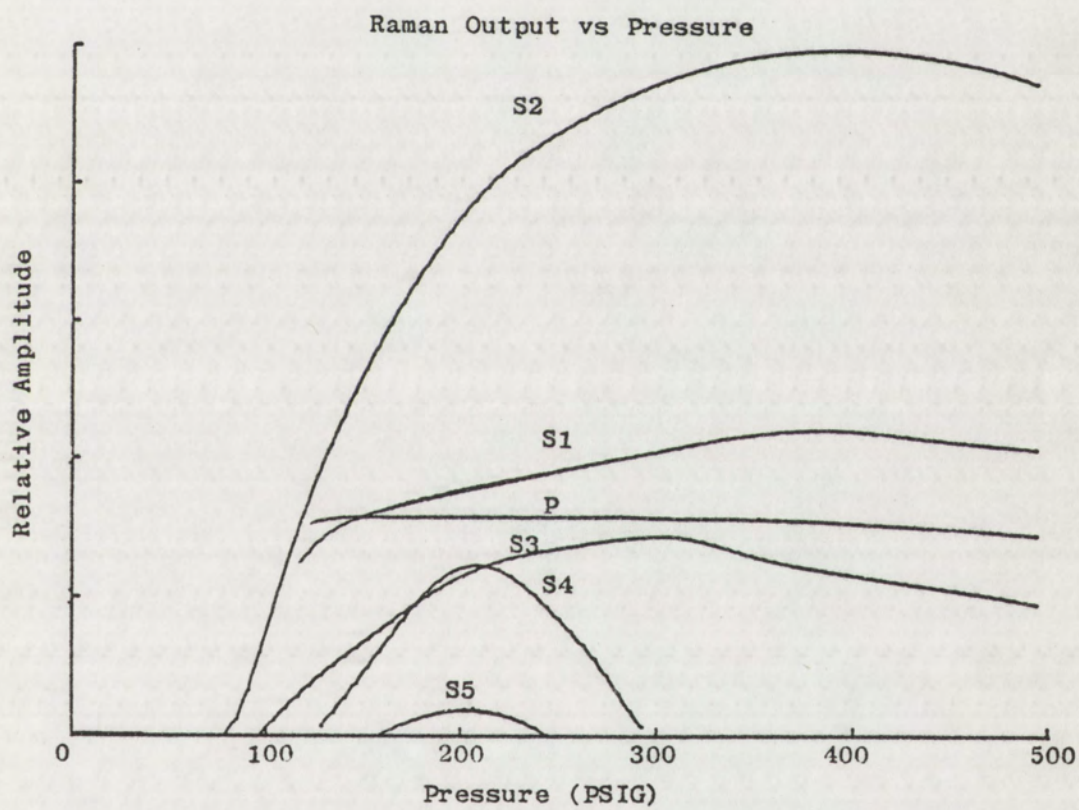Figure 39. Raman Scattering of ArF in D_2 with 0.5 m Lens

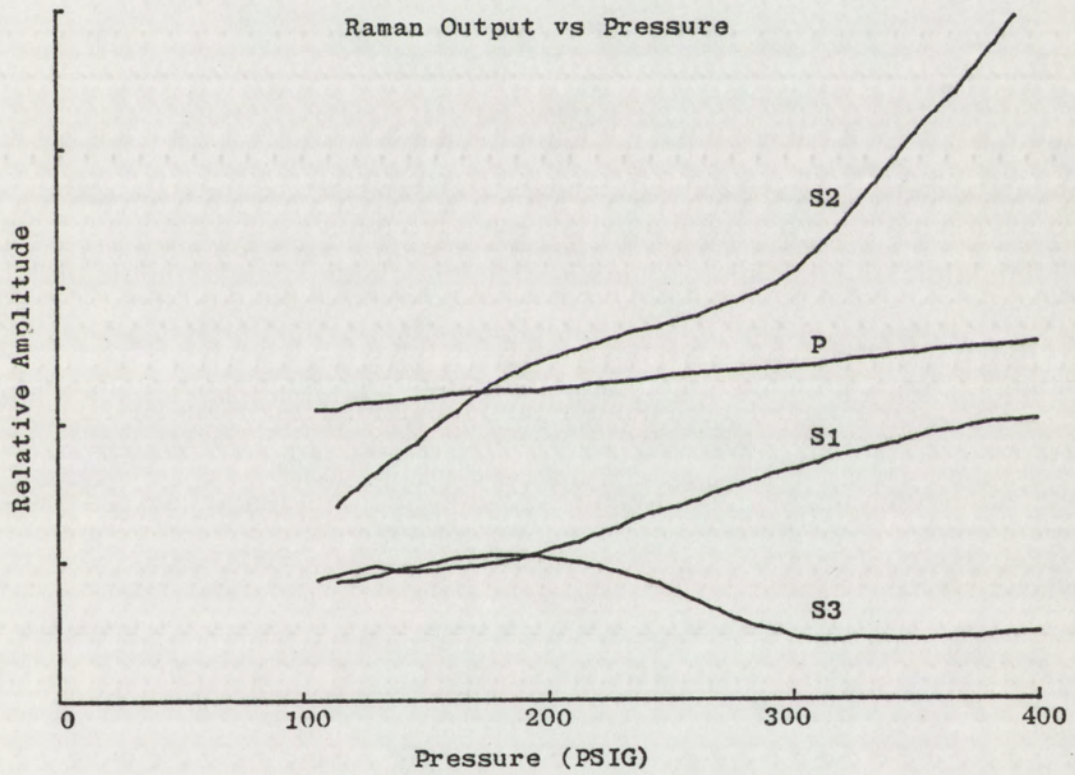Figure 40. Raman Scattering of ArF in D_2 with 0.35 m Lens

Figure 41. Raman Scattering of ArF in D_2 with 1.0 m Lens

absorption and permit the measurement of the first Anti-Stokes data presented in Figure 42, taken with the 350 mm focal length lens and 300 mm length D_2 cell.

Note that the amplitudes on any given figure are normalized to the largest amplitude observed, and cannot be compared between figures. It is also interesting to note that the second Stokes line always exceeds the first Stokes line in amplitude, and in some cases even exceeds the transmitted pump signal. This condition required a very careful alignment of the output coupler to optimize the power density. Once this alignment was obtained even reducing the pump energy below 50 mJ/pulse did not result in the first Stokes exceeding the second. No attempt was made to measure the energy at the output of the D_2 cell, however, in the case of the severely depleted pump signal it is believed that nearly all the pump is converted to Stokes lines.

The 193 nm pump was strongly absorbed in the cell containing methane gas, with no signal of any kind at the exit end. This was believed to be absorption by impurities in the methane, but was not pursued further.

Raman scattering in a mixture of two gases having different Stokes shifts can produce interesting results. When the pressure ratio of the two gases is correct for approximately equal output in the first Stokes of both gases, the lines observed include not only the Stokes lines of each gas, but combination lines as well.

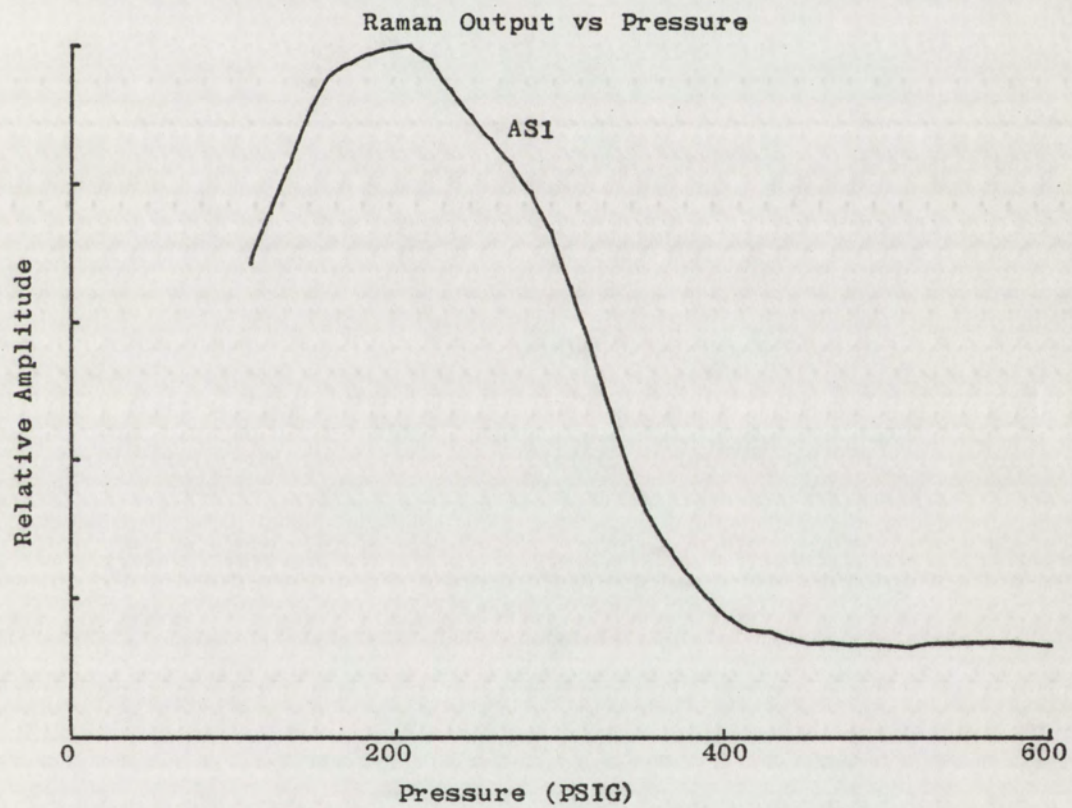Figure 43 shows the results obtained from a mixture of 82% H_2 and

Figure 42.   First Anti-Stokes Line of ArF in D_2
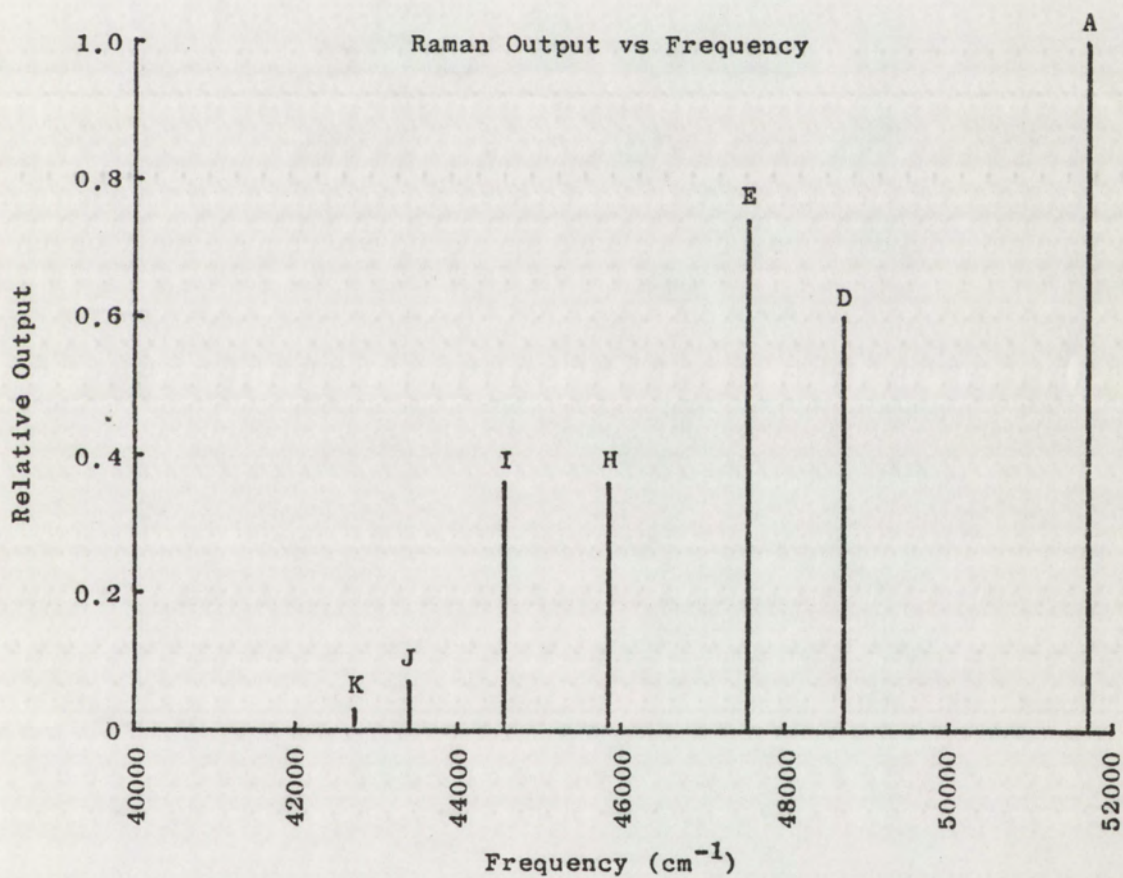
Figure 43. Strong Raman Lines of ArF in H_2/D_2 Mixture

18% D_2, at 450 psig. The Stokes shift in H_2 is 4155 cm^{-1} while the shift in D_2 is 2993 cm^{-1}. Line A is the pump at 51700 cm^{-1} (193nm). Lines D, H, and K are S_1, S_2, S_3 of D_2 at 48700 cm^{-1} (205nm), 45700 cm^{-1} (219nm), and 42700 cm^{-1} (234nm). Lines E and J are S_1 and S_2 of H_2 at 47600 cm^{-1} (210 nm) and 43400 cm^{-1} (230 nm). Line I is a combination line resulting from one downshift in each gas, which is at 44600 cm^{-1} (224nm).

Several other weaker lines were also identified, and are shown on Figure 44. As shown lines A, D, E, H, I, and J are all saturated. The weaker lines are referenced to line K, i.e. S_3 of D_2. Two more simple combination lines were identified (M and N) at 41600 cm^{-1} (241nm) and 40400 cm^{-1} (247nm). Line M results from 2 downshifts in D_2 and one in H_2, while line N results from 2 downshifts in H_2 and one in D_2. Lines B, G, and L are identified as S_1, S_2, and S_3 in H_2 scattered off the first Anti-Stokes line of D_2. They occur at 50500 cm^{-1} (198nm), 46400 cm^{-1} (216nm), and 42200 cm^{-1} (237nm). Lines C and F likewise are the result of S_2 and S_3 in D_2 scattered off the first Anti-Stokes line in H_2. They occur at 49900 cm^{-1} (200nm) and 46900 cm^{-1} (213nm). Although no measurements were made above the pump frequency, it is apparent that the first anti-Stokes lines of H_2 and D_2 should have been observed at 55900 cm^{-1} (179nm) and 54700 cm^{-1} (183nm). In addition, the S_1 line in D_2 scattered off the first Anti-Stokes in H_2 should have been observed at 52900 cm^{-1} (189nm).
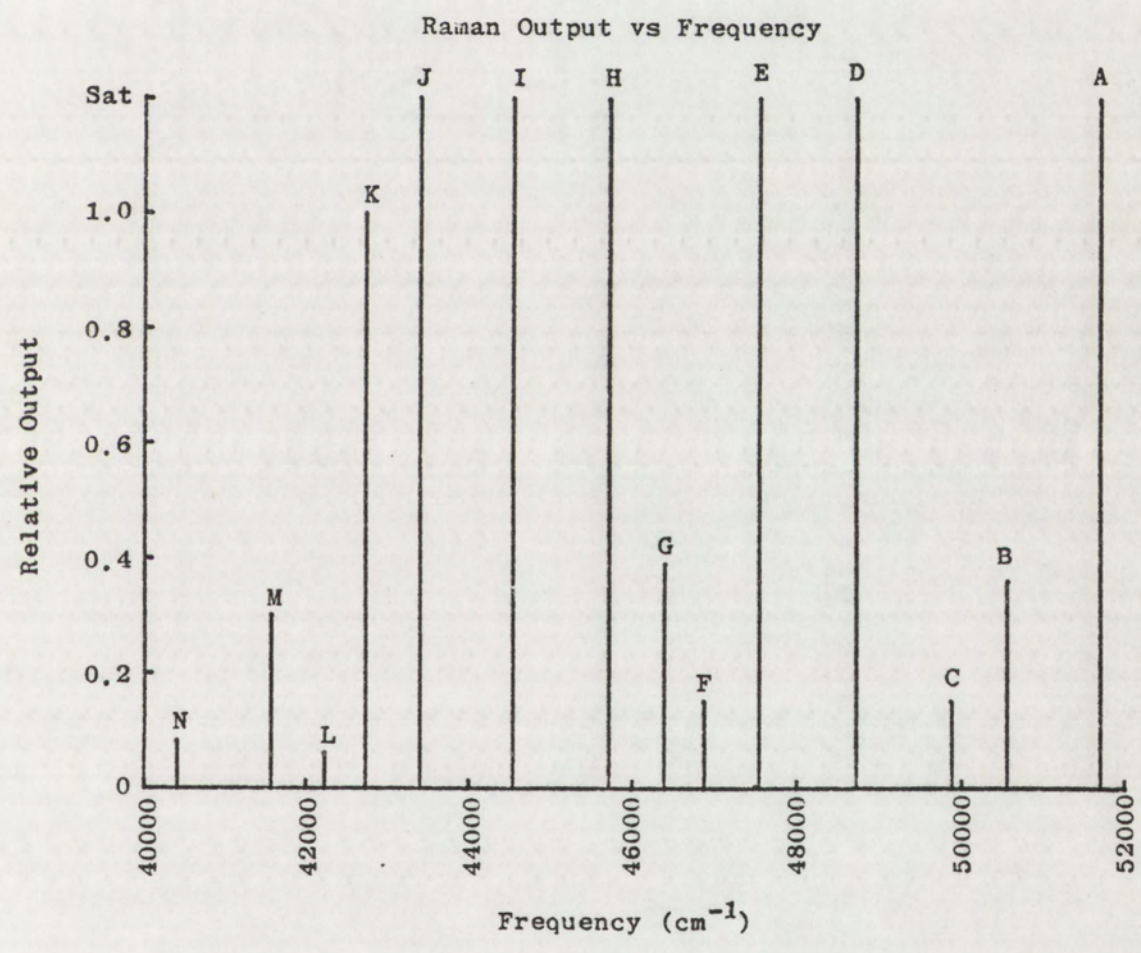
Figure 44. Observed Raman Lines of ArF in H_2/D_2 Mixture

CHAPTER V. SUMMARY

Rare gas excimer lasers are finding increased usage in a wide
variety of fields. A better understanding of the characteristics of
these lasers is essential to improving performance and versatility.

Several materials were found to be poor choices for use with
excimer lasers. Acrylic and polycarbonate, although used by the laser
industry, develop cracks after relatively short exposures to low con-
centrations of F_2 gas. Other materials, notably epoxy and teflon TFE,
are much more resistant, if not immune to this problem.

Some form of pre-ionization is required to successfully use elec-
trical discharge pumping in excimer lasers. The time delay between pre-
ionization and the main discharge is shown to be more important than the
magnitude of pre-ionization. Different excimers are shown to behave
differently with respect to time delay.

The voltage and current in the discharge are used to calculate a
number of electrical parameters. Equations describing the voltage,
current, and impedance of the discharge are presented. A computer
simulation of the discharge reproduces the measured values of voltage
and current quite well.

Conclusions are drawn from the derived electrical parameters and
measured values of energy, pressure, and charging voltage. Data are
presented showing that the laser output energy is related to the rate of
deposition of energy in the gas, the gas mixture, the risetime of the
voltage pulse, the impedance of the PFN, and the gas pressure. Equa-
tions describing the breakdown voltage of the gas and output energy

are presented. The efficiency of the laser is shown to be a function of
initial voltage on the PFN driver and the gas pressure. The length of
the active volume is shown to be of little importance in such a high
gain system.

Experiments in Raman scattering and optical air breakdown are described. A coarse measurement of the threshold for air breakdown at 193
nm and 248 nm is discussed. Experiments in Raman scattering resulting
in energy levels and wavelengths not previously attained are presented.
Coherent energy was observed at over twenty different wavelengths
ranging from 183 nm to 513 nm.

The data presented and some of the conclusions drawn are based on a
rather narrow range of data. The present known operating range of
excimer lasers is also quite narrow, and physical considerations tend to
place limits on many of the parameters. It is unlikely that parameters
such as pressure, voltage, inductance, and capacitance will vary greatly
in future excimer laser systems. The time dependent impedance of the
discharge reduces the chances of designing a perfect PFN to achieve
impedance matching. With these constraints the conclusions reached
should provide a reasonable estimate of future laser performance.

References

D. Barker and T. Loree, "Improved Beam Quality in Double Discharge Excimer Lasers," Appl. Optics, Vol. 16, No. 7, p. 1792, July 1977.

C. DeMichelis, "Laser Induced Gas Breakdown: A Bibliographical Review," IEEE J. Quantum Electronics, Vol. QE-S, No.4, P. 188, April 1969.

T. Loree, D. Barker, R. Sze, "Efficient Raman Shifting of KrF and ArF Laser Wavelength," Appl. Phys. Lett., Vol. 31, No. 1, p. 37, July 1, 1977.

J. C. Martin, "Multichannel Gaps," SSWA/JCM/703/27

R. C. Sze, P. B. Scott, "1/4 Joule Discharge Pumped KrF Laser," to be published.

W. Willis, unpublished internal memo